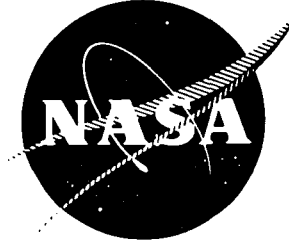


NASA CR 165360



NASA CR-165360
FR-13370



NASA-CR-165360
19810019556

COATING FOR PREVENTION OF TITANIUM COMBUSTION

by **V. G. Anderson, M. E. Funkhouser**

LANGLEY RESEARCH CENTER
LIBRARY

AUG 10 1981

LANGLEY RESEARCH CENTER
LIBRARY, NASA
HAMPTON, VIRGINIA

PRATT & WHITNEY AIRCRAFT GROUP
GOVERNMENT PRODUCTS DIVISION

Prepared for
NATIONAL AERONAUTICS AND SPACE ADMINISTRATION

NASA Lewis Research Center
Contract NAS3-21815

1. Report Number NASA CR-165360		2. Govt Accession No.		3. Recipient's Catalog Number	
4. Title (and Subtitle) COATING FOR PREVENTION OF TITANIUM COMBUSTION				5. Report Date September 1980	
				6. Performing Organization Code	
7. Author(s) V. Anderson and M. Funkhouser P. McDaniel				8. Performing Organization Report No. FR-13370	
9. Performing Organization Name and Address United Technologies Corporation Pratt & Whitney Aircraft Group Government Products Division P.O. Box 2691, West Palm Beach, FL 33402				10. Work Unit No.	
				11. Contract or Grant No. NAS3-21815	
12. Sponsoring Agency Name and Address National Aeronautics and Space Administration Washington, D. C. 20546				13. Type of Report and Period Covered Final - 9 Feb 1979 through 9 June 1980	
				14. Sponsoring Agency Code	
15. Supplementary Notes NASA-Lewis Research Center, Cleveland, Ohio 44135, Project Manager — John Merutka					
16. Abstract This program explored a limited number of coating options for titanium gas turbine engine components with the objective of minimizing potential combustion initiation and propagation without adversely affecting component mechanical properties. The program objectives were met by two of the coatings, ion-plated platinum plus electroplated copper plus electroplated nickel (Pt/Cu/Ni) and ion vapor deposited aluminum (IVD Al).					
17. Key Words Laser Ignition Titanium Alloy Burn Severity Sustained Combustion Combustibility				18. Distribution Statement Unclassified — Unlimited	
IVD Aluminum Ion Plated Platinum Chordwise Velocity Cascade (Molten Metal Ignition) Compressor Environment					
19. Security Classif. (of this report) Unclassified		20. Security Classif. (of this page) Unclassified		21. No. of Pages 82	22. Price* 3.00

*For sale by the National Technical Information Service, Springfield, Virginia 22151

N81-28094#

TABLE OF CONTENTS

<i>Section</i>	<i>Page</i>
SUMMARY.....	1
INTRODUCTION.....	3
Program Overview.....	3
EXPERIMENTAL APPROACH.....	5
Materials.....	5
Test Apparatus and Procedures.....	7
TEST RESULTS AND DISCUSSION.....	19
Combustion Tests.....	19
High-Cycle Fatigue Tests.....	27
Tensile Testing.....	30
Creep Testing.....	30
Stress Rupture Testing.....	30
Hot Salt Stress Corrosion Testing.....	32
Erosion Testing.....	34
Adhesion Testing.....	34
Static Oxidation Testing.....	34
Diffusion Testing.....	37
Thermal Shock Testing.....	37
Stress Analysis Testing.....	37
SUMMARY OF RESULTS.....	44
Combustion — Cascade Test Configuration.....	44
High-Cycle Fatigue (HCF) Testing.....	44
Tensile Testing.....	50
Creep Testing.....	50
Stress Rupture Testing.....	50
Hot Salt Stress Corrosion Testing.....	50
Erosion Testing.....	51
Adhesion Testing.....	51
Static Oxidation Testing.....	51
Diffusion Testing.....	51
Thermal Shock Testing.....	51
Stress Analysis Testing.....	51
CONCLUSIONS.....	52
RECOMMENDATIONS.....	52
APPENDIX A — AFWAL/PL Titanium Fire Program Combustion Test Results.....	53
APPENDIX B — Electrodeposition Processes.....	54
APPENDIX C — Test Specimen Configurations.....	63

LIST OF ILLUSTRATIONS

<i>Figure</i>		<i>Page</i>
1	Reverse Bending Fatigue Results of Coated AMS 4916 (Ti 8-1-1).....	2
2	Titanium Combustion Test Rig — Laser Ignition.....	8
3	Titanium Combustion Test Rig Setup.....	9
4	Arrangement of Laser Ignition and Photographic Recording Systems.....	10
5	Titanium Combustion Rig — Cascade Ignition.....	11
6	Combustion Rig Specimen Holder.....	11
7	Model 76 NAC Film Motion Analyzer.....	12
8	Determination of Specimen Ignition.....	14
9	Establishment of Burn Through.....	15
10	Hot Salt Stress Corrosion Specimen Holder.....	16
11	Erosion Test Station.....	18
12a	Specimen Appearance After Test at Indicated Temperatures.....	21
12b	Specimen Appearance After Test at Indicated Temperatures.....	22
12c	Specimen Appearance After Test at Indicated Temperatures.....	23
13	Typical Compressor Conditions.....	26
14	Typical Compressor Conditions.....	26
15	Reverse Bending Fatigue Results of Uncoated AMS 4916 (Ti 8-1-1).....	27
16	Reverse Bending Fatigue Results of Coated AMS 4916 (Ti 8-1-1).....	28
17	Reverse Bending Results of Ti 8-1-1 (AMS 4916) Coating Evaluation, R = -1, Alt Stress = ± 414 MPa (60 ksi), Temp = 425°C (800°F).....	29
18	Reverse Bending Results of Ti 6-4 (AMS 4911) Coating Evaluation, R = -1, Alt Stress = ± 414 MPa (60 ksi), Temp = 315°C (600°F).....	29
19	Reverse Bending Results of Ti 3Al-8V-6Cr-0.4Mo-4Zr Coating Evaluation, R = -1, Alt Stress = ± 240 MPa (35 ksi), Temp = 425°C (800°F)....	30
20	Tensile Test Results at 427°C (for Ti 8-1-1) and 315°C (for Ti 6-4).....	31
21	Stress Rupture Results.....	32
22	Hot Salt Stress Corrosion.....	33

LIST OF ILLUSTRATIONS (Continued)

<i>Figure</i>		<i>Page</i>
23	Scanning Electron Microscopy Photos of Cross-Sectioned Adhesion Specimens.....	35
24	Oxidative Weight Gain for Coated and Uncoated Titanium Specimens at 500°C in Air.....	36
25	Mapping of Elements by X-ray Emission Spectroscopy.....	38
26	Thermal Shock Results.....	39
27	Peak Dynamic Stress* vs Tip Double Amplitude F100, PWA 1202, 6th-Stage HPC Blades P/N 4034806 Vibrated in the First Mode of Vibration.....	40
28	Peak Dynamic Stress* vs Tip Double Amplitude F100, PWA 1202, 6th-Stage HPC Blades P/N 4034806 Vibration in the Second Mode of Vibration.....	41
29	Peak Dynamic Stress* vs Tip Double Amplitude F100, PWA 1202, 6th-Stage HPC Blades P/N 4034806 Vibrated in the Third Mode of Vibration.....	42
30	F100, PW 1202, 6th-Stage Compressor Blade, P/N 4034806, Illustration Showing Strain Gage Locations Used for Calibrations in the First Bending Mode of Vibration.....	43
31	F100, PWA 1202, 6th-Stage Compressor Blade, P/N 4034806, Illustration Showing Strain Gage Locations Used for Calibrations in the Second Mode of Vibration.....	43
32	F100, PWA 1202, 6th-Stage Compressor Blade, P/N 4034806, Illustration Showing Strain Gage Locations Used for Calibrations in the Third Mode of Vibration.....	44
33	F100, PWA 1202, 6th-Stage HPC Blade, P/N 4034806, Showing Stress Coat Patterns for the First Bending Mode of Vibration (Frequency = 620 to 630 Hz) for the Coating Configurations Indicated.....	45
34	F100, PWA 1202, 6th-Stage HPC Blade, P/N 4034806, Showing Stress Coat Patterns for the Second Mode of Vibration (Frequency = 2500 to 2600 Hz) for the Coating Configurations Indicated.....	46
35	F100, PWA 1202, 6th-Stage HPC Blade, P/N 4034806, Showing Stress Coat Patterns for the Third Mode of Vibration (Frequency = 2890 to 3000 Hz) for the Coating Configuration Indicated.....	47
36	Peak (σ_{max}) Dynamic Stress Vs Cycles to Failure F100, PWA 1202, 6th-Stage HPC Blades P/N 4034806 from Engine FX-209 Vibrated in the First Bending Mode of Vibration.....	50

LIST OF ILLUSTRATIONS (Continued)

<i>Figure</i>		<i>Page</i>
37	Schematic Diagram of the Ion Plating Process.....	59
38	Schematic Diagram of the Sputtering Process.....	62
39	Specimen Configuration.....	64
40	Specimen Thickness Measurement Points.....	64
41	Cascade Combustion Specimen.....	65
42	Ignitor Combustion Specimen.....	65
43	High-Cycle Fatigue Specimen.....	66
44	High-Cycle Fatigue Specimen.....	66
45	High-Cycle Fatigue Specimen.....	67
46	High-Cycle Fatigue Specimen.....	67
47	Stress Rupture/Creep/Tensile Test Specimen.....	68

LIST OF TABLES

<i>Table</i>		<i>Page</i>
1	Combustion Test Results.....	1
2	Summary of Test Results.....	2
3	Screening Test Results for Burn Severity.....	19
4	Task II Combustion Results.....	24
5	Burn Severity Empirical Equations.....	25
6	Burn Severity — Typical Compressor Conditions.....	25
7	Creep Test Results.....	32
8	Creep Test Results.....	32
9	Erosion Rates of Coating.....	34
10	TGA Oxidation Data for Titanium Specimens.....	36
11	Frequency Check Data for F100, PWA 1202, 6th-Stage Compressor Blades, P/N 4034806, Airfoils Coated and Uncoated, Vibrated at Room Temperature.....	48
12	First Bending Mode Fatigue Test Data for F100, PWA 1202, 6th-Stage HPC Blades, P/N 4034806, Uncoated, Vibrated at Room Temperature...	49
13	First Bending Mode Fatigue Test Data for F100, PWA 1202, 6th-Stage Compressor Blades, P/N 4034806, Airfoils Coated With Pt/Cu/Ni, Vibrated at Room Temperature.....	49
14	First Bending Mode Fatigue Test Data for F100, PWA 1202, 6th-Stage Compressor Blades, P/N 4034806, Airfoils Coated With IVD Aluminum, Vibrated at Room Temperature.....	49
15	Stress Rupture/Creep/Tensile Test Specimen.....	68

SUMMARY

The use of combustion-resistant alloys and ignition-preventive coatings represent two approaches to reduce the probability of titanium ignition and/or combustion due to blade rubbing, rotor imbalance, aerodynamic heating, or other conditions encountered in gas turbine engine compressors. This program explored a limited number of coating options for titanium components with the objective of minimizing potential combustion initiation and propagation. A critical criterion for any combustion-preventive coating demands that the mechanical properties of the titanium alloy are not degraded below a minimum design level.

Establishing a combustion-preventive coating requires combustion screening tests followed by mechanical properties testing. The combustion screening tests utilized laser ignition to identify the most combustion-resistant coating systems from the fifteen initially selected. Testing at 370°C, 0.76 MPa, 245 m/sec (700°F, 110 psia, 800 ft/sec), conditions which are typical of gas turbine engine compressors, and then at the more severe conditions of 455°C, 0.76 MPa, 245 m/sec (850°F, 110 psia, 800 ft/sec) enabled the selection of seven coating systems for further evaluation.

These seven coating systems were then subjected to combustion tests at even more severe conditions (455°C, 0.965 MPa, 245 m/sec (850°F, 140 psia, 800 ft/sec)) and to high-cycle fatigue (HCF) screening tests at 425°C (800°F). Test results for all laser ignition combustion tests are outlined in table 1, while those for the HCF screening tests are shown in figure 1. Based on these results, IVD aluminum and Pt/Cu/Ni were chosen for further evaluation on both Ti 8Al-1Mo-1V and Ti 6Al-4V.

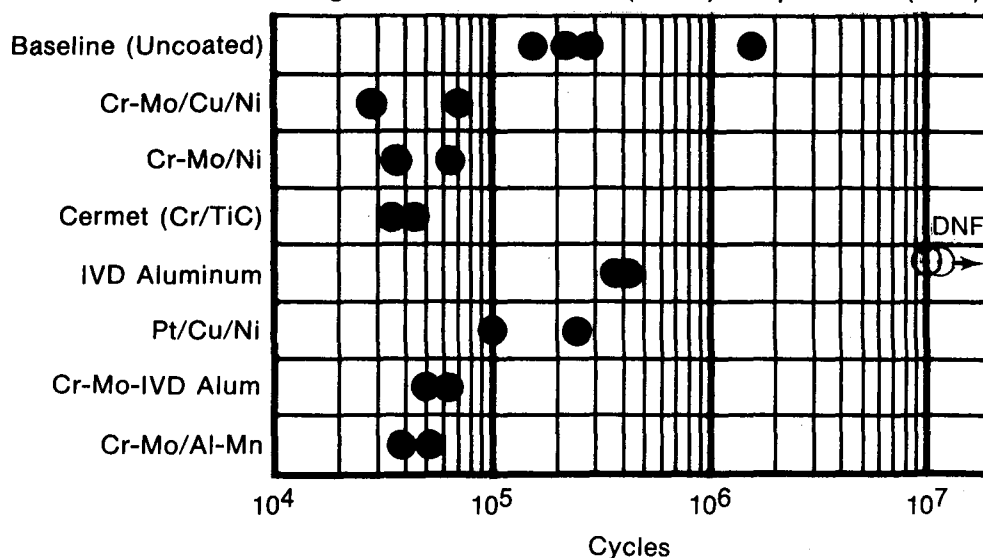
TABLE 1. COMBUSTION TEST RESULTS

Coating	Percent Burn (Airflow = 245 m/s)		
	Nominal Engine Conditions	Accelerated Test I	Accelerated Test II
	(370°C/0.76 MPa)	(455°C/0.76 MPa)	(455°C/0.97 MPa)
Cr - Mo + Cu + Ni	0	0	44.6*
Pt + Cu + Ni	0	0	47.0
IVD Al	0	<1	47.5
Cr - Mo + Ni	0	0	58.8
Cr - Mo + IVD Al	13	—	60.0
Cr - Mo + Al - Mn	0	0	64.7
Cr - TiC Cermet	0	<1	100.0
Cr - Mo (Sputtered)	0	18	—
Pt + Ni - P	—	25	—
Cr - Mo	0	37	—
Pt + IVD Al	0	38	—
Al - Mn	0	55	—
Pt + Al - Mn	56	—	—
Cr	67	—	—
Pt	100	—	—

*Test conditions for this coating were 482°C/0.76 MPa.

All four coating/substrate combinations were subjected to tensile, creep, and additional HCF testing. After these tests, both coatings over a substrate of Ti 8Al-1Mo-1V proved to be the best coating systems. These two coating systems were then subjected to further mechanical property tests. In addition, the two coating systems underwent cascade combustion testing in a concurrent Air Force contract (Contract No. F33615-79-C-2005). This cascade testing utilized molten metal ignition rather than laser ignition.

R = -1 Alternating Stress = ± 380 MPa (55 ksi) Temp = 27°C (80°F)



FD 201880

Figure 1. Reverse Bending Fatigue Results of Coated AMS 4916 (Ti 8-1-1)

Table 2 shows a summary of the test results of the two final coating systems. Although both coating systems exhibited more severe static oxidation than the uncoated substrate material, the amount of oxidation experienced would not prohibit the application of these coatings in a compressor environment. In most of the mechanical properties tests, the difference between the coatings was minimal. However, in the cascade combustion testing, the IVD aluminum performed significantly better than the Pt/Cu/Ni coating. The better performance in combustion testing and equal performance in mechanical property testing resulted in the selection of IVD aluminum as the best coating.

TABLE 2. SUMMARY OF TEST RESULTS

	Pt/Cu/Ni	IVD Al
Combustion	+	++
HCF	0	0
Tensile	0	0
Creep	0	0
HSSC	0	0
Stress Rupture	+	0
Erosion	+	+
Adhesion	Fair	Good
Static Ox.	-	-
Diffusion	0	0
Thermal Shock	0	0
Stress Analysis	0	0

where: 0 = No significant influence due to coating
 - = Coating had degrading effect on baseline
 + = Coating appeared to provide improvement over baseline

INTRODUCTION

Rapid developments in high performance aircraft gas turbine engines necessitate corresponding advances in material technology, including titanium alloys for fan and compressor components. These alloys contribute to gains in performance and efficiency because of their high strength and low density, resulting in favorable strength-to-weight ratios. Titanium alloys have gained wide acceptance in operating environments up to 480°C (900°F). Typical titanium components in current use include static structures, such as fan and compressor vanes and cases, and rotating components, such as fan and compressor disks and blades.

Titanium, like several other metals, can be made to ignite and react in a rapid oxidation (exothermic) process. In the specific case of titanium, a unique combination of thermophysical properties, including high heat of combustion, low thermal conductivity, and a spontaneous ignition temperature below its melting point, enhance this reactivity. This latter property favors ignition, rather than melting, thus producing additional rapid local temperature increases and rapid propagation of the resultant combustion, once ignition occurs. This combustion potential has limited the use of titanium.

Several instances of titanium blade and vane ignition and combustion have occurred in gas turbine compressors over a wide range of ambient pressure and temperatures. Initiating conditions may include blade tip rubbing on adjacent casing or blade/structure rubbing as a result of compressor stalls where blades deflect into the casing, rotor imbalance, entrapment of broken airfoil elements, and aircraft maneuvers. Aerodynamic heating of compressor components during a stall also contributes to ignition of titanium gas turbine components. Improved compressor seals help reduce the blade tip rubbing problem. However, the high-velocity airstream in axial-flow compressors enhances the continued combustion of any titanium blade or vane that does ignite, causing burning particles and molten metal to be sloughed off. These particles can be entrained in the airstream and impinge on downstream components, thereby spreading combustion. The results and extent of this spreading depend largely on the environmental conditions prevalent at the time of ignition, and can vary from burning the tips of a few compressor blades to the catastrophic destruction of an entire engine. This latter condition has been minimized by the substitution of Inconel stators for titanium stators past the 4th-stage of the compressor. Titanium blades are still used back to the 7th-stage of the compressor.

Program Overview

This program explored a limited number of coating options for titanium gas turbine engine components with the objective of minimizing potential combustion initiation and propagation without adversely affecting component mechanical properties.

Task I effort involved the application of 15 coating specimens to a substrate of Ti 8Al-1Mo-1V and subjecting the samples to an initial series of combustion tests with the objective of identifying the four best coating systems for an in-depth study. As a result of the initial screening combustion tests conducted at the environmental conditions of 370°C, 0.76 MPa, 245 m/sec (700°F, 110 psia, 800 ft/sec), only four coating systems experienced sustained combustion. The remaining coating systems then underwent testing at the more severe environmental conditions of 455°C, 0.965 MPa, 245 m/sec (850°F, 110 psia, 800 ft/sec). In the second round of screening tests, six coating systems experienced no combustion or limited combustion (<1%).

Based on the above combustion screening test results, the Task II technical effort was redirected by NASA so that further coating selection could be made. Additional combustion tests were conducted at environmental conditions of 455°C, 0.965 MPa, 245 m/sec (850°F, 140 psia, 800 ft/sec) and high-cycle fatigue (HFC) tests at a temperature of 425°C (800°F). To

compensate, planned Task III rub tests were eliminated. These rub tests were judged to be meaningless in light of rub test results achieved under the Air Force Wright Aeronautical Laboratories/Materials Laboratory (AFWAL/ML) Blade Tip Coating Program (Contract No. F33615-78-C-5159).

The additional combustion tests and HCF tests resulted in the selection of ion vapor deposited (IVD) aluminum and Pt/Cu/Ni as the two best coating systems. Due to the widespread application of Ti 6Al-4V in the compressor section of gas turbine engines, it was added as a second substrate material. The four best coating systems resulted from all combinations of the components listed below:

1. Coating — IVD aluminum and Pt/Cu/Ni
2. Substrate — Ti 8Al-1Mo-1V and Ti 6Al-4V
3. Thickness — 0.0025 cm (0.001 in.).

Task III mechanical properties test plans were modified by testing additional coating combinations (adding Pt/IVD aluminum) and eliminating room temperature tests. The number of coating thicknesses was increased from one to two for tensile testing by eliminating the room temperature phase of this testing.

From the four best coating systems, IVD aluminum and Pt/Cu/Ni applied to a substrate of Ti 8-1-1 were selected as the two best coating systems based on the titanium component hierarchy and the test results from HCF testing, tensile testing, and creep testing. A review of the titanium component hierarchy resulted in the selection of a Ti 8-1-1 substrate since it was the predominant candidate for current and potential coating applications. A coating thickness of 0.005 cm (0.002 in.) was selected since it represented one of the thicknesses used in a parallel Air Force Wright Aeronautical Laboratories/Propulsion Laboratory (AFWAL/PL) titanium combustion contract (F33615-79-C-2005). Thus, the two best coating systems selected for Task III evaluations were; 0.005 cm (0.002 in.) IVD aluminum on Ti 8Al-1Mo-1V and 0.005 cm (0.002 in.) Pt/Cu/Ni on Ti 8Al-1Mo-1V.

NASA modified Task III by replacing 50 Task III combustion tests with an equivalent amount of work consisting of high-cycle fatigue and diffusion tests. A concurrent AFWAL/PL titanium fire program conducted combustion tests on the Task III coating systems. The data for the 50 combustion tests are included in this report as Appendix A. The equivalent work testing included the application of the two coatings on an AFWAL/PL-selected alloy of Ti 3Al-8V-6Cr-0.4Mo-4Zr for HCF testing. In addition, diffusion tests were run on the four best coatings mentioned above to determine the effect that an exposure to 425°C (800°F) for 168 hr produced on the coating/alloy interface.

The two coating systems on Ti 8-1-1 were then subjected to the following Task III property characterization tests:

1. Hot salt stress corrosion
2. Erosion
3. Stress rupture
4. Stress analysis
5. Adhesion
6. Static oxidation
7. Thermal shock.

Results from the above tests and the 50 combustion tests in the AFWAL/PL titanium fire program then formed the basis of the selection of the best coating system.

EXPERIMENTAL APPROACH

Materials

Alloy Selection

Ti 8Al-1Mo-1V and Ti 6Al-4V

These are probably the two most widely used titanium alloys. The first, Ti 8Al-1Mo-1V, finds use as compressor blade material in the TF30, F100, JT9D, and JT8D engines; fan exit guide vane material in the F100; and material for construction of seals, cases, supports, and disks in several gas turbine engines. The second alloy, Ti 6Al-4V, finds use as both blade and vane material for the JT9D, TF30, and JT8D engines; F100 engine fan and compressor ducts; and disk material in the JT8D engine.

Ti 3Al-8V-6Cr-0.4Mo-4Zr

This alloy was selected at the suggestion of AFWAL/PL due to the reportedly low combustibility of the alloy.

Coatings

The 15 coating systems chosen for initial evaluation included the following:

Single Coatings

- Chromium (electroplate and diffuse)
- Chromium-molybdenum (electroplate and diffuse)
- Chromium-molybdenum (sputtered)
- Aluminum (ion vapor deposited)
- Aluminum-manganese (electroplate)
- Platinum (ion-plated)
- Cermet plate of chromium with TiB, ZrB, ZrC, or TiC.

Duplex Coatings

- Chromium-molybdenum (electroplate and diffuse) plus aluminum (ion vapor deposited)
- Chromium-molybdenum (electroplate and diffuse) plus aluminum-manganese (electroplate)
- Chromium-molybdenum (electroplate and diffuse) plus copper (electroplate) plus nickel (electroplate)
- Chromium-molybdenum (electroplate and diffuse) plus nickel (electroplate)
- Platinum (ion-plated) plus aluminum (ion vapor deposited)
- Platinum (ion-plated) plus aluminum-manganese (electroplate)
- Platinum (ion-plated) plus copper (electroplate) plus nickel (electroplate)
- Platinum (ion-plated) plus nickel-phosphorus (electroless).

Electrodeposition

Appendix B details the electrodeposition procedures used to apply coatings studied in this program. Unless otherwise specified, conventional plating procedures and processes were used.

Chromium

Electroplated chromium was selected since it represents a simplified cost-effective variation of the chromium-molybdenum coating which has demonstrated some fire resistance. It was applied as a single coating by a conventional chromium electrodeposition process.

Chromium Cermet

A chromium cermet coating was developed in this program and included in the preliminary combustion screening tests. The chromium cermet coating consisted of an electroplated chromium with occluded titanium carbide.

Chromium-Molybdenum

Chromium-molybdenum was selected for evaluation as an electroplated coating due to the degree of fire control demonstrated in previous tests. In addition, this coating was believed to not adversely affect titanium mechanical properties.

Nickel-Phosphorus

Due to difficulties encountered in obtaining satisfactory adhesion of electroplated nickel to ion-plated platinum, electroless nickel-phosphorus was substituted. This self-sustaining process, also called autocatalytic plating, uses a hypophosphite-based plating bath and yields a coating containing up to 15% phosphorus.

Nickel

Electroplated nickel over chromium-molybdenum was selected to provide data on the mechanism of how coatings affect the combustion characteristics of titanium. Also, a thin nickel coating was applied over copper to provide oxidation resistance from the normal gas turbine compressor environment. The coating was applied utilizing a conventional high-speed, nickel-sulfamate plating bath.

Copper

Copper electrodeposits applied to either electrodeposited chromium-molybdenum or ion-plated platinum were evaluated in this program based on its established fire protection capability. This coating was applied from a conventional Rochelle copper-cyanide plating bath.

Aluminum-Manganese

Aluminum-manganese coating applied by electrodeposition directly on the titanium alloy or as an overcoat to electrodeposited chromium-molybdenum was evaluated in this program.

Sputter Coatings: Chromium-Molybdenum

Sputtered chromium-molybdenum was selected as a variation of the electroplated chromium-molybdenum that had demonstrated a degree of fire control in previous tests. Also, without a requirement for diffusion heat treatment, this coating should not adversely affect titanium mechanical properties.

Ion-Plating and Ion Vapor Deposition

Ion-plating and ion vapor deposition are synonymous terms defining essentially the same method of coating application. Two materials were selected for use with this process:

Platinum

Platinum, applied by ion-plating, was selected primarily for its favorable effects on titanium mechanical properties and, although it did not provide a significant degree of fire protection, it found application as a base or barrier coat for other coatings.

Aluminum

Aluminum, applied by ion vapor deposition (IVD) directly onto the titanium, as an overcoat to chromium-molybdenum, and as an overcoat to ion-plated platinum, was evaluated during this program. IVD aluminum can be used alone as a coating without mechanical property degradation because the application temperature of the aluminum is low enough to prevent any intermetallic formation. The combination coatings were used to provide fire resistance and minimize the effects on mechanical properties.

Test Apparatus and Procedures

Combustion Tests

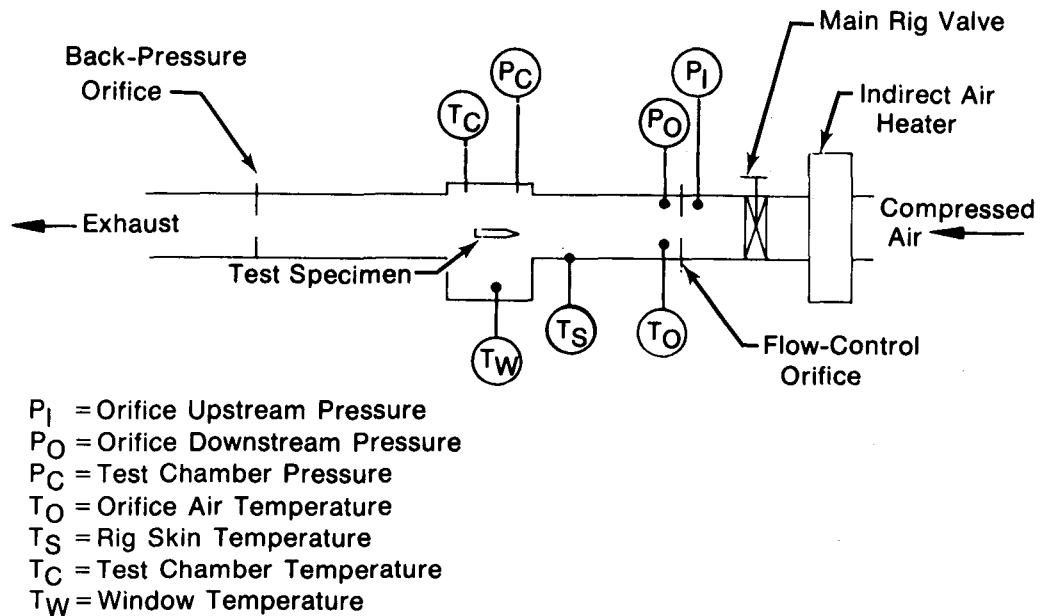
Combustion Rig — Laser Ignition

The Pratt & Whitney Aircraft Group (P&WA) titanium combustion test rig consists of a small wind tunnel driven from a 2.4 MPa (350 psi) compressed air supply. Ancillary conditioning equipment permits the simulation of a wide range of environmental combinations of air pressure (up to 15 atmospheres), temperature (up to 550°C), and velocity (up to 350 m/sec). Small test specimens are mounted in a rectangular test chamber. Installed instrumentation provides a vehicle to determine pressure and temperature at strategic locations in and around the rig.

Air, supplied from a large compressor, passes through a gas-fired indirect heater and a flow-measuring orifice prior to entering the test section. The test section, shown schematically in figure 2, consists of a 2 by 5 cm (0.75 by 2.0 in.) rectangular channel with a bellmouth and 7.5 cm (3.0 in.) of straight section upstream of the test specimen leading edge. The test specimen mounts in a carrier which is inserted into the test section. Orifice plates, upstream and downstream of the test section, provide control of flowrate and pressure level. Thermocouples provide temperatures at the flow-measuring orifice, in the specimen test chamber, on the rig skin, and on the laser and camera windows. Airstream flow is determined by calculation using the ΔP across the orifice.

The test section contains two windows: one for laser irradiation of the specimen and one for photographic viewing of the test specimen. These windows mount in a port on the side of the rig approximately 20 cm (8 in.) from the test specimen. The window for the camera is optically flat fused quartz which is 6.4 cm (2.5 in.) in diameter by 1.3 cm (0.5 in.) thick. The laser beam window is zinc selenide 3.8 cm (1.5 in.) in diameter by 6.4 cm (0.25 in.) thick.

This zinc selenide offers excellent transmissivity for the 10.6 μ wavelength emission of the CO₂ laser beam. This window has an antireflective coating on both faces to minimize reflection and beam scatter. The quartz window exhibits excellent optical clarity for visible light, but will not transmit the CO₂ laser light, thus protecting the camera lens from scattered reflections of the laser beam. A water jacket to absorb conducted heat in the metal housing, and an air injection system to film-cool optical surfaces protect the windows from the high-temperature test environment.



FD 139565

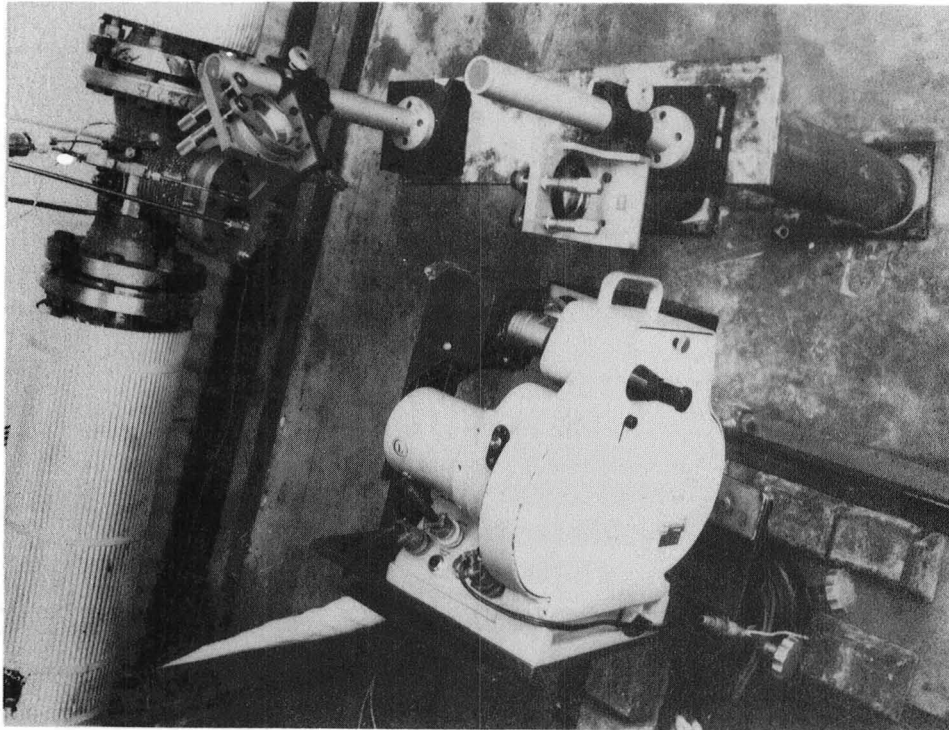
Figure 2. Titanium Combustion Test Rig — Laser Ignition

The arrangement of the test section and other supporting test equipment appear in figures 3 and 4. Because of environmental restrictions, the laser equipment is located in the air-conditioned control room and the beam passed through a port in the concrete blast wall. A high-speed Hycam motion picture camera and a video camera with a tape recording/playback system permit, through the use of a beamsplitter, simultaneous photographic recording and real-time video observation.

A CRL Model 41 laser provides the energy required for specimen ignition. This electric-discharge, water-cooled CO_2 laser system is capable of providing an output of 250 watts in the TEM 00 mode at a transmission frequency of 10.6μ . The beam defocuses at the specimen to diameter of approximately 0.3 cm (0.12 in.) to yield an incident average power density of approximately 1.25 kw/cm^2 absorbed by the specimen. A coincident helium-neon laser provides a visible red beam for alignment of the hot CO_2 laser beam on the titanium test specimen. The videotape system enables observation of this red alignment beam. Specimen configuration is detailed in Appendix C.

Combustion Rig — Cascade Ignition

A concurrent Air Force contract (F33615-79-C-2005), Titanium Coatings Ignition Test, accomplished the Task III combustion testing. Modification of the combustion rig permitted molten metal ignition (cascade), as shown in figure 5. Enlargement of the specimen holder to a capacity where two specimens could be held is shown in figure 6. The upstream specimen, composed of anodized Ti 8Al-1Mo-1V, ignites by use of the laser (as described earlier), thereby subjecting the downstream specimen to molten metal impingement. The configurations of the two specimens are shown in Appendix C.



FC 44036

Figure 3. Titanium Combustion Test Rig Setup

Film Analyzer

A Model 76 Data Analyzer, as shown in figure 7, enabled review and analysis of the high-speed film. This system combines a film motion analyzer with sonic digitizer, teletype, and minicomputer, including interface and software for computing line length, inside or outside angles, and area. The special test equipment achieves an improvement in the quality of combustion data extracted from the run films when compared to previously employed techniques. Additionally, its capability to provide rapid, direct readout and printout of distance, angles, and area measurements significantly decreased the time required to extract this data from the resulting large quantity of test run film.

The Model 76 Film Data Analyzer, from Instrument Marketing Corporation, Burbank, CA, consists of the following hardware:

1. NAC Film Motion Analyzer Model 160B, 350B, or 700B
2. Graphic pen sonic digitizer Model GP-3, electronically interfaced to the computer and mechanically interfaced to the film analyzer
3. Data General NOVA3 computer system, including teletype.

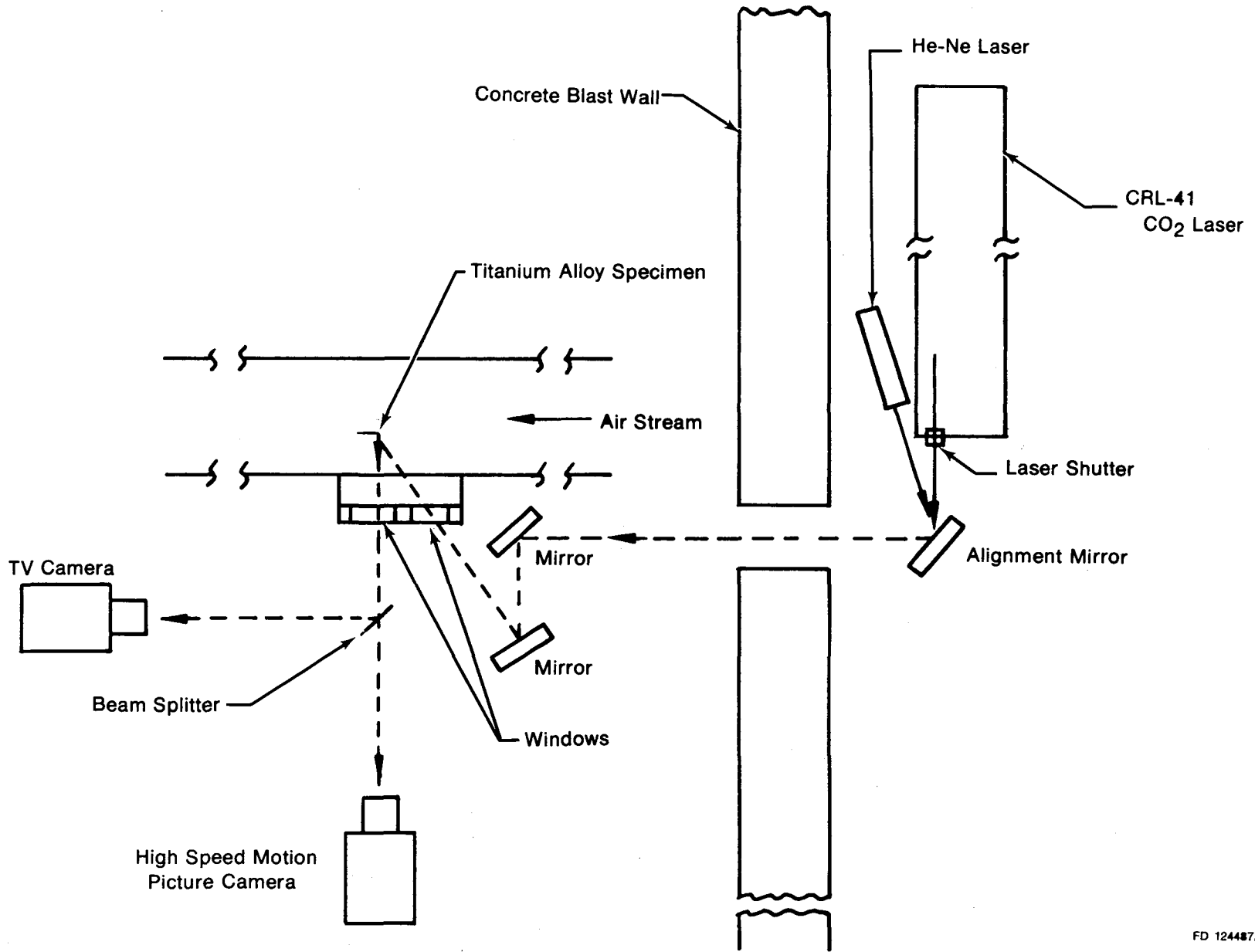
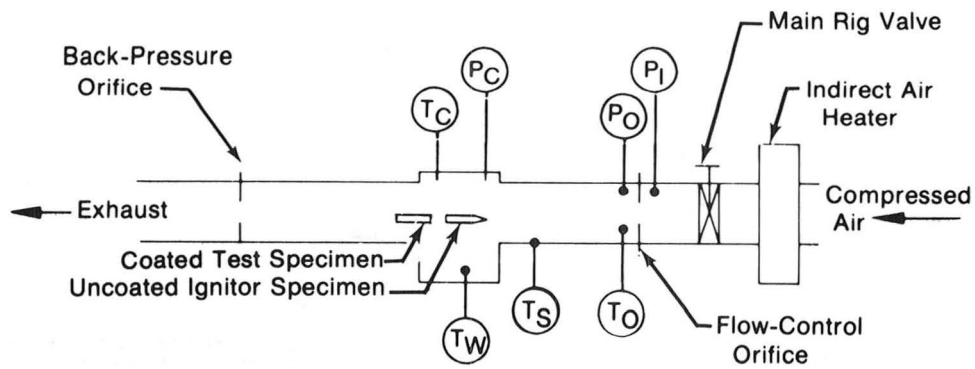


Figure 4. Arrangement of Laser Ignition and Photographic Recording Systems



- P_1 = Orifice Upstream Pressure
- P_0 = Orifice Downstream Pressure
- P_C = Test Chamber Pressure
- T_0 = Orifice Air Temperature
- T_S = Rig Skin Temperature
- T_C = Test Chamber Temperature
- T_W = Window Temperature

FD 139565A

Figure 5. Titanium Combustion Rig — Cascade Ignition

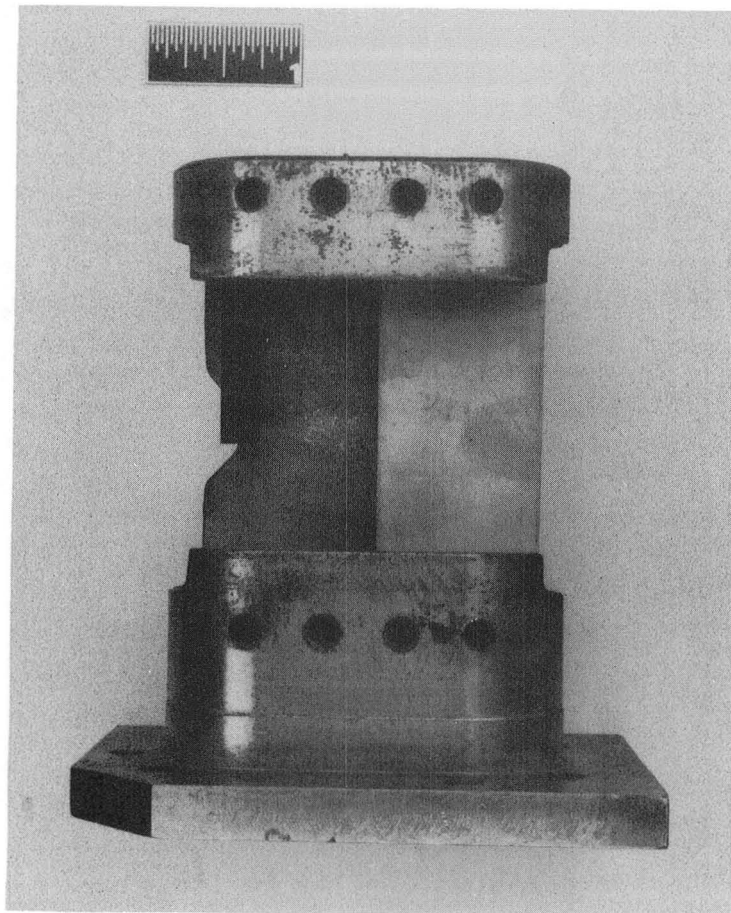


Figure 6. Combustion Rig Specimen Holder

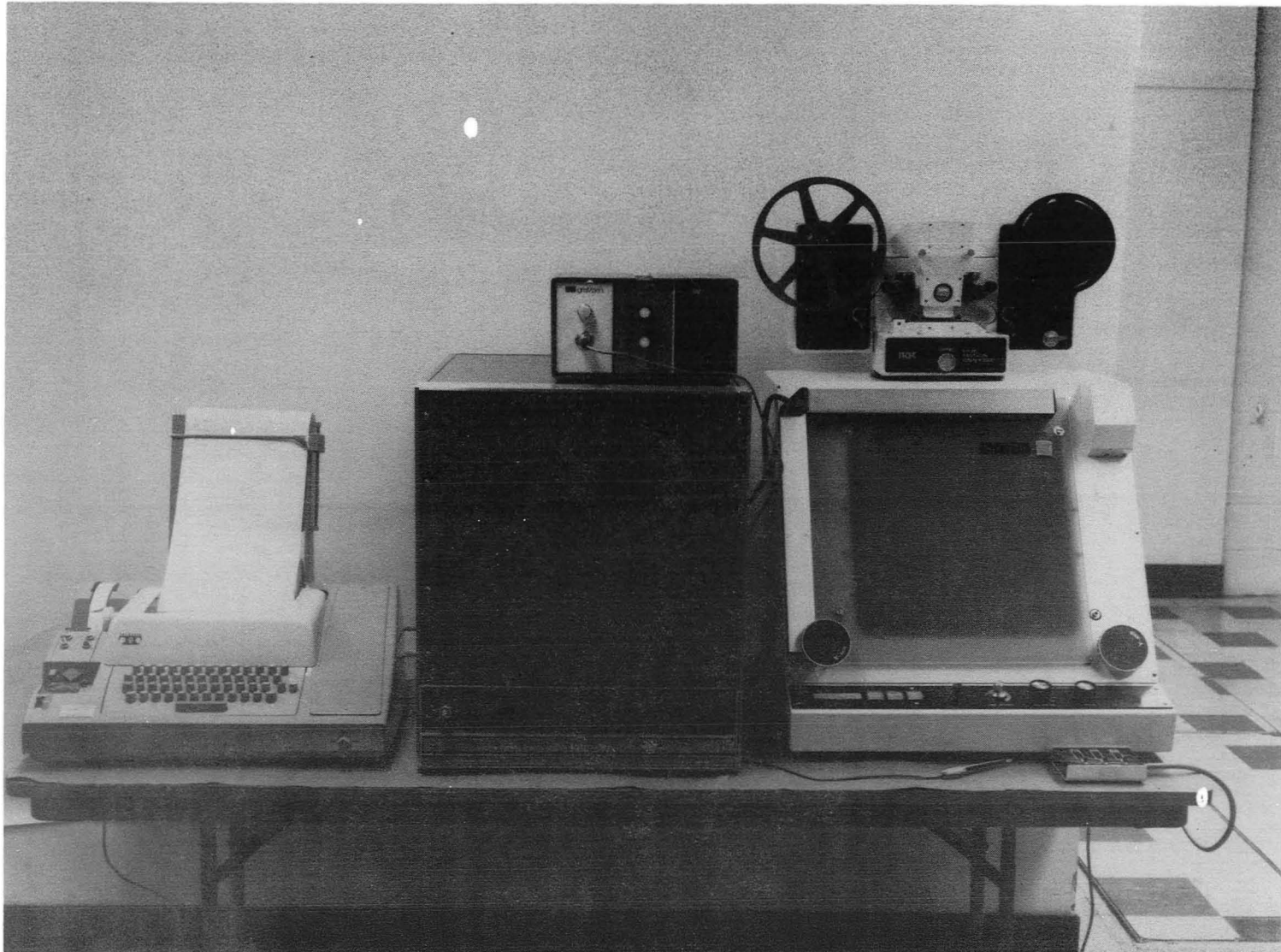


Figure 7. Model 76 NAC Film Motion Analyzer

Combustion Test Procedure

Prior to the combustion test run, test specimens are placed in the specimen holder which is then mounted in the test chamber. Installing a specific combination of flow-measuring and back-pressure orifices in the test rig establishes individual run values of air velocity and chamber pressure. After setting the heater to the desired temperature, airflow is introduced into the system and the test chamber allowed to reach thermal equilibrium. Once thermal equilibrium has been reached, the laser optics are aligned using the visible helium-neon laser beam and the videotape system. A high-intensity light transmitted from its source by fiber optics provides specimen illumination during alignment. For high-speed photographic coverage, the camera is focused on the specimen at all times during the test run. Sufficiently intense light from the specimen ignition and burning permits photodocumentation of burn propagation and movement of the melted material. An event marker (light pulse) recorded on the side of the film on all runs annotates the start and finish of the laser action during the run. Light pulses from a 1 kHz timing generator also mark the high-speed films to provide an absolute time reference for event sequences.

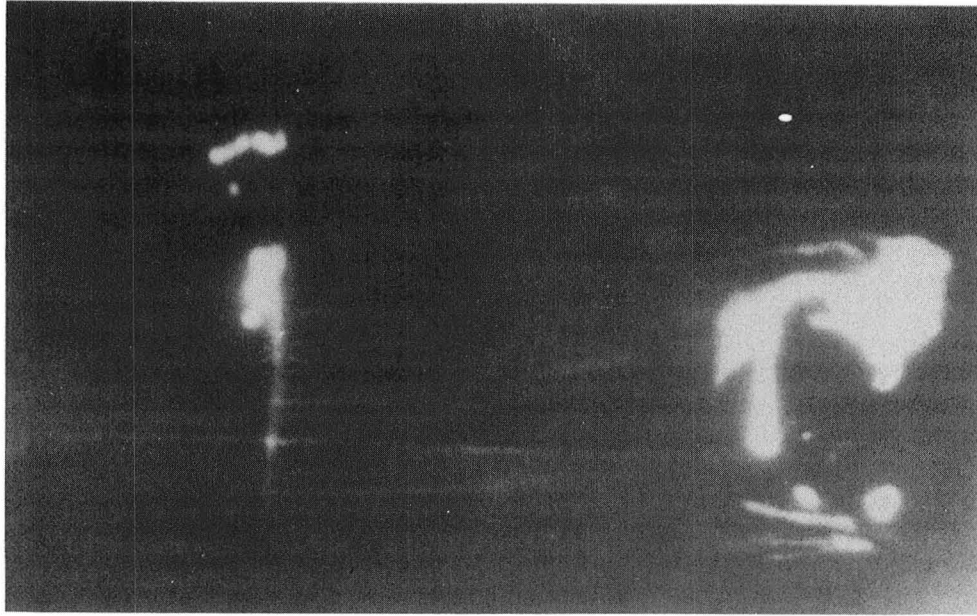
Just prior to the start of a particular run, the following sequence occurs: (1) final temperature and pressure adjustments are made by judicious throttling of the hot air valve and a cold air bleed input valve, (2) final adjustment is made, as necessary, to laser alignment, and (3) final run parameters are then recorded. A time-sequenced switch initiates the test by starting the high-speed camera. Approximately 2 sec after camera start, the sequencer opens the laser shutter to irradiate the specimen, thereby starting the run. The laser remains on for 5 sec before the sequencer closes the shutter. This time can be overridden manually when ignition occurs before the 5 sec have elapsed. The camera runs until it is out of film (about 16 sec) and is sequenced off at approximately 20 sec. The video system remains on at all times in the CCTV mode. Videotape recording is controlled manually during a run sequence. The instant replay and slow-motion/stop-action capability of the color video recording permits immediate review of the test run for its potential impact on the next test run.

A majority of test data came from the high-speed film coverage of each test run in the form of:

1. Ignition time
2. Burn through time
3. Chordwise burn velocity.

To determine specimen ignition time, the number of photographic frames between igniter ignition and specimen ignition was divided by the number of frames per sec. Ignitor ignition was considered to be the first visible yellowing of the red (helium-neon) laser indicating heating by the CO₂ laser beam. Specimen ignition was established as the first visible indication that the leading edge of the specimen was being consumed through sustained combustion, as shown in figure 8. Location of the leading edge was most readily identified from a frame containing sparks or flares of sufficient intensity to permit specimen definition.

Chordwise burn velocity was calculated by dividing the initial specimen width by the burn through time. Burn through time represents the number of frames between specimen ignition and burn through divided by the number of frames per sec for the particular test run and roll of film. A printed grid on transparent acetate film was overlaid on the Data Analyzer screen. The grid was used with X and Y cursors to define specimen boundaries. Burn through time was recorded when the burn traveled across the width of the specimen, as shown in figure 9.



FD 204298

Figure 8. Determination of Specimen Ignition

Data for the determination of burn severity (area burned %) was obtained by reconstructing and photographing the burned specimen. Specimen length, width, area, and burn area were measured directly from the photograph using the Model 76 Data Analyzer. Because of the heat-sink effect at the ends of the specimen holder, only the middle 5.3 cm (2.1 in.) exposed portion of the specimen was considered in this determination.

High-Cycle Fatigue Tests

High-cycle fatigue testing was accomplished utilizing a standard electromagnetic high-cycle fatigue test rig. Specimen configuration is shown in Appendix C. The initial phase of high-cycle fatigue testing involved the generation of a stress vs cycles to failure curve for the baseline uncoated alloy at test temperature by interactively selected stress levels to determine the 10^7 cycle fatigue strength. Six specimens were used for each curve. Further testing consisted of evaluation of four samples representative of each coating system for comparison with the baseline curve at the determined stress level. Specimens were electromagnetically vibrated to failure in the first bending mode at resonance between constant deflection limits. Deadweight load vs deflection calibration of each specimen at test temperature established test deflection limits. Loads to obtain stress levels were calculated based on Mc/I .

Tensile Tests

The apparatus used for tensile testing was a Tinius Olsen 267 kN (60,000 lb) capacity hydraulic tensile machine with a Class B-1 extensometer and a strain-rate pacer. Specimens were fabricated as shown in Appendix C. The tensile test procedure was performed in accordance with ASTM Standard E-8-69 with the following parameters measured:

1. 0.2% yield strength
2. Ultimate strength
3. Elongation.



FD 204299

Figure 9. Establishment of Burn Through

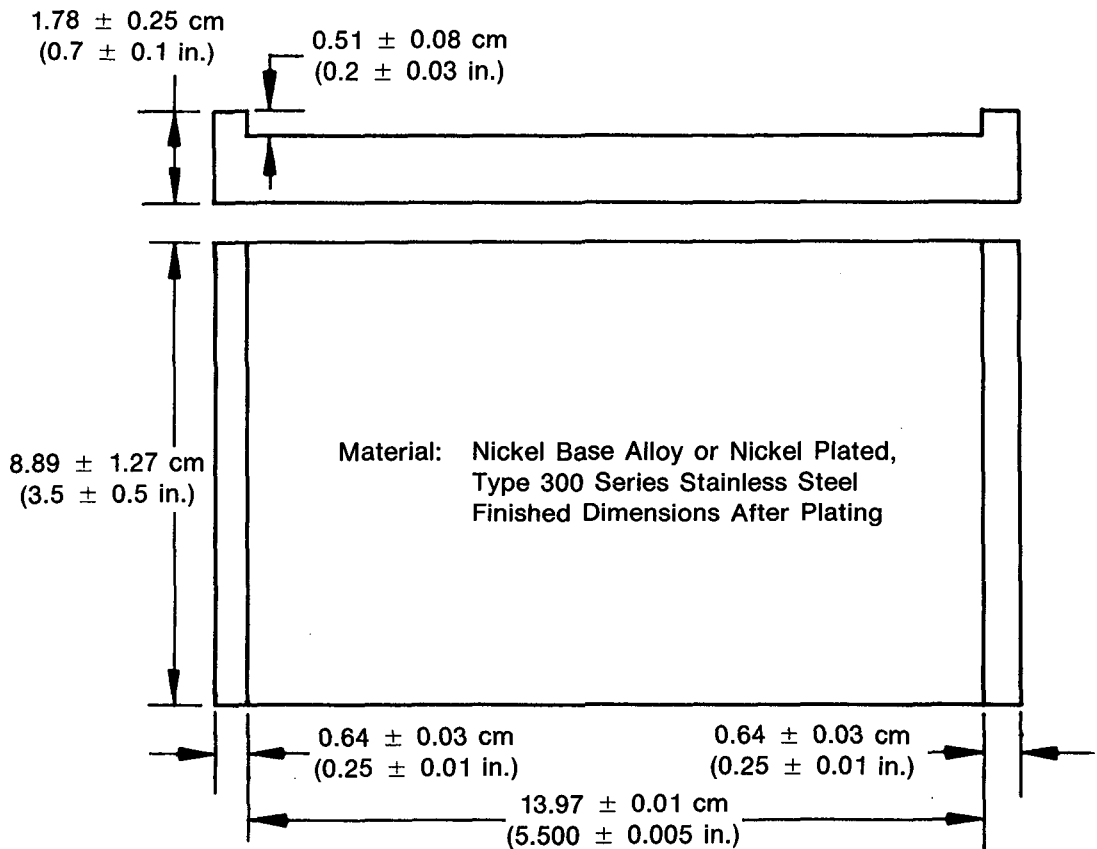
Creep and Stress-Rupture Tests

The creep and stress rupture tests were conducted on a Satec dual range 53.4 kN (12,000 lb) creep rupture machine dead-weight loaded through a lever arm with an automatic beam leveling device. The configuration of the test specimens is illustrated in Appendix C. The creep-rupture test procedure was performed in accordance with ASTM Standard E-139-66T. Stress-rupture test was conducted in accordance with ASTM Standard E-139-70. Three thermocouples, each making intimate contact with the specimen gage section, monitored and provided control of test temperature.

Hot Salt Stress Corrosion Tests

The following apparatus were used for hot salt stress corrosion testing:

1. Specimen holder, as shown in figure 10.
2. Oven — circulating air capable of heating the specimens and maintaining $480^{\circ} \pm 5^{\circ}\text{C}$ ($900^{\circ} \pm 10^{\circ}\text{F}$) for 100 hr
3. Microscope — capable of 10X magnification
4. Sodium chloride solution — an aqueous solution of 3g NaCl dissolved into 100 ml of distilled or demineralized water.



FD 132419A

Figure 10. Hot Salt Stress Corrosion Specimen Holder

Specifications for test specimens are detailed in Appendix C.

The following procedure was utilized for hot salt stress corrosion testing:

1. Clean the specimens with acetone. Handling the specimens with lint-free gloves prevented contamination.
2. Bend the specimens into the specimen holder, allowing some space between specimens.
3. Apply a 3% solution chloride aqueous solution to the uncoated control specimen and a specimen of each coating system (i.e., IVD Al and Pt/Cu/Ni).
4. Dry the specimens at approximately $88^{\circ} \pm 5^{\circ}\text{C}$ ($190^{\circ} \pm 10^{\circ}\text{F}$). A solid white residue should remain on the treated specimens.
5. Place the specimen holder in an air-circulating oven at $480^{\circ} \pm 5^{\circ}\text{C}$ ($900^{\circ} \pm 10^{\circ}\text{F}$) for 100 hr.
6. After 100-hr exposure, examine the specimens for breaks and obvious cracks while the specimens are still in the holder.

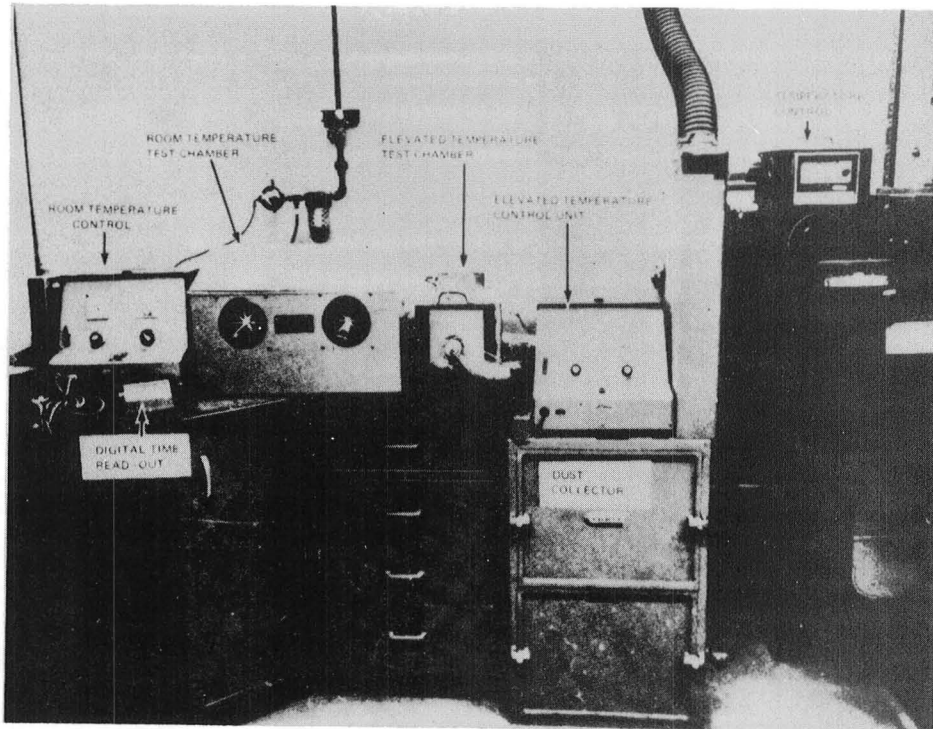
After the 100-hr exposure, when the control specimen showed no breaks or cracks, the specimen was removed from the holder and vapor blasted. The specimen was then immersed in a freshly prepared solution of 5 parts nitric acid, 1 part hydrofluoric acid, and 1 part sulfuric acid at approximately $60^{\circ} \pm 5^{\circ}\text{C}$ ($140^{\circ} \pm 10^{\circ}\text{F}$) until red fumes were liberated. The time of immersion until red fumes are generated is not to exceed 30 sec. The control specimen was rinsed immediately in running water and dried. Upon examination, cracks had formed in the treated control specimen.

Erosion Tests

An S. S. White Industrial Airabrasive Unit, Model F, as shown in figure 11, formed the nucleus of the erosion test rig. The equipment causes a small mass of abrasive particles to be impinged on the test specimen and then collects them on a dust filter. To conduct a test using this equipment, abrasive powder, placed in a pressurized hopper connected to a vibrating unit, falls into an airstream that carries the abrasive particles through a nozzle to the specimen. Powder flowrate is controlled by changing the amplitude of vibration. The design of the specimen holder permits the particle impingement angle to be varied. The axis of specimen rotation lies on the specimen surface facing the nozzle, thus maintaining a constant distance for particle-free travel beyond the nozzle as the impingement angle is varied. Specimen dimensions are given in Appendix C.

Aluminum oxide was used as the erosive agent and was procured from the S. S. White Co. in two controlled particle sizes designated as No. 1 (27μ) and No. 3 (50μ).

Erosion testing was conducted under room temperature conditions. The S. S. White Airabrasive Unit injected SC240 grit abrasive grains into a nitrogen carrier gas stream impelled at the coated specimens at angles of 30, 60, and 90 deg with a gun-to-work distance of 2.5 cm (1.0 in.). Since coating thicknesses were assumed to be equal, relative erosion rates were determined by the time required to break through the coating. At least five erosion tests were performed on each coating system at each of the above angles. Times were averaged and normalized to establish the relative erosion resistance of each coating system.



FD 132430

Figure 11. Erosion Test Station

Adhesion Tests

The equipment involved in adhesion testing was a Bend Tester with a 0.38 cm (0.15 in.) mandrel. Specimen dimensions are given in Appendix C. Adhesion testing required the specimen be bent approximately 105 deg over the mandrel. The appearance of the coating and underlying substrate after bending was observed and recorded.

Static Oxidation Tests

The apparatus used for static oxidation testing was a Cahn thermobalance. Specimen dimensions are given in Appendix C. The static oxidation specimen was placed in a Cahn thermobalance at a temperature of 500°C (935°F) for 50 hr. A recorder plotted specimen weight vs time.

Diffusion Tests

Diffusion testing was conducted in an air-circulating oven capable of maintaining a temperature of 425°C (800°F). Specimen dimensions are given in Appendix C. Diffusion test specimens were placed in an oven at a temperature of 425°C (800°F) for 168 hr. After this exposure, specimens were cross sectioned, mounted, and inspected metallographically.

Thermal Shock Tests

The thermal shock test apparatus consisted of a C-type oven capable of maintaining temperatures to 550°C (1025°F). Specimen dimensions are given in Appendix C. Thermal shock specimens were placed in a C-type oven and maintained at a temperature of 425°C (800°F) for 4 hr to ensure the specimens had reached thermal equilibrium. After 4 hr, the

specimens were subjected immediately to a room temperature water quench. Specimens were then dried, examined for detrimental effects, and photographed. This cycle was repeated three times.

Stress Analysis

The test equipment used to determine stress analysis characteristics was a Ling Series E-390 Electrodynamic Shaker on an F100 6th-stage broached fixture. Specimens are described in Appendix C. The three sets of blades (8 uncoated, 8 coated with Pt/Cu/Ni, and 8 coated with aluminum) used for testing were frequency checked in the first three modes of vibration. The location and orientation of calibration strain gages for the first three modes of vibration were established from stresscoat patterns for each coating configuration in the corresponding mode of interest. Calibration curves of peak dynamic stress vs tip double-amplitude were obtained for the first three modes of vibration for all coatings tested.

Each blade underwent fatigue testing to failure (or 10^7 cycles) at room temperature in the first bending mode of vibration. S-N curves for coated and uncoated blades were then generated.

TEST RESULTS AND DISCUSSION

Combustion Tests

Screening Tests (Laser Ignition)

Combustion screening tests utilized laser ignition to identify the four most combustion-resistant coating systems from the 15 that were tested. These systems, along with screening test conditions and results, appear in table 3.

TABLE 3. SCREENING TEST RESULTS FOR BURN SEVERITY

Coating Tested	Burn Severity	Burn Severity
	370°C-0.76 MPa-245 m/sec (700°F - 110 psia - 800 ft/sec) (%)	455°C-0.76 MPa-245 m/sec (850°F - 110 psia - 800 ft/sec) (%)
Cr	67	
Cr-Mo	0	37
Cr-Mo (Sputtered)	0	18
IVD Al	0	<1
Al-Mn	0	55
Pt	100	
Cr-TiC Cermet	0	<1
Cr-Mo + IVD Al	13	
Cr-Mo + Al-Mn	0	0
Cr-Mo + Cu + Ni	0	0
Cr-Mo + Ni	0	0
Pt + IVD Al	0	38
Pt + Al-Mn	56	
Pt + Cu + Ni	0	0
Pt + Ni-P	No Test	25

Figure 12 shows the appearance of the specimens after tests at the indicated temperatures. It is evident from table 3 that, at the higher temperature, six coatings either did not burn or experienced very limited combustion (less than 1%). This testing enabled the selection of seven coating systems for high-cycle fatigue and combustion testing at more severe conditions. These coating systems and test conditions, along with the corresponding burn severity results, are detailed in table 4. The Cr-Mo/Cu/Ni coating system exhibited the lowest burn severity, i.e., the best protection against sustained combustion.

Cascade Combustion (Molten Metal Ignition)

The combustion environmental test conditions encompassed the following parameters:

Pressure	0.275-0.550 MPa	(40-80 psia)
Temperature	315-440°C	(600-825°F)
Air Velocity	183-305 m/sec	(600-1000 ft/sec)

While temperature and pressure can be precisely regulated, air velocity depends on the size of the downstream orifice installed in the combustion rig. Due to a limited number of orifice sizes available, variations from the nominal air velocity occurred, depending on temperature and pressure values.

Appendix A to this report contains the results from this testing. The combustion data of the concurrent AFWAL contract was subjected to statistical analysis. Parameters of coating thickness, temperature, pressure, and air velocity determined the significance of each coating type as it impacted chordwise burn velocity (combustion rate) and burn severity.

Chordwise Burn Velocity

Upon analysis, the type of coating did not significantly influence chordwise burn velocity. Pressure and air velocity seem to be the parameters which exhibited the greatest effect. The following empirical equation shows this relationship:

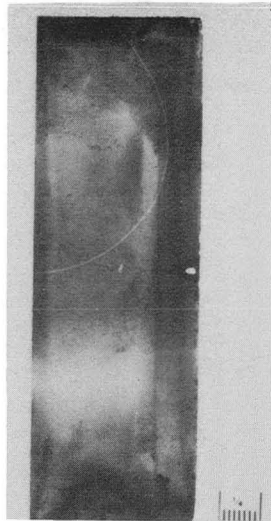
$$CBV = -3.53 - 55.11C + 0.02683P + 0.00025T + 0.00574V - 0.0000026V^2$$

subject to, Correlation Coefficient (R^2) = 0.914
Standard Estimate of Error (SEE) = 0.158

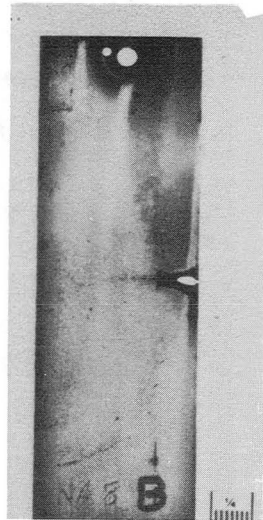
where,

CBV	=	chordwise burn velocity, in./sec
C	=	coating thickness, in.
P	=	pressure, psia
T	=	airstream temperature, °F
V	=	airstream velocity, ft/sec

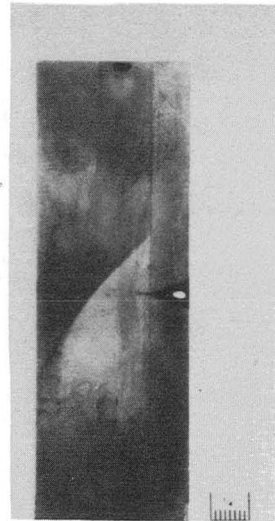
In this relationship, as pressure and/or airstream velocity increase, chordwise burn velocity increases. A straightforward explanation exists for this relationship. As pressure increases, the amount of oxidizer available for reaction increases, which in turn increases the reaction rate (chordwise burn velocity). The effect of airstream velocity is in the same direction as the pressure parameter, but to a lesser extent. Airstream velocity affects the rate at which the molten substrate material "wets" the specimen surface, i.e., moves across the specimen surface. An increase in the rate of molten metal propagation results in an increase in the rate of heat transfer, which in turn results in an increase in combustion rate and, thus, chordwise burn velocity.



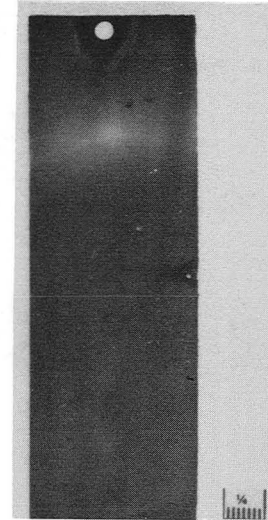
370°C FE 345223



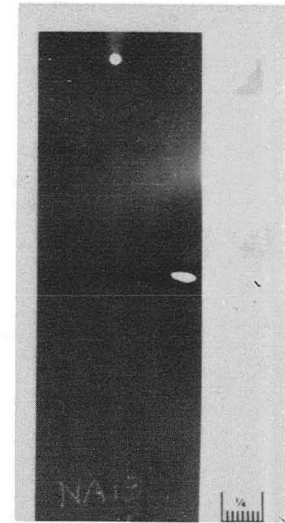
370°C FE 345048



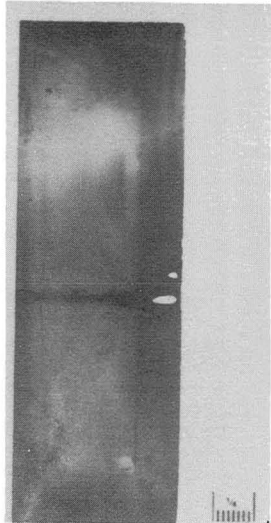
370°C FE 345051



370°C FE 345221

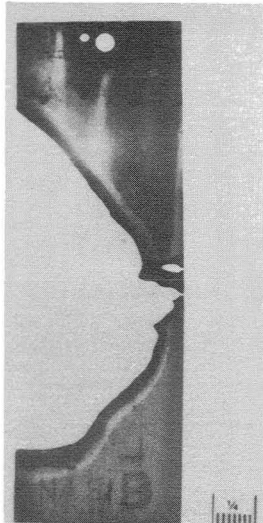


370°C FE 345050



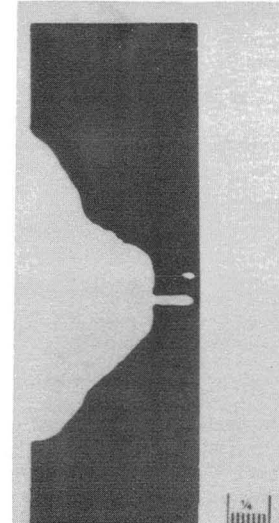
455°C FE 345243

Cr + TiC



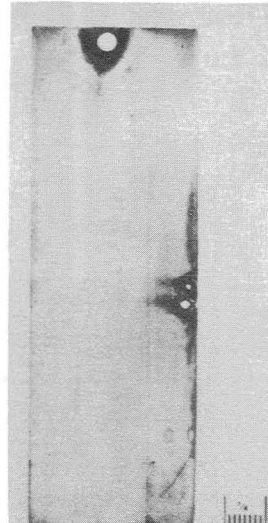
455°C FE 345225

Aluminum-
Manganese



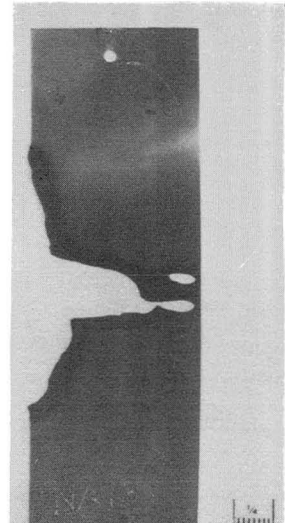
455°C FE 345226

Chromium-
Molybdenum



455°C FE 345245

Cr-Mo +
Aluminum-
Manganese

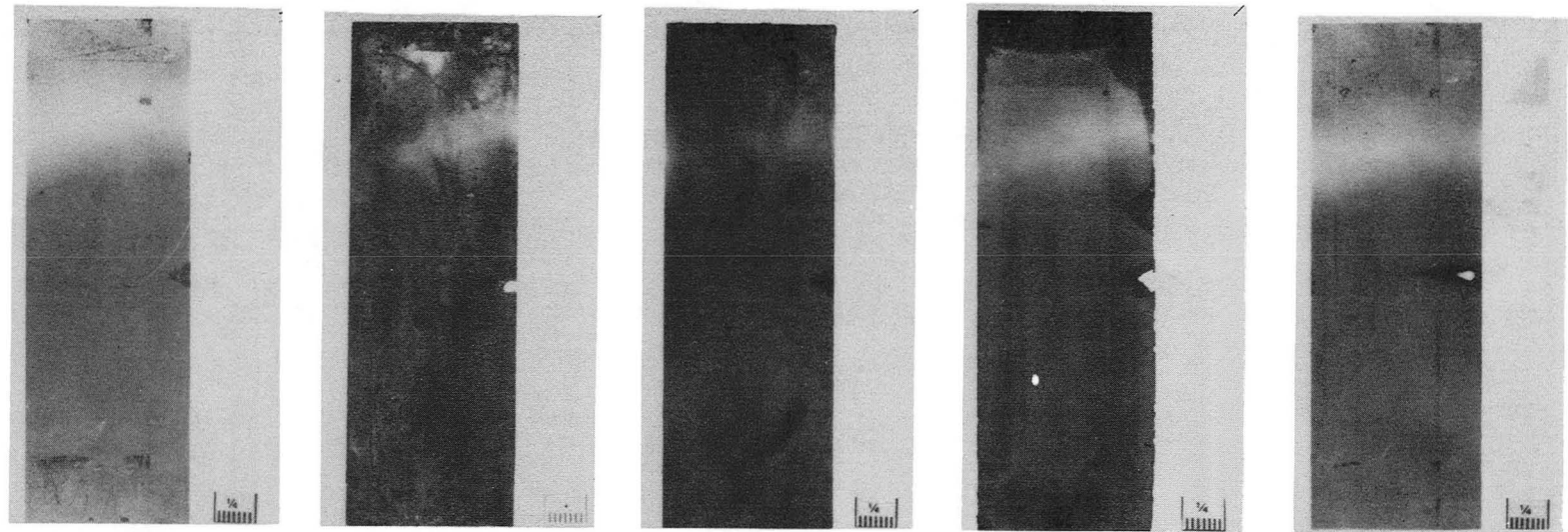


455°C FE 345244

Cr - 5% Mo
(Sputtered)

FD 166842

Figure 12a. Specimen Appearance After Test at Indicated Temperatures



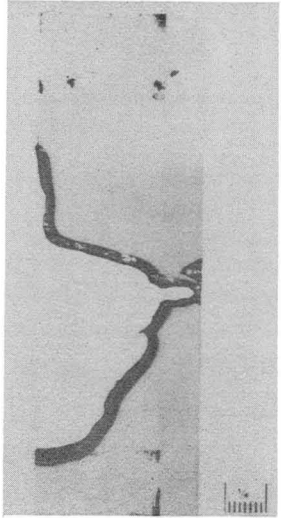
370°C FE 345219

370°C FE 345242

370°C FE 345220

370°C FE 345255

370°C FE 345222



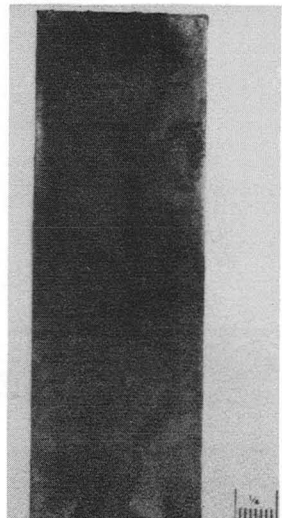
455°C FE 345246

Platinum +
IVD Aluminum



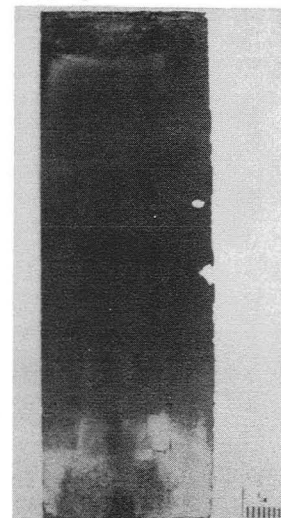
455°C FE 345266

Cr-Mo +
Copper +
Nickel



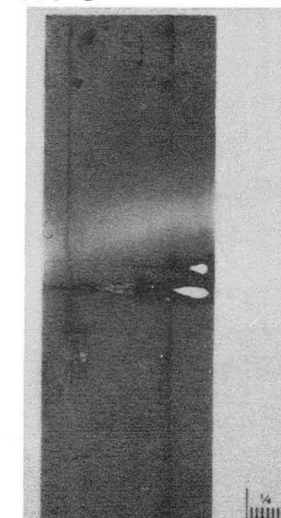
455°C FE 345264

Platinum +
Copper +
Nickel



455°C FE 345265

Cr-Mo +
Nickel



455°C FE 345263

IVD Aluminum

FD 166842A

Figure 12b. Specimen Appearance After Test at Indicated Temperatures

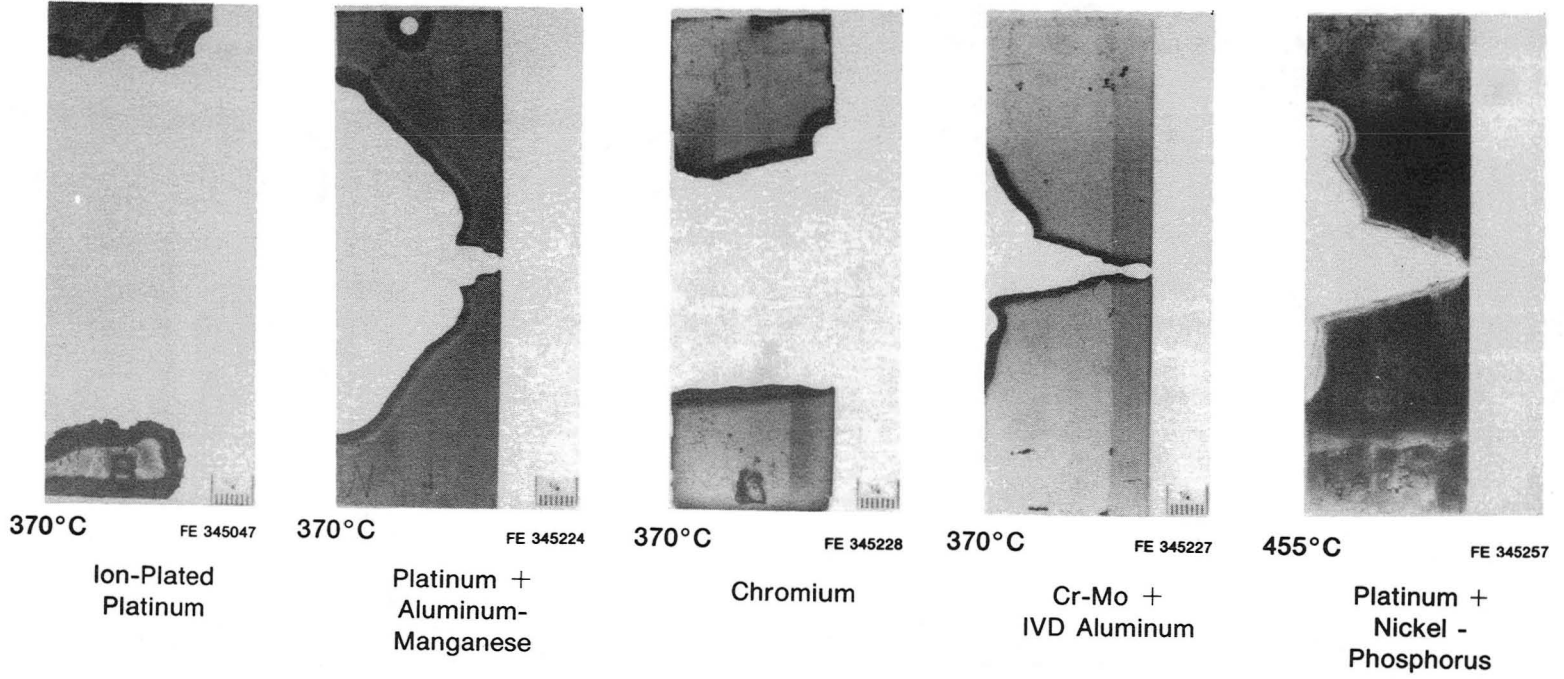


Figure 12c. Specimen Appearance After Test at Indicated Temperatures

FD 204796

TABLE 4. TASK II COMBUSTION RESULTS

Coating System	Pressure		Temperature		Air Velocity		Burn Severity
	MPa	(psia)	°C	(°F)	m/s	(ft/s)	%
IVD Al	0.76	(110)	482	(900)	245	(800)	47.5
Pt + Cu + Ni	0.97	(140)	455	(850)	245	(800)	47.0
Cr-Mo + Cu + Ni	0.97	(140)	455	(850)	245	(800)	44.6
Cr-Mo + Ni	0.97	(140)	455	(850)	245	(800)	58.8
Cr-Mo + IVD Al	0.97	(140)	455	(850)	245	(800)	60.0
Cr-Mo + Al-Mn	0.97	(140)	455	(850)	245	(800)	64.7
Cr-TiC Cermet	0.97	(140)	455	(850)	245	(800)	100.0

Airstream temperature affects chordwise burn velocity in the same direction as pressure and airstream velocity. An increase in airstream temperature increases substrate temperature, thereby decreasing the temperature gradient between the molten material and the substrate. All things considered, such as decreased heat transfer rate, the lower the temperature gradient the higher will be the rate of molten metal propagation. An increase in this propagation corresponds to an increase in chordwise burn velocity.

While the type of coating was not significant, the thickness of an applied coating did affect chordwise burn velocity. From the previous equation, an increase in coating thickness results in a decrease in chordwise burn velocity. A reasonable mechanism for this is that the moving molten substrate material melts the coating before the substrate is heated adequately enough to propagate combustion. Because the melted coating exhibits different viscosity and surface tension characteristics than the propagating molten titanium, the difference could cause the molten substrate and coating to become entrained in the airstream more readily instead of propagating further across the specimen surface. The loss of molten material to the airstream results in a decrease in chordwise burn velocity.

Burn Severity

Stepwise regression analysis was used to identify which parameters were important in determining trends in the dependent variable, i.e., burn severity. Only parameters which were significant at a 90% confidence level were included in the development of the models. These parameters included coating thickness, temperature, pressure, and airstream velocity, depending upon coating type. The empirical equations shown in table 5 describe the relationships for each coating type between burn severity and the significant parameters. These equations provide useful tools in showing trends and evaluating the coating systems, but due to relatively low correlation coefficients, caution must be exercised when using these empirical equations for predicting burn severity. To evaluate the two coating systems selected in this program, a comparison of the coating thickness coefficients was made by substituting typical compressor environmental conditions into the equations in table 5. The resultant equations are shown in table 6 and graphically illustrated in figures 13 and 14. The slope of the IVD aluminum coating equation is approximately twice the slope of the Pt/Cu/Ni equation, indicating that the aluminum coating exhibits a greater effect on minimizing burn severity than the other coating system. Due to the low correlation coefficients of these equations, however, the difference between the two coatings on burn severity is difficult to quantify.

TABLE 5. BURN SEVERITY EMPIRICAL EQUATIONS

<i>Specimen Type</i>	<i>Empirical Equation</i>	<i>R</i> ²	<i>SEE</i>
Titanium Substrate	$B = 458.9 + 0.312P + 1.5525T - 0.001122T^2$	0.411	11.6
IVD Aluminum	$B = -405.7 - 8829C + 0.581P + 0.00005T^2 + 0.9907V - 0.0005545V^2$	0.669	16.3
Pt/Cu/Ni	$B = 535.0 - 4477.5C + 0.006891P^2 + 1.52341T - 0.00103102T^2 + 0.00003317V^2$	0.540	17.4

where: B = burn severity
C = coating thickness, in.
P = pressure, psia
T = airstream temperature, °F
V = airstream velocity, ft/sec

TABLE 6. BURN SEVERITY — TYPICAL COMPRESSOR CONDITIONS

<i>Specimen Type</i>	<i>Empirical Equation</i>	<i>Compressor Conditions</i>					
		<i>Pressure</i>		<i>Temperature</i>		<i>Air Velocity</i>	
		<i>kPa</i>	<i>(psia)</i>	<i>°C</i>	<i>(°F)</i>	<i>m/sec</i>	<i>(ft/sec)</i>
Baseline	B = 90.6	345	(50)	335	(640)	350	(1150)
Baseline	B = 95.5	385	(56)	365	(690)	350	(1150)
IVD Aluminum	B = 49.8 - 8829.2C	345	(50)	335	(640)	350	(1150)
IVD Aluminum	B = 56.6 - 8829.2C	385	(56)	365	(690)	350	(1150)
Pt/Cu/Ni	B = 79.3 - 4477.5C	345	(50)	335	(640)	350	(1150)
Pt/Cu/Ni	B = 91.4 - 4477.5C	385	(56)	365	(690)	350	(1150)

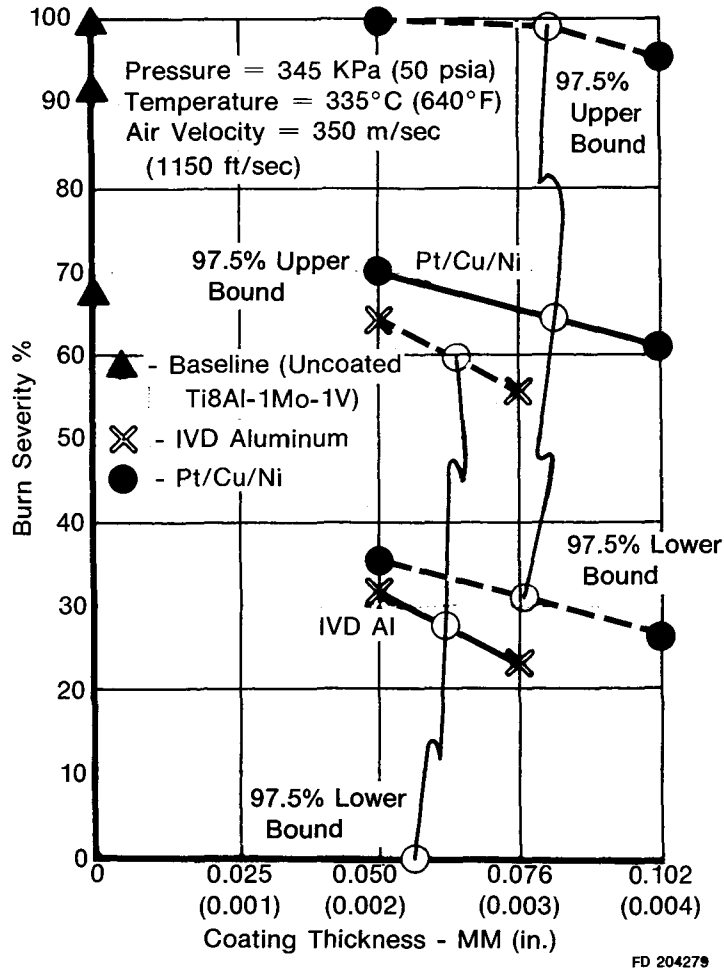


Figure 13. Typical Compressor Conditions

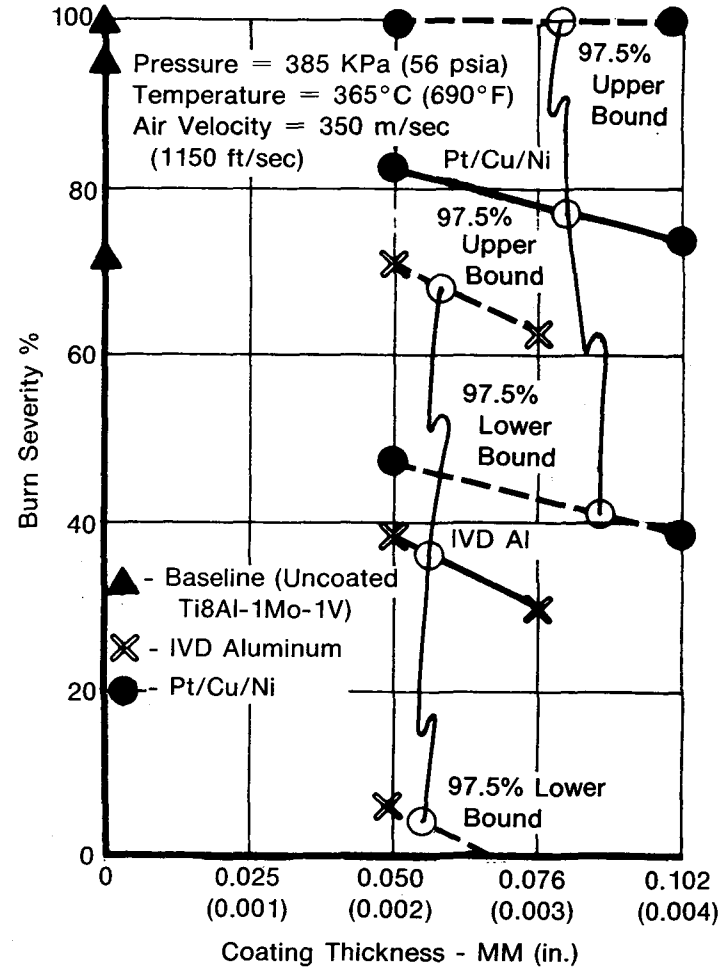


Figure 14. Typical Compressor Conditions

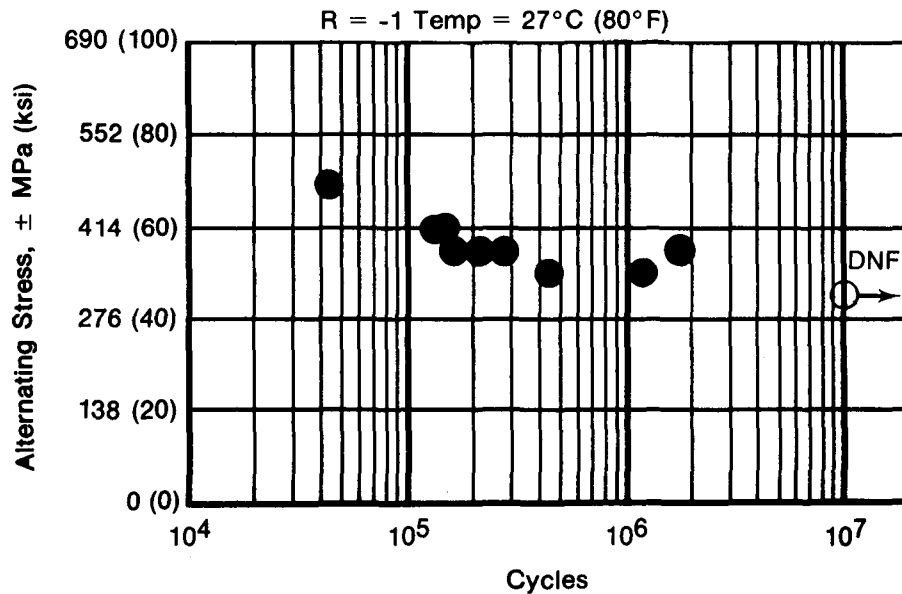
High-Cycle Fatigue Tests

Screening Tests

High-cycle fatigue (HCF) screening tests were conducted on the following seven coatings in addition to baseline determinations on the uncoated material:

1. Chromium-molybdenum + copper + nickel
2. Chromium-molybdenum + nickel
3. Cermet (chromium + occluded TiC)
4. IVD aluminum
5. Platinum + copper + nickel
6. Chromium-molybdenum + IVD aluminum
7. Chromium-molybdenum + aluminum-manganese

A stress vs cycle to failure (S-N) curve (figure 15) was developed using uncoated Ti 8-1-1 material as a baseline. From this curve, a stress level of ± 380 MPa (± 55 ksi) was obtained and used for comparative testing of the coated specimens.



FD 201881

Figure 15. Reverse Bending Fatigue Results of Uncoated AMS 4916 (Ti 8-1-1)

Based on the test results, as shown in figure 16, the following conclusions were reached: All failed coated specimens exhibited an origin location on the coated side in the specimen gage area, and IVD aluminum produced the most favorable results, followed by Pt/Cu/Ni. The rest of the coatings were approximately equal in their relative rank order with reduced fatigue properties compared with the uncoated baseline material.

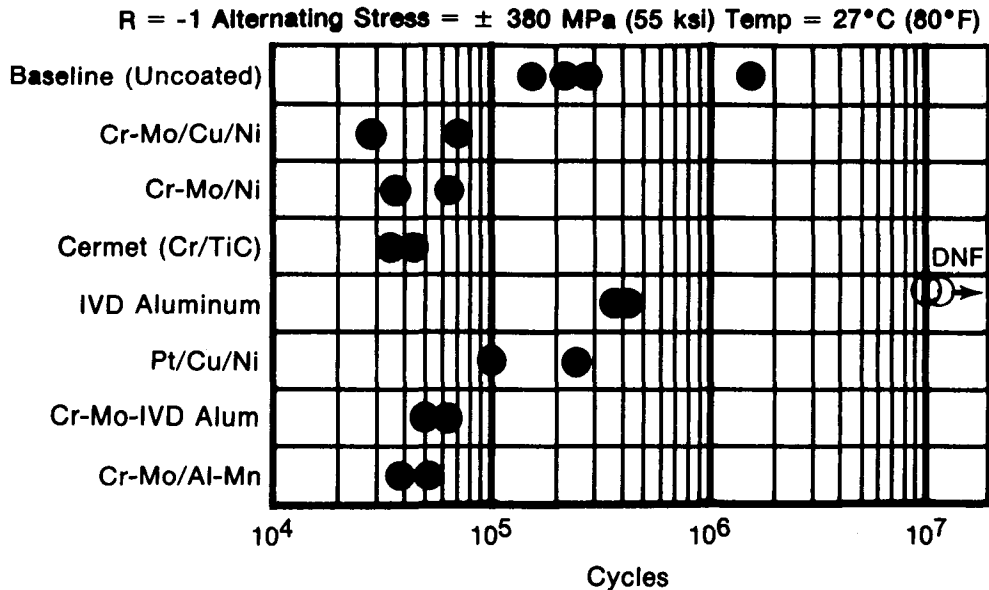


Figure 16. Reverse Bending Fatigue Results of Coated AMS 4916 (Ti 8-1-1)

Testing of Selected Coatings

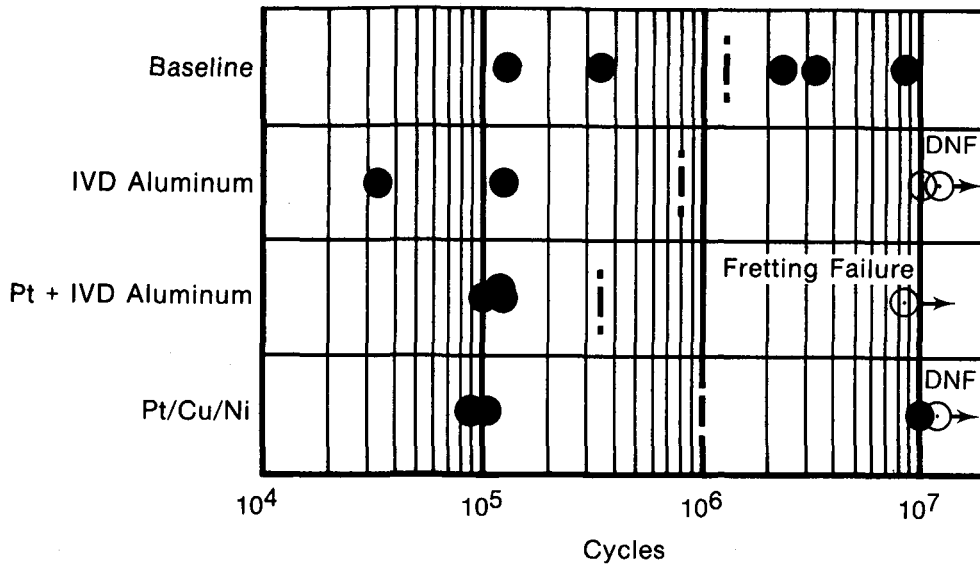
The following coating systems, selected as best based upon the HCF screening tests, were then subjected to additional HCF testing and analysis:

- Alloy Ti 8-1-1 with coatings of IVD aluminum, Pt + IVD aluminum, and Pt/Cu/Ni
- Alloy Ti 6-4 with coatings of IVD aluminum, Pt + IVD aluminum, and Pt/Cu/Ni.

This test series employed an additional coating variation involving ion-plated platinum as an undercoat to IVD aluminum. This enabled the determination of whether or not platinum would significantly improve the fatigue strength of the IVD aluminum coating. As shown in figures 17 and 18, no improvement was noted. Therefore, all subsequent mechanical properties testing was concerned only with IVD aluminum and Pt/Cu/Ni. For all coatings tested, no significant effect was evident in the baseline HCF properties.

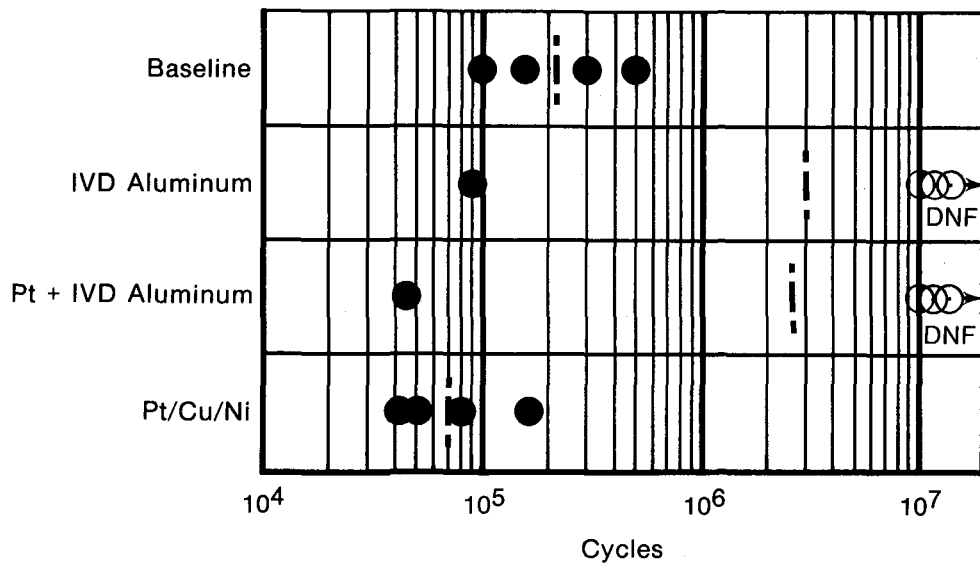
Testing of Air Force-Selected Alloy

IVD aluminum and Pt/Cu/Ni coatings were also tested on a Ti 3Al-8V-6Cr-0.4Mo-4Zr substrate. Figure 19 shows the results of this testing. No significant difference occurred between the results of the baseline (uncoated) specimen and the two coating systems at a temperature of 425°C (800°F) to 10⁶ cycles. The life cycle (10⁶) of the baseline specimens at a steady stress of \pm 240 MPa (\pm 35 ksi) is significantly below the AMS specification for identical material. Inspection showed the reason for this short life cycle to be poor quality specimen edge preparation.



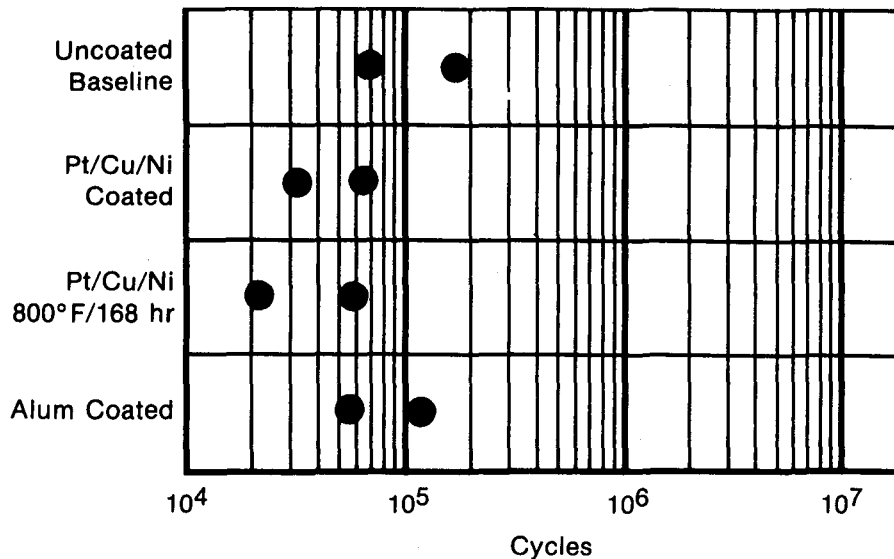
FD 201882

Figure 17. Reverse Bending Results of Ti 8-1-1 (AMS 4916) Coating Evaluation, $R = -1$, Alt Stress = ± 414 MPa (60 ksi), Temp = 425°C (800°F)



FD 201883

Figure 18. Reverse Bending Results of Ti 6-4 (AMS 4911) Coating Evaluation, $R = -1$, Alt Stress = ± 414 MPa (60 ksi), Temp = 315°C (600°F)



FD 201884

Figure 19. Reverse Bending Results of Ti 3Al-8V-6Cr-0.4Mo-4Zr Coating Evaluation, $R = -1$, Alt Stress = ± 240 MPa (35 ksi), Temp = 425°C (800°F)

Tensile Testing

Both coatings were tested at thicknesses of 0.025 mm (0.001 in.) and 0.076 mm (0.003 in.). Raw data from individual test results of specimens employing coating thickness variations established that this parameter exhibited no influence on tensile values. The average values shown in figure 20, therefore, include the individual values for both coating thicknesses.

When compared to the uncoated baseline specimens, neither coating produced a statistically significant (i.e., confidence level $\geq 90\%$) influence on ultimate tensile strength, yield strength, or percent elongation.

Creep Testing

Both coatings were applied to a thickness of 0.025 mm (0.001 in.). The test results appear in tables 7 and 8. Neither coating appreciably affected the creep characteristic of the Ti 8Al-1Mo-1V substrate. While the values for the Pt/Cu/Ni and IVD aluminum on Ti 6Al-4V were less than the baseline values, the difference in values becomes insignificant when the number of specimens and the test result spread is considered.

Stress Rupture Testing

Coating thickness was 0.050 mm (0.002 in.). The results of this testing appear in figure 21. As noted therein, both coating systems significantly enhanced the stress rupture characteristics of the substrate alloy.

When a specimen develops a crack on the surface of the substrate, the crack propagates rapidly, thereby causing rupture. It is reasonable to assume that the coatings delayed the initiation of a substrate surface crack. In addition, neither coating system significantly affected the percent elongation of the substrate.

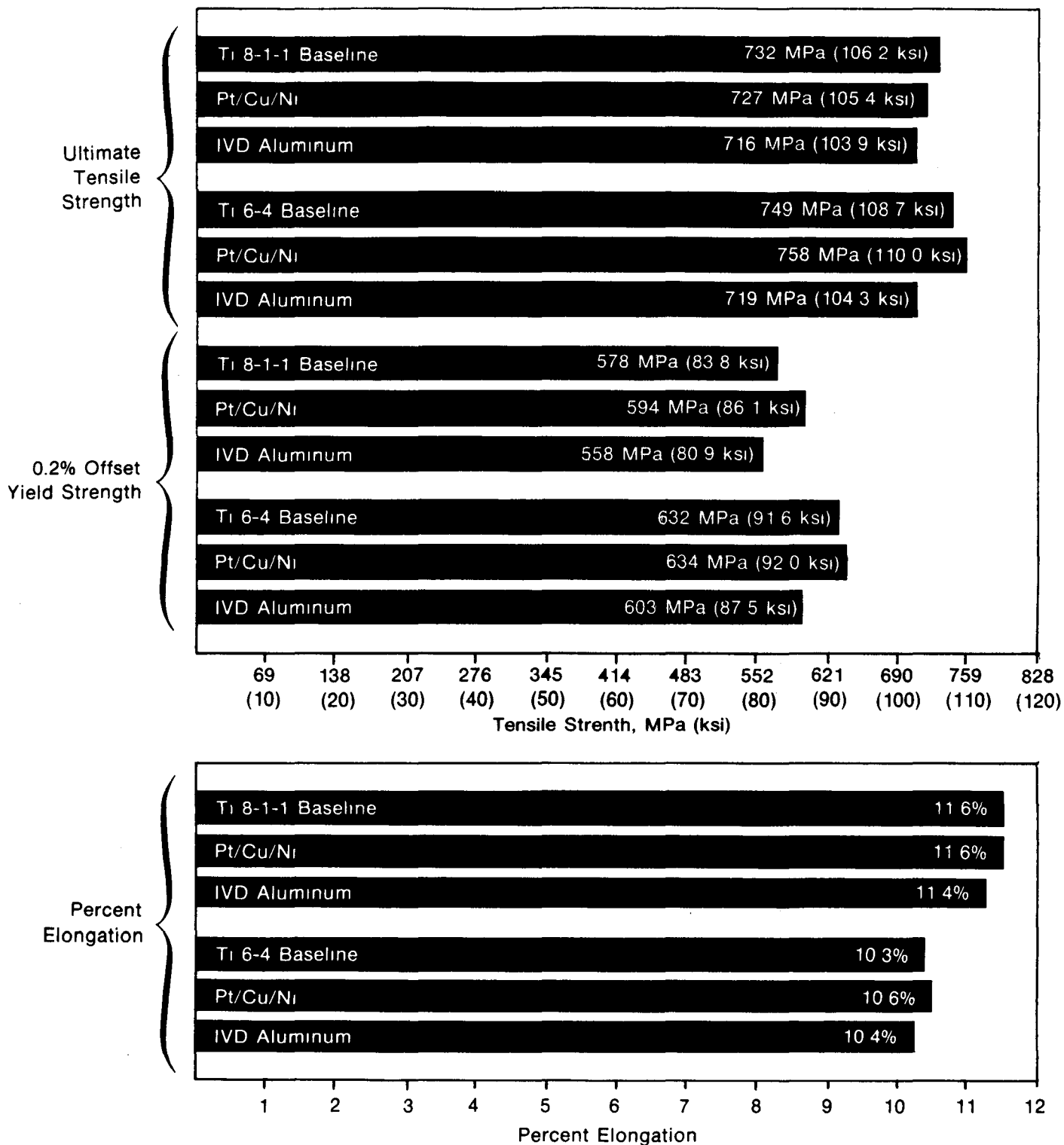


Figure 20. Tensile Test Results at 427°C (for Ti 8-1-1) and 315°C (for Ti 6-4)

TABLE 7. CREEP TEST RESULTS

Substrate Material: Ti 8-1-1
 Test Temperature: 427°C (800°F)
 Stress Level: 445 MPa (65 ksi)

Coating	Hours to reach 1.0% Creep	
Uncoated	218	
Uncoated	210	
Uncoated	200	avg = 216
Uncoated	273	SD = 29.7
Uncoated	202	
Uncoated	190	
Pt/Cu/Ni	230	
Pt/Cu/Ni	182	avg = 207
Pt/Cu/Ni	235	SD = 29.8
Pt/Cu/Ni	180	
IVD Al	213	
IVD Al	206	avg = 200
IVD Al	189	SD = 11.6
IVD Al	191	

TABLE 8. CREEP TEST RESULTS

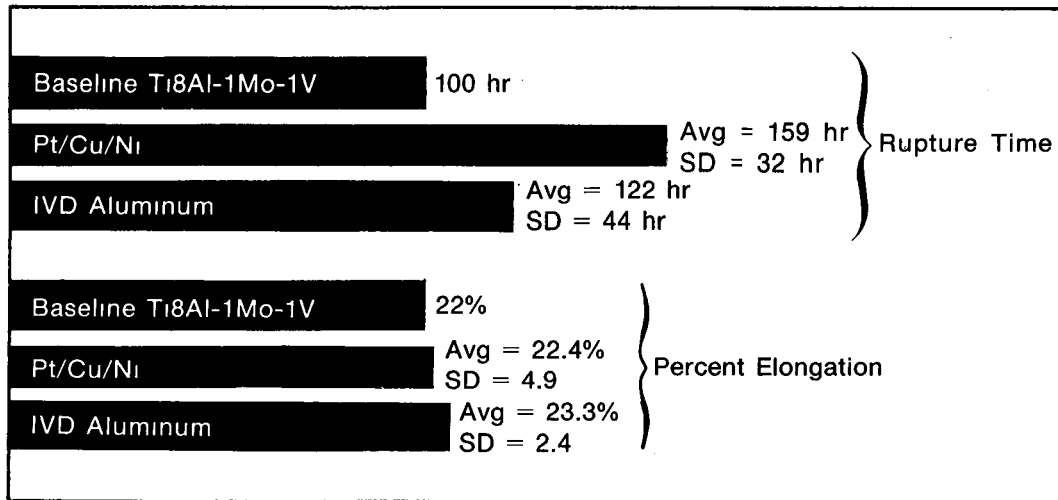
Substrate Material: Ti 6-4
 Test Temperature: 315°C (600°F)
 Stress Level: 414 MPa (60 ksi)

Coating	Hours to reach 1.0% Creep	
Uncoated	1070	
Uncoated	1910	
Uncoated	1940	avg = 1524
Uncoated	1730	SD = 380
Uncoated	1250	
Uncoated	1245	
Pt/Cu/Ni	1050	
Pt/Cu/Ni	1060	avg = 1028
Pt/Cu/Ni	690*	SD = 255
Pt/Cu/Ni	1310	
IVD Al	1118	
IVD Al	1431	avg = 1258 (+)
IVD Al	1081	SD = 184
IVD Al	1400+**	

*Data point in question
 **Test stopped at 1400 hr (Creep was at 0.08%)

Test Stress Level = 638 MPa (92.5 ksi)

Test Temperature = 427°C (800°F)



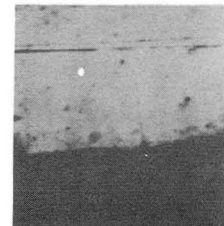
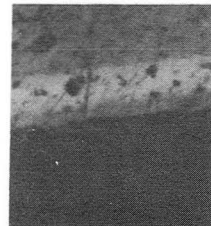
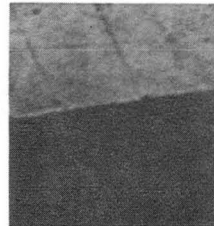
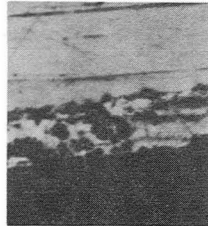
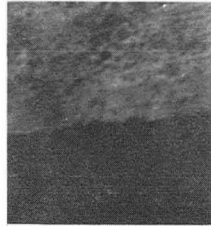
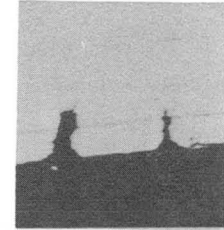
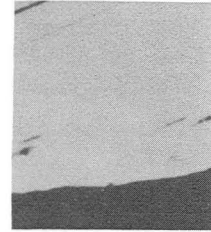
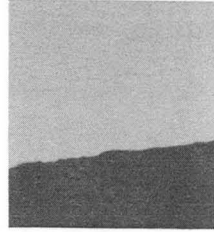
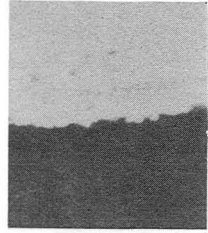
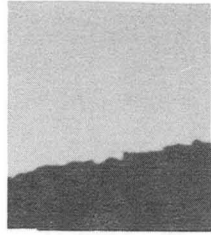
FD 201886

Figure 21. Stress Rupture Results

Hot Salt Stress Corrosion Testing

Coating thickness was 0.050 mm (0.002 in.). Results of the testing appear in figure 22. The occurrence of stress corrosion cracking in the salt solution-treated baseline Ti, combined with the nonoccurrence of stress corrosion cracking in the untreated baseline Ti, confirms the validity of the test. No stress corrosion cracking appeared in the Pt/Cu/Ni or IVD aluminum coating systems, both with and without salt solution applied.

Test Duration: 100 hr
Test Temperature: 800°F
Stress Applied: 60 ksi



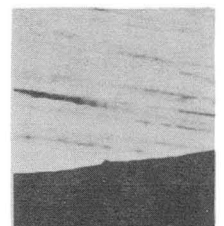
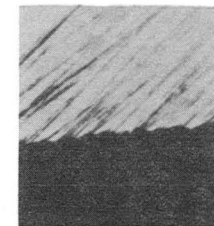
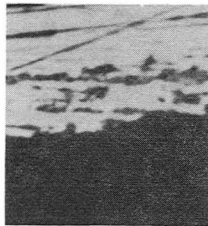
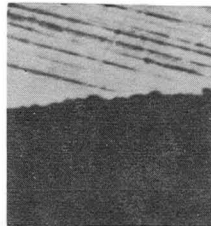
Aluminum Coating
Removed

Aluminum

Pt/Cu/Ni Coating
Removed

Pt/Cu/Ni

Baseline (Ti 8-1-1)



Aluminum Coating
Removed

Aluminum

Pt/Cu/Ni Coating
Removed

Pt/Cu/Ni

Baseline (Ti 8-1-1)

Figure 22. Hot Salt Stress Corrosion

Erosion Testing

Erosion testing was conducted for both coating systems with a Ti 8Al-1Mo-1V substrate and a coating thickness of 0.050 mm (0.002 in.). Due to the thinness of the coatings and the small area eroded during test, a weight loss rate determination was not practical. Because the Pt/Cu/Ni showed better protection against 90 deg impingement, the rate of erosion of Pt/Cu/Ni was used as the basis for comparison with the aluminum coating, as shown in table 9.

TABLE 9. EROSION RATES OF COATING

<i>Angle of Incidence</i>	<i>IVD Aluminum</i>	<i>Pt/Cu/Ni</i>
90°	1.6 rate	1 rate
60°	1.2 rate	1 rate
30°	0.6 rate	1 rate

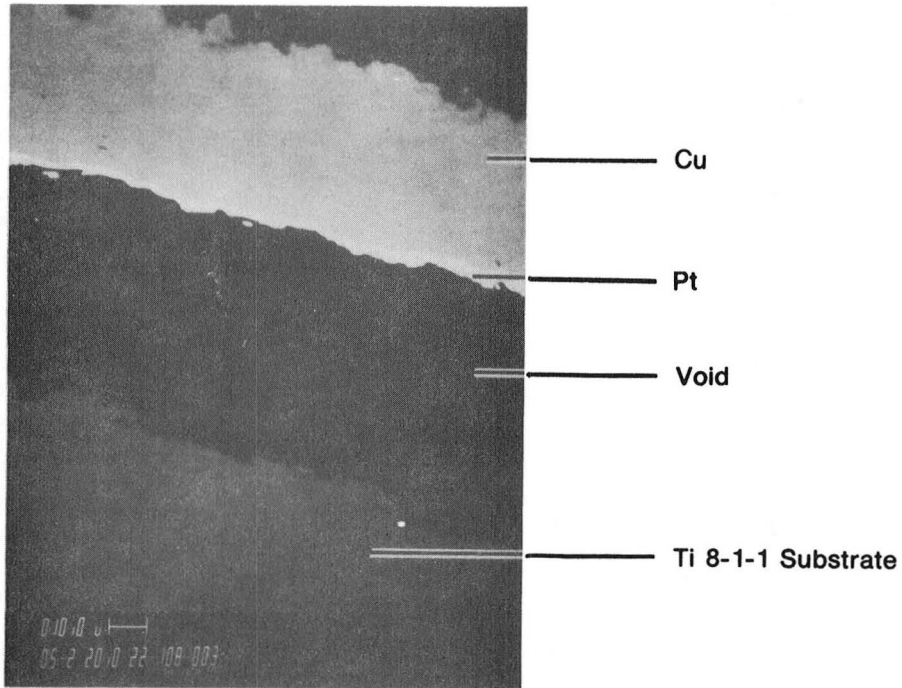
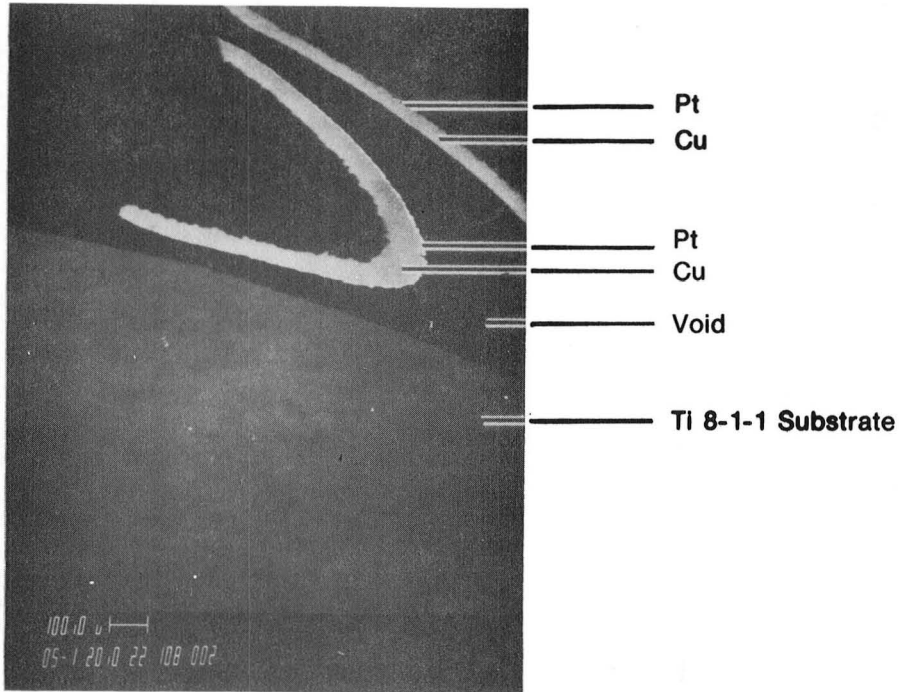
Adhesion Testing

During testing IVD aluminum exhibited better adhesion to the substrate than the Pt/Cu/Ni coating. In one test the IVD aluminum coating specimen was bent greater than 105 deg before the specimen fractured. At this point the aluminum still adhered to the titanium and did not flake. The Pt/Cu/Ni coating separated from the substrate when subjected to bend testing. The flaked-off coating was analyzed by X-ray emission spectroscopy (XES) to determine the separation interface. At the interface side of the coating, platinum with traces of copper and titanium was found. The bend specimen was then cross sectioned, mounted, and analyzed by scanning electron microscopy (SEM). The SEM photos shown in figure 23 show all of the platinum adhering to the copper.

Both coatings, IVD aluminum and Pt/Cu/Ni, were applied by an ion-plating process. This process theoretically produces metallic coatings that adhere very strongly to the substrate. There are two reasons why a strongly adhering coating is expected: (1) the very clean surface that results prior to coating from a sputter cleaning step and (2) the very large driving force created from the bias applied to the specimen. The strong adhesion exhibited by the aluminum coating demonstrates the possible strength of the ion-plating process. A possible reason for the poor adhesion exhibited by the platinum coating is that some specimens were shadowed by other specimens in the coating chamber. This would cause inadequate cleaning of the substrate, which interferes with the adhesion of the coating applied. As result, therefore, it is assumed that the poor adhesion of the Pt/Cu/Ni coating was the result of processing problems and not the inherent capability of the coating system.

Static Oxidation Testing

Coating thickness for this testing was 0.050 mm (0.002 in.). The coating system of Pt/Cu/Ni provided the better oxidation protection (smallest weight gain). The IVD aluminum coating showed a nearly twofold increase in weight at 50 hr compared to the Pt/Cu/Ni coating. Both coating systems exhibited greater weight gains than the baseline uncoated Ti 8-1-1 by a factor of about four for the aluminum and a factor of about three for the platinum, as shown in table 10 and figure 24.



FD 201888A

Figure 23. Scanning Electron Microscopy Photos of Cross-Sectioned Adhesion Specimens

TABLE 10. TGA OXIDATION DATA FOR TITANIUM SPECIMENS

Material	Sample Weight (mg)	Temperature °C (°F)	Footnote	Time (hr)	Weight Gain (mg/cm ²)			Rate Constant (mg/sq cm/min)		
Ti 8-1-1 Baseline	123.1	500 (932)	1	0.00	—	—	—	—	—	—
				2.58	4.125	×	10 ⁻²	2.661	×	10 ⁻⁴
				22.45	5.041	×	10 ⁻²	3.743	×	10 ⁻⁵
				45.58	8.249	×	10 ⁻²	3.016	×	10 ⁻⁵
				50.98	8.249	×	10 ⁻²	2.697	×	10 ⁻⁵
Ti 8-1-1 IVD Al	164.7	500 (932)	2	0.00	—	—	—	—	—	—
				1.00	2.336	×	10 ⁻²	3.894	×	10 ⁻⁴
				10.00	1.525	×	10 ⁻¹	2.542	×	10 ⁻⁴
				20.00	2.408	×	10 ⁻¹	2.006	×	10 ⁻⁴
				30.00	2.687	×	10 ⁻¹	1.493	×	10 ⁻⁴
				40.00	2.888	×	10 ⁻¹	1.203	×	10 ⁻⁴
50.00	3.199	×	10 ⁻¹	1.066	×	10 ⁻⁴				
Ti 8-1-1 Pt/Cu/Ni	139.7	500 (932)	3	0.00	—	—	—	—	—	—
				5.00	3.150	×	10 ⁻²	1.050	×	10 ⁻⁴
				15.00	1.031	×	10 ⁻¹	1.145	×	10 ⁻⁴
				25.00	1.613	×	10 ⁻¹	1.075	×	10 ⁻⁴
				35.00	1.899	×	10 ⁻¹	9.042	×	10 ⁻⁵
				50.00	2.386	×	10 ⁻¹	7.952	×	10 ⁻⁵

Footnote:

Specimen	Weight Loss to Dryness (mg)	Specimen Surface Area Calculations (sq cm)	(sq in.)
1	0.02	2.182	(0.3383)
2	0.21	1.541	(0.2389)
3	0.24	1.048	(0.1624)

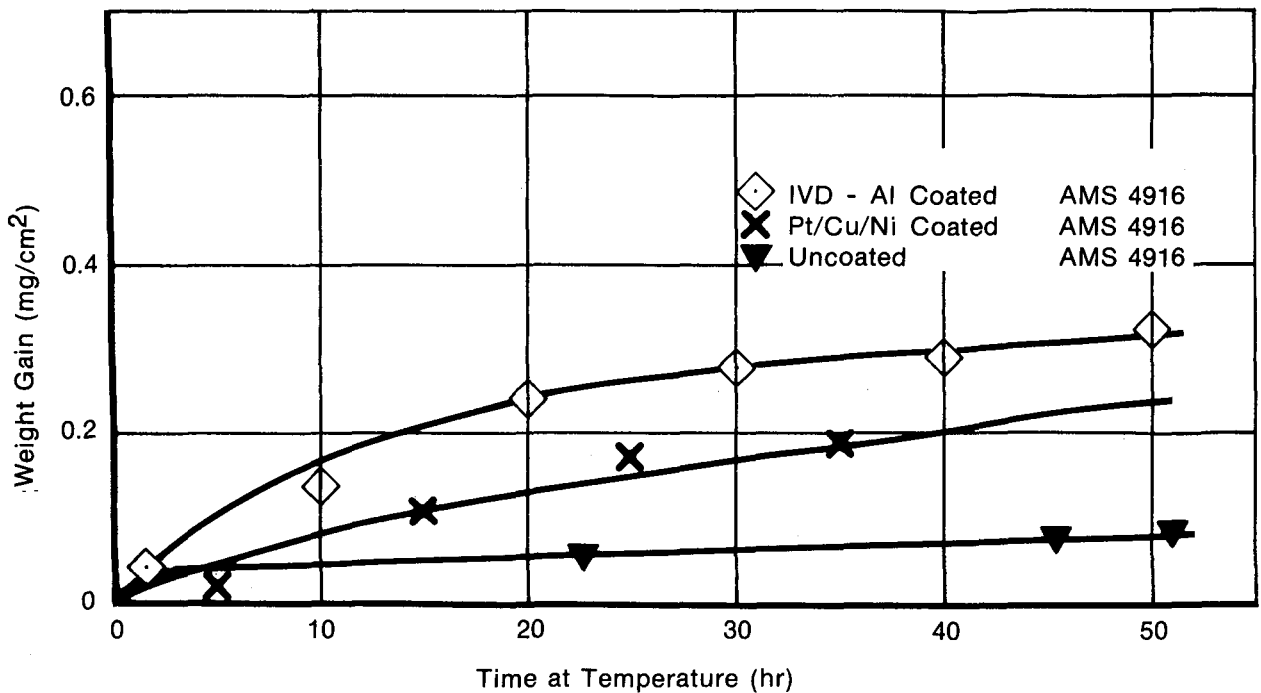


Figure 24. Oxidative Weight Gain for Coated and Uncoated Titanium Specimens at 500°C in Air

FD 201889

Diffusion Testing

Coating thickness was 0.050 mm (0.002 in.). Diffusion tests consisted of subjecting coated specimens to a temperature of 425°C (800°F) in air for 168 hr. Tested specimens were then cross sectioned, mounted, and analyzed with XES. A set of XES photographs taken of each coating system provide a mapping of each element of the coating and substrate base material. The XES photographs, shown in figure 25, indicate essentially no overlap of elements at the coating/substrate interface. From this it can be concluded that very little diffusion occurred between coatings and substrate.

Thermal Shock Testing

Coating thickness for this test was 0.050 mm (0.002 in.). For each cycle the specimens were heated to equilibrium at a temperature of 425°C (800°F) and then rapidly water quenched to room temperature. Figure 26 shows photographs of the results. The coating of IVD aluminum exhibited no detrimental effects after three thermal shock cycles. The coating of Pt/Cu/Ni showed minimal detrimental effects after the first cycle in the form of flaking in one small area. After examination it was determined that the oxidation prevention coating of nickel flaked, leaving the copper intact. The second cycle resulted in additional nickel flaking. The exposed copper did not flake. More of the nickel coating flaked off and the copper oxidized during the third cycle. Although the nickel coating flaked off in all cycles, the copper coating remained intact. It should be emphasized that the function of the nickel coating was to protect the copper from oxidation. For purposes of this study, a conclusion can be drawn that the IVD aluminum coating is more resistant to thermal shock than Pt/Cu/Ni, but that the Pt/Cu/Ni coating could be adequate if optimized by means of a more adherent nickel coating.

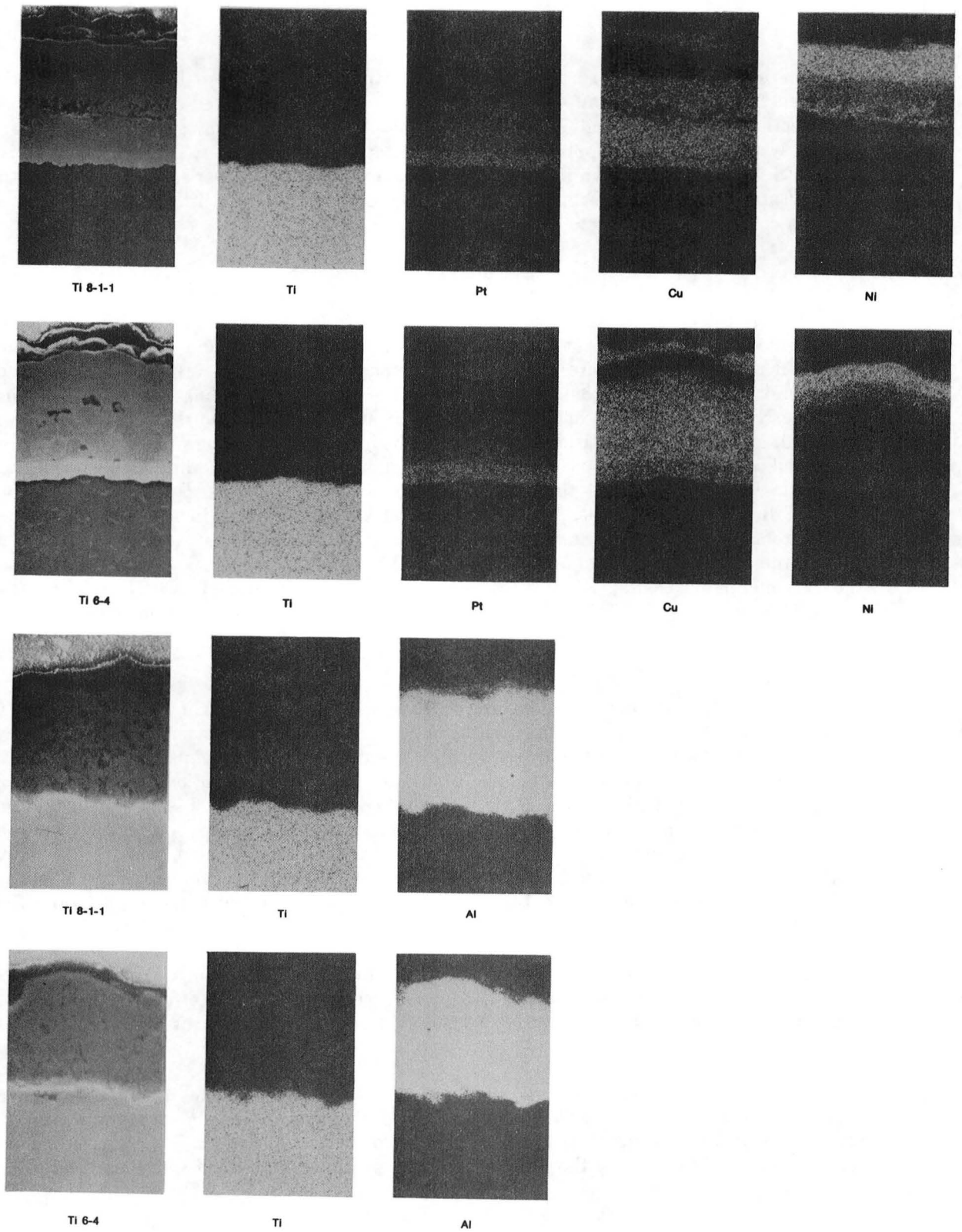
Stress Analysis Testing

Stress analysis testing was conducted on baseline (uncoated), Pt/Cu/Ni coated, and IVD aluminum-coated 6th-stage F100 compressor blades. Prior to destructive HCF testing, stresscoat patterns in the first three modes of vibration were determined. A comparison of stress vs tip double amplitude for the first three modes of vibration for each coating configuration are shown in figures 27 through 29. Figures 30 through 32 show the strain gage locations used for calibrations in the first, second, and third bending modes of vibration, respectively. Photographs of the stresscoat patterns for the first, second, and third bending modes of vibration for each coating configuration appear in figures 33 through 35, respectively. Neither coating appreciably changed the mode shape of the stresscoat patterns of the baseline substrate in the first three modes of vibration.

Table 11 lists the resonant frequencies of the first three modes of vibration for coated and uncoated blades. The aluminum coating produced no appreciable effect on the frequencies, but the Pt/Cu/Ni coating lowered the resonant frequencies slightly (by approximately 2 to 4%).

The results of the first bending mode fatigue tests appear in tables 12 through 14. S-N curves for baseline and coated blades tested at room temperature are shown in figure 36. The standard estimate of error (SEE), and coefficient of determination (R^{**2}), representing the relative amount of scatter in the fatigue data, are given below for each specimen:

<u>Specimen</u>	<u>SEE</u>	<u>R^{**2}</u>
Baseline (uncoated)	0.281	0.915
Aluminum	1.012	0.145
Pt/Cu/Ni	0.463	0.763



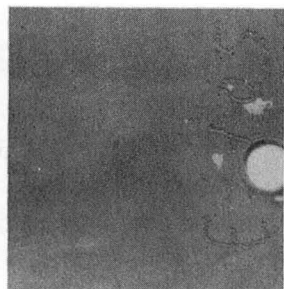
FD 201800

Figure 25. Mapping of Elements by X-ray Emission Spectroscopy



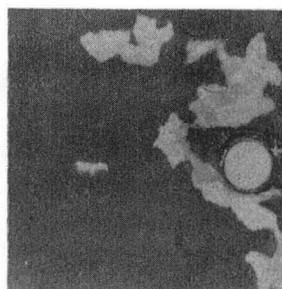
FE 187548

Initial



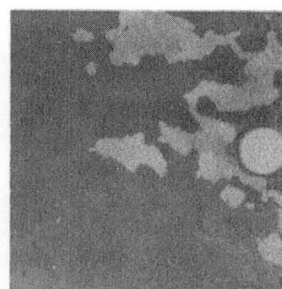
FE 187672

First Cycle



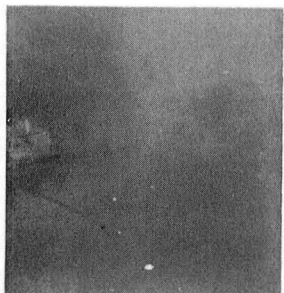
FE 187705

Second Cycle

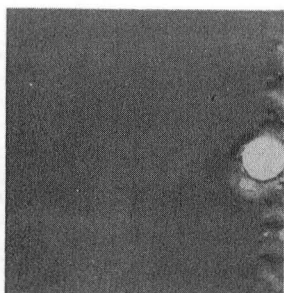


FE 187824

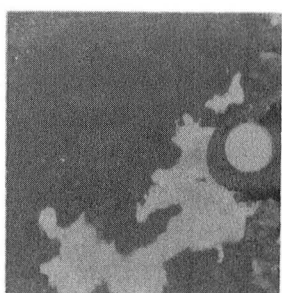
Third Cycle



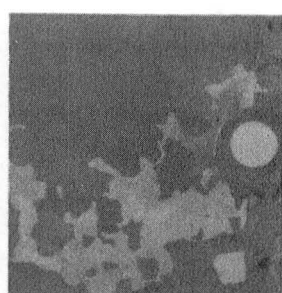
FE 187547



FE 187673

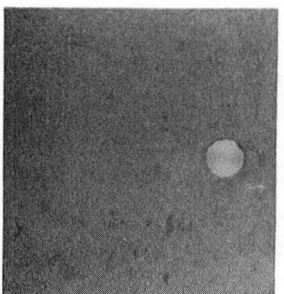


FE 187706



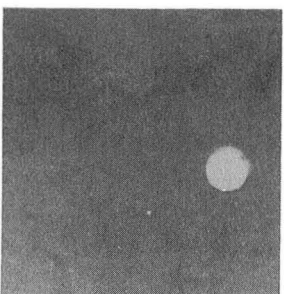
FE 187827

Pt/Cu/Ni



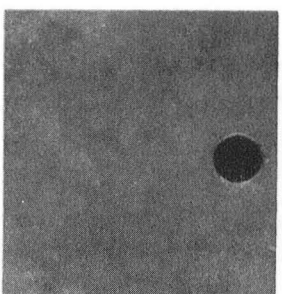
FE 187549

Initial



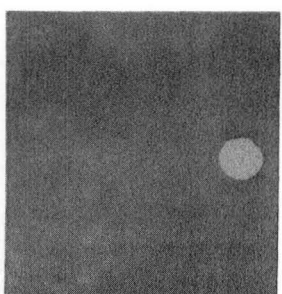
FE 187674

First Cycle



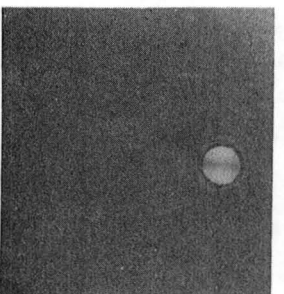
FE 187704

Second Cycle

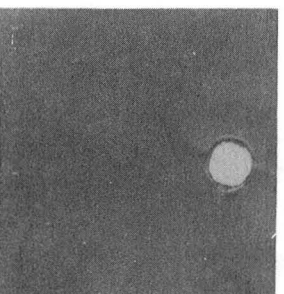


FE 187825

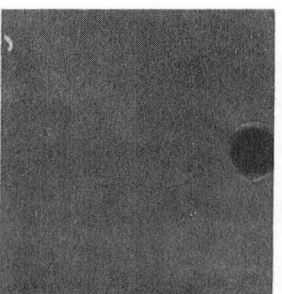
Third Cycle



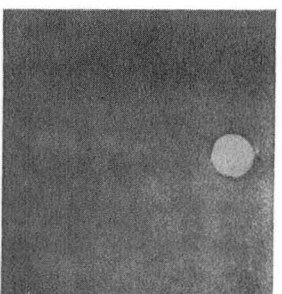
FE 187550



FE 187675



FE 187703



FE 187826

IVD Aluminum

FD 195108

Figure 26. Thermal Shock Results

*Stress Based on $E = 1.28 \times 10^5 \text{ MPa}$ ($18.5 \times 10^6 \text{ psi}$)
and Measured at Locations Noted in Figure 30

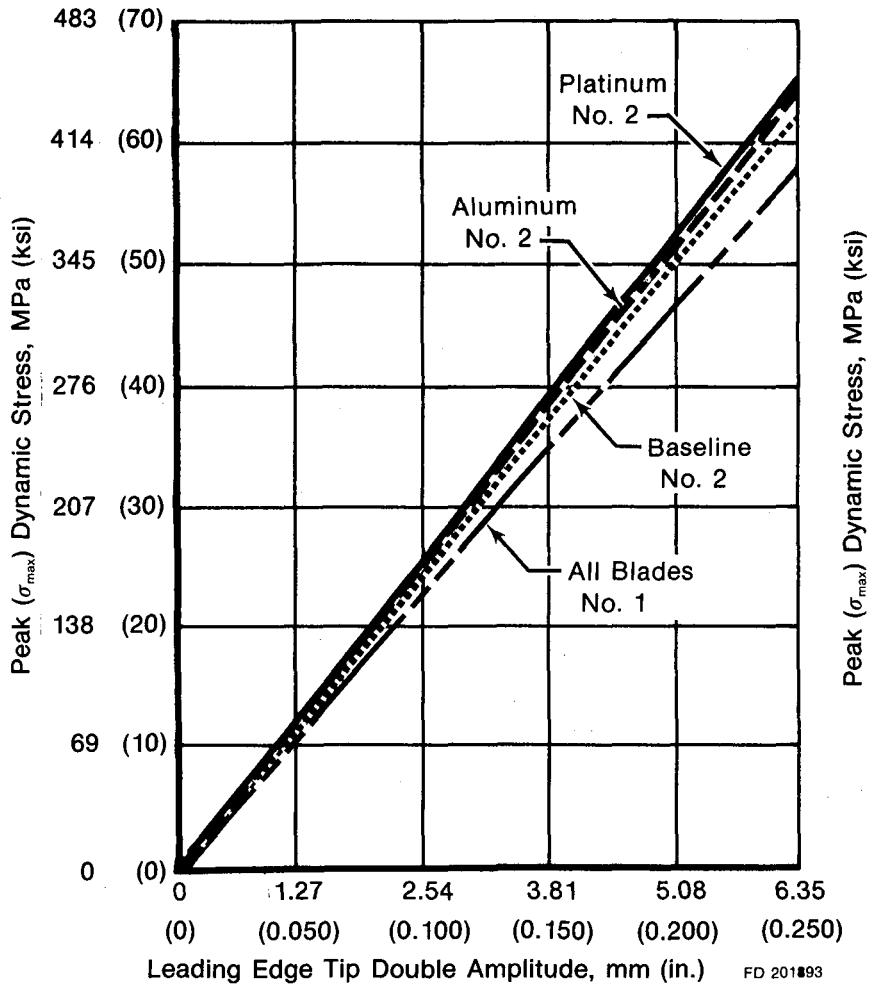


Figure 27. Peak Dynamic Stress* vs Tip Double Amplitude F100, PWA 1202, 6th-Stage HPC Blades P/N 4034806 Vibrated in the First Mode of Vibration

*Stress Based on $E = 1.28 \times 10^5 \text{ MPa}$ ($18.5 \times 10^6 \text{ psi}$)
and Measured at Locations Noted in Figure 31

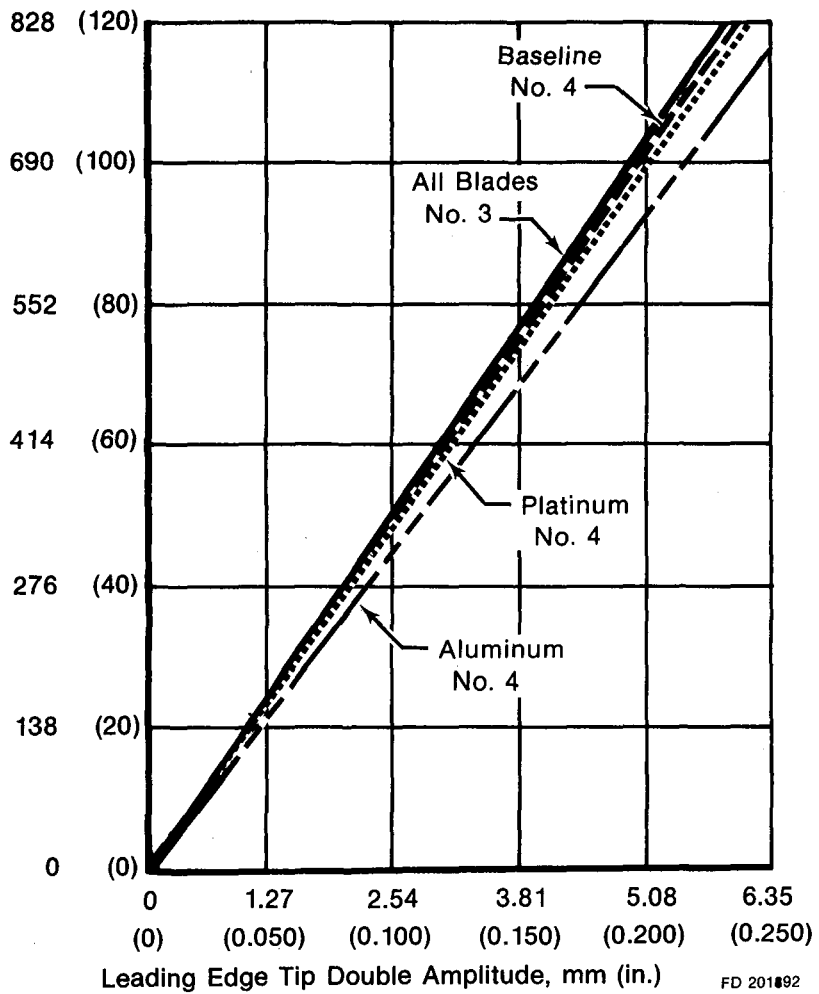
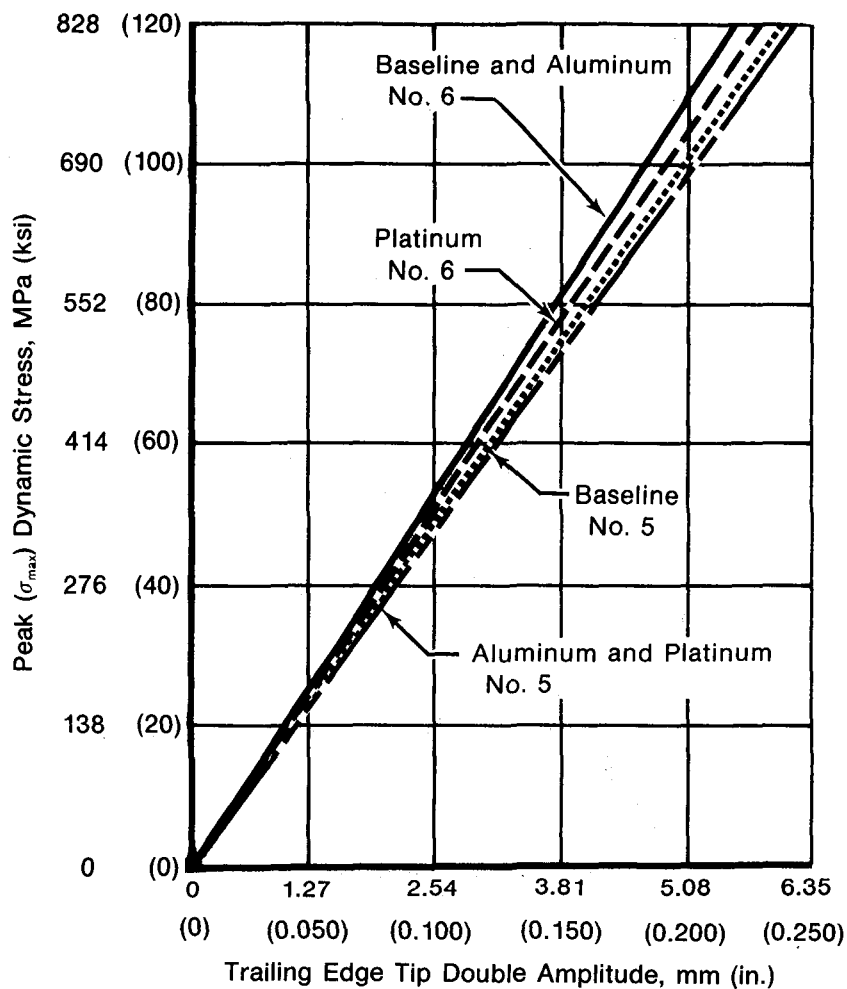


Figure 28. Peak Dynamic Stress* vs Tip Double Amplitude F100, PWA 1202, 6th-Stage HPC Blades P/N 4034806 Vibration in the Second Mode of Vibration

*Stress Based on $E = 1.28 \times 10^5 \text{ MPa}$ ($18.5 \times 10^6 \text{ psi}$)
 and Measured at Locations Noted in Figure 32



FD 201894

Figure 29. Peak Dynamic Stress* vs Tip Double Amplitude F100, PWA 1202, 6th-Stage HPC Blades P/N 4034806 Vibrated in the Third Mode of Vibration

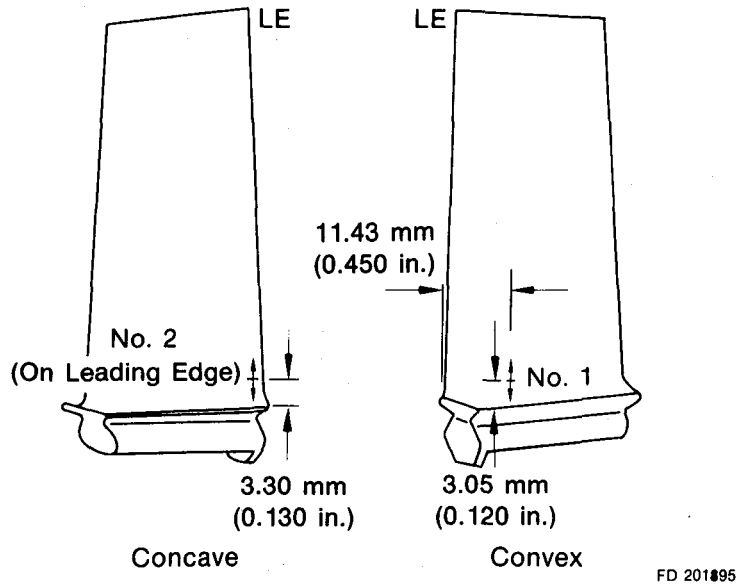


Figure 30. F100, PW 1202, 6th-Stage Compressor Blade, P/N 4034806, Illustration Showing Strain Gage Locations Used for Calibrations in the First Bending Mode of Vibration

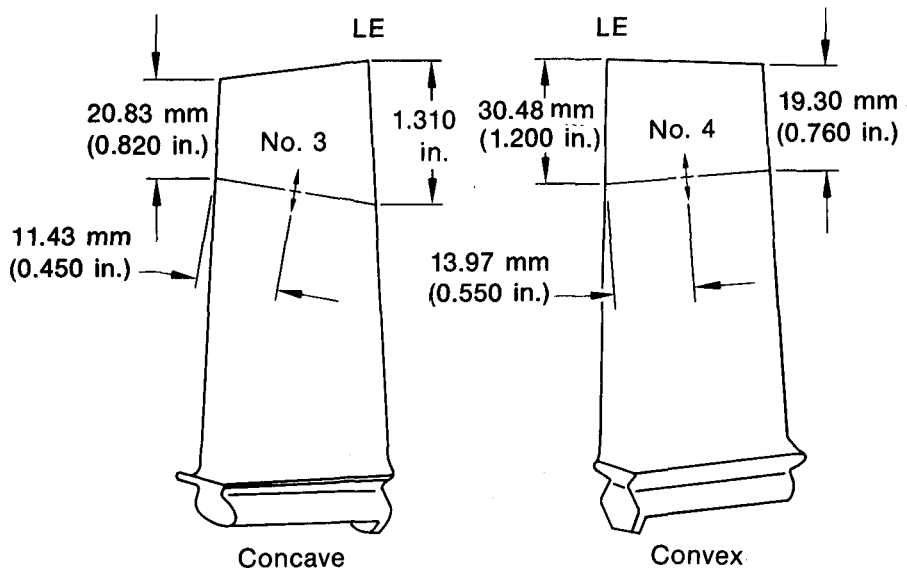
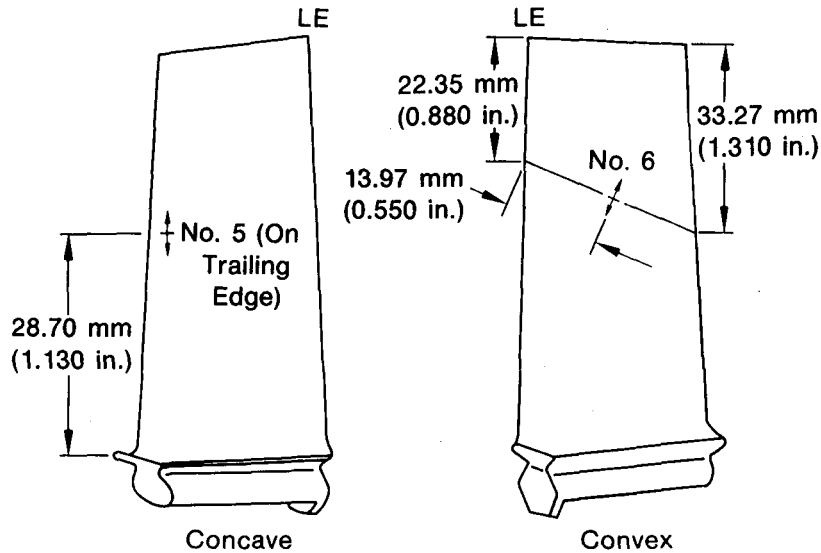


Figure 31. F100, PWA 1202, 6th-Stage Compressor Blade, P/N 4034806, Illustration Showing Strain Gage Locations Used for Calibrations in the Second Mode of Vibration



FD 201897

Figure 32. F100, PWA 1202, 6th-Stage Compressor Blade, P/N 4034806, Illustration Showing Strain Gage Locations Used for Calibrations in the Third Mode of Vibration

For small amounts of scatter, SEE equals zero, while R^{**2} equals 1.0. For large amounts of scatter, SEE equals 1.0, while R^{**2} equals zero. The amount of scatter experienced by the aluminum-coated specimen is comparable to the scatter experienced during HCF testing of aluminum-coated Ti 8Al-1Mo-1V specimens, suggesting that the effect of the coating on the blades is the same as that on the HCF test specimens.

SUMMARY OF RESULTS

Combustion — Cascade Test Configuration

Burn Severity

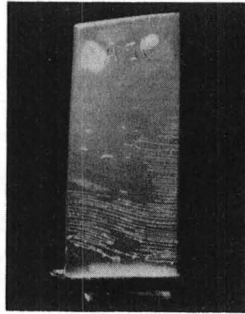
Pressure is the most significant test parameter. Burn severity increases as pressure is increased. The coated specimens have lower burn severities than those that are uncoated. Furthermore, increased coating thickness decreases burn severity.

Chordwise Burn Velocity

No significant difference exists between the chordwise burn velocities of the coated and uncoated specimens. Pressure and air velocity are the significant parameters in relation to chordwise burn velocity. Chordwise burn velocity increases with increasing pressure. The air velocity parameter affects chordwise burn velocity to a considerably lesser degree.

High-Cycle Fatigue (HCF) Testing

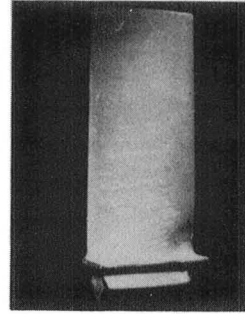
Tests conducted at an alternating stress of ± 414 MPa and temperatures of 427°C (800°F) (for Ti 8-1-1) and 315°C (600°F) (for Ti 6-4) indicate that IVD aluminum coatings enhance HCF life on both substrates. However, no statistically significant difference exists between the baseline and the two coatings (IVD Al and Pt/Cu/Ni). The HCF results for these coating systems on Ti 3Al-6Cr-8V-0.4Mo-4Zr proved inconclusive.



FAL 58287

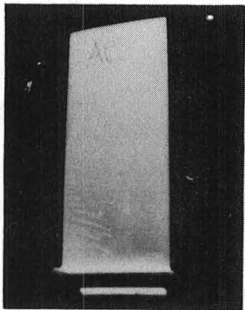
Concave

Baseline
(Uncoated)



FAL 58288

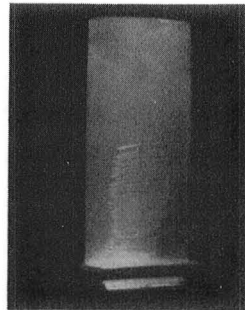
Convex



FAL 58317

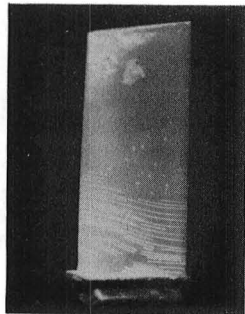
Concave

Al Coating



FAL 58318

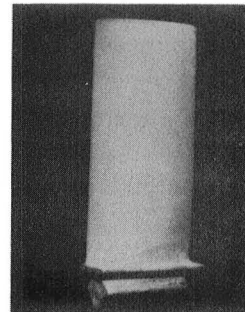
Convex



FAL 58289

Concave

P₁/Cu/Ni Coating

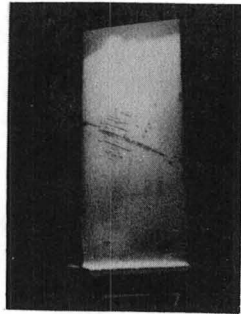


FAL 58290

Convex

FD 199493

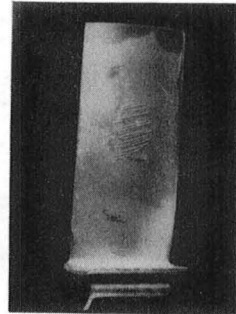
Figure 33. F100, PWA 1202, 6th-Stage HPC Blade, P/N 4034806, Showing Stress Coat Patterns for the First Bending Mode of Vibration (Frequency = 620 to 630 Hz) for the Coating Configurations Indicated



FAL 58432

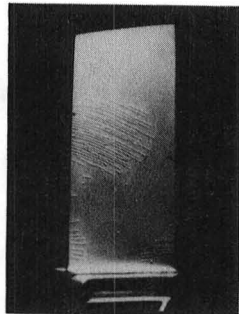
Concave

Baseline
(Uncoated)



FAL 58433

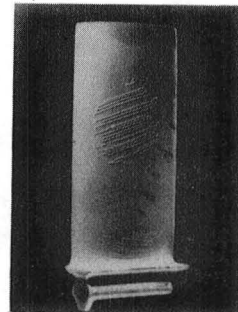
Convex



FAL 58428

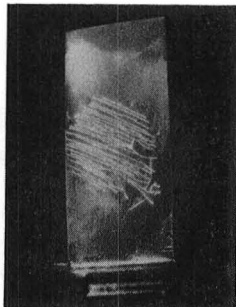
Concave

AL Coating



FAL 58429

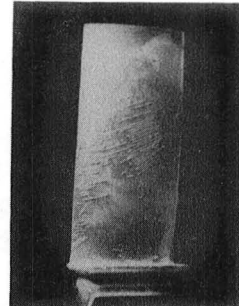
Convex



FAL 58424

Concave

P₁/Cu/Ni Coating

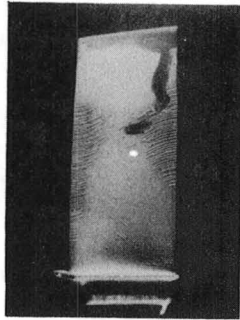


FAL 58425

Convex

FD 199494

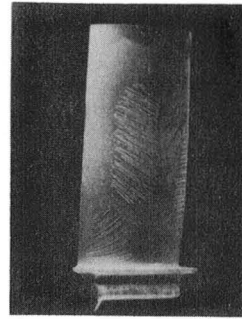
Figure 34. F100, PWA 1202, 6th-Stage HPC Blade, P/N 4034806, Showing Stress Coat Patterns for the Second Mode of Vibration (Frequency = 2500 to 2600 Hz) for the Coating Configurations Indicated



FAL 58430

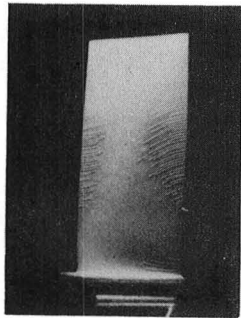
Concave

Baseline
(Uncoated)



FAL 58431

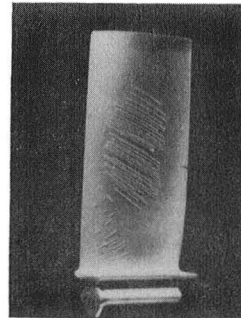
Convex



FAL 58426

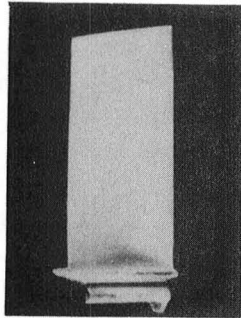
Concave

AL Coated



FAL 58427

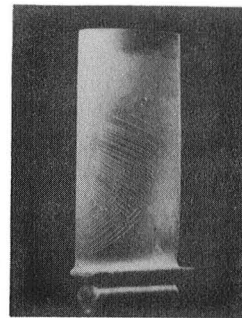
Convex



FAL 58422

Concave

Pt/Cu/Ni Coating



FAL 58423

Convex

FD 199495

Figure 35. F100, PWA 1202, 6th-Stage HPC Blade, P/N 4034806, Showing Stress Coat Patterns for the Third Mode of Vibration (Frequency = 2890 to 3000 Hz) for the Coating Configurations Indicated

TABLE 11. FREQUENCY CHECK DATA FOR F100, PWA 1202, 6TH-STAGE COMPRESSOR BLADES, P/N 4034806, AIRFOILS COATED AND UNCOATED, VIBRATED AT ROOM TEMPERATURE

Specimen Serial Number	Resonant Frequency (Hz)		
	1st Mode	2nd Mode	3rd Mode
<i>Uncoated</i>			
1	639	2600	3032
2	633	2595	3016
3	629	2585	3003
4	636	2601	3018
5	631	2563	3021
6	623	2574	2989
7	636	2581	3031
8	<u>631</u>	<u>2562</u>	<u>2978</u>
Mean	632	2583	3011
Std. Dev.	5	16	19
<i>Pt/Cu/Ni Coating</i>			
2	625	2560	2939
3	628	2526	2933
4	615	2480	2860
5	624	2530	2890
6	621	2506	2854
7	609	2475	2833
8	<u>615</u>	<u>2533</u>	<u>2889</u>
Mean	620	2516	2885
Std. Dev.	7	31	40
<i>IVD Aluminum Coating</i>			
1	643	2625	3032
2	650	2656	3053
3	635	2588	3014
4	629	2588	2995
5	611	2555	2905
6	633	2595	3022
7	636	2620	3036
8	<u>636</u>	<u>2613</u>	<u>3001</u>
Mean	634	2605	3007
Std. Dev.	11	30	45

TABLE 12. FIRST BENDING MODE FATIGUE TEST DATA FOR F100, PWA 1202, 6TH-STAGE HPC BLADES, P/N 4034806, UNCOATED, VIBRATED AT ROOM TEMPERATURE

Specimen Serial Number	Test Frequency (Hz)	Dynamic Stress*		Cycles to Failure	Remarks
		MPa	(ksi)		
1	637	518	(75)	7.26×10^6	Failed on LE, 0.015 in. A/P
2	630	552	(80)	8.32×10^6	Failed on LE, 0.240 in. A/P
3	628	587	(85)	1.0×10^7	Failed on LE, 0.150 in. A/P
4	635	587	(85)	8.92×10^6	Failed on LE, 0.120 in. A/P
5	631	552	(80)	10^7	Did not fail
6	622	587	(85)	1.79×10^6	Failed on LE, 0.120 in. A/P
7	634	587	(85)	10^7	Did not fail
8	635	656	(95)	4.6×10^5	Failed on LE, 0.130 in. A/P
9	635	621	(90)	1.52×10^5	Failed on LE, 0.130 in. A/P
10	640	621	(90)	1.60×10^6	Failed on LE, 0.250 in. A/P
5	631	656	(95)	1.1×10^5	Failed on LE, 0.120 in. A/P

*Stress based on $E = 1.28 \times 10^5$ MPa (18.5×10^6 psi) and measured at stress location No. 2 shown in figure 30.

TABLE 13. FIRST BENDING MODE FATIGUE TEST DATA FOR F100, PWA 1202, 6TH-STAGE COMPRESSOR BLADES, P/N 4034806, AIRFOILS COATED WITH Pt/Cu/Ni, VIBRATED AT ROOM TEMPERATURE

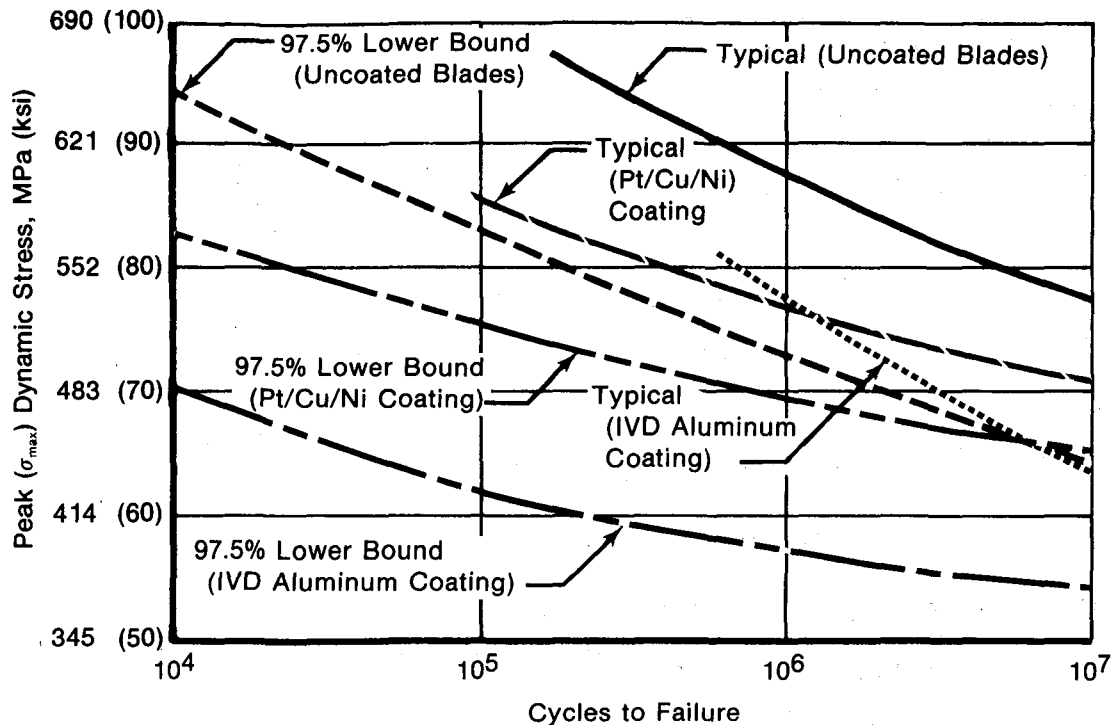
Specimen Serial Number	Test Frequency (Hz)	Dynamic Stress*		Cycles to Failure	Remarks
		MPa	(ksi)		
2	603	518	(75)	1.23×10^6	Failed on LE, 0.200 in. A/P
3	614	483	(70)	10^7	Did not fail
4	608	587	(85)	1.82×10^5	Failed on LE, 0.170 in. A/P
6	600	552	(80)	2.65×10^5	Failed on LE, 0.150 in. A/P
7	607	518	(75)	10^7	Did not fail
8	600	552	(80)	1.4×10^5	Failed on LE, 0.150 in. A/P

*Stress based on $E = 1.28 \times 10^5$ MPa (18.5×10^6 psi) and measured at stress location No. 2 shown in figure 30.

TABLE 14. FIRST BENDING MODE FATIGUE TEST DATA FOR F100, PWA 1202, 6TH-STAGE COMPRESSOR BLADES, P/N 4034806, AIRFOILS COATED WITH IVD ALUMINUM, VIBRATED AT ROOM TEMPERATURE

Specimen Serial Number	Test Frequency (Hz)	Dynamic Stress*		Cycles to Failure	Remarks
		MPa	(ksi)		
1	638	578	(75)	2.68×10^5	Failed on LE, 0.130 in. A/P
2	646	483	(70)	1.94×10^5	Failed on LE, 0.260 in. A/P
3	633	483	(70)	10^7	Did not fail
4	606	518	(75)	10^7	Did not fail
5	629	483	(70)	10^7	Did not fail
6	631	552	(80)	10^7	Did not fail
7	637	449	(65)	10^7	Did not fail
8	635	552	(80)	0.38×10^5	Failed on LE, 0.150 in. A/P

*Stress based on $E = 1.28 \times 10^5$ MPa (18.5×10^6 psi) and measured at stress location No. 2 shown in figure 30.



FD 201898

Figure 36. Peak (σ_{max}) Dynamic Stress Vs Cycles to Failure F100, PWA 1202, 6th-Stage HPC Blades P/N 4034806 from Engine FX-209 Vibrated in the First Bending Mode of Vibration

Tensile Testing

Tensile tests conducted at 427°C (800°F) (for Ti 8-1-1) and 315°C (600°F) (for Ti 6-4) indicate that Pt/Cu/Ni and IVD aluminum coatings have no significant effect on ultimate tensile strength, yield strength, or percent elongation, compared to baseline (uncoated) specimens.

Creep Testing

By measuring the time to reach 1.0% creep at 427°C (800°F) with a stress level of 445 MPa (65 ksi) (Ti 8-1-1) and at 315°C (600°F)/414 MPa (60 ksi) (Ti 6-4), it was determined that no appreciable difference in creep exists between coating systems and the baseline materials.

Stress Rupture Testing

Stress rupture tests conducted at 427°C (800°F) and a stress level of 638 MPa (92.5 ksi) indicate that a Pt/Cu/Ni coating increases the stress rupture life of Ti 8-1-1 by an average of 59%, compared to a 22% increase for IVD Al. Neither coating affects the percent elongation of the substrate.

Hot Salt Stress Corrosion Testing

HSSC tests conducted at 482°C (900°F) and a stress of 345 MPa (50 ksi) indicate that both Pt/Cu/Ni and IVD Al, applied to a thickness of 0.050 mm (0.002 in.) will protect Ti 8-1-1 from stress corrosion cracking.

Erosion Testing

Pt/Cu/Ni is more resistant to erosion than IVD Al at impingement angles of 60 and 90 deg, but IVD Al is superior at an angle of 30 deg.

Adhesion Testing

Bend testing of Ti 8-1-1 specimens indicate that IVD Al adheres more strongly to the substrate than Pt/Cu/Ni. However, it is likely that the relatively poor adhesion exhibited by Pt/Cu/Ni is attributable to processing problems.

Static Oxidation Testing

Thermal gravimetric analysis (TGA) conducted at 500°C (932°F) indicates that the Pt/Cu/Ni coating provides better oxidation protection (smallest oxidative weight gain) than the IVD Al coating. Both coating systems experienced more oxidation than the uncoated baseline Ti 8-1-1 specimen.

Diffusion Testing

After 168 hr at 427°C (800°F), neither coating, IVD Al or Pt/Cu/Ni, exhibited measurable diffusion into Ti 8-1-1 or Ti 6-4 substrates.

Thermal Shock Testing

The IVD aluminum coating withstood thermal shock testing (427 to 25°C) (800 to 77°F) better than Pt/Cu/Ni, but both coatings were acceptable.

Stress Analysis Testing

Stress analysis testing of F100 6th-stage compressor blades showed four results. These were:

1. The 97.5% lower bound HCF life for the Pt/Cu/Ni coated specimens exhibited little degradation, as compared to the fatigue strength of uncoated blades at 10^7 cycles.
2. Fatigue test results of compressor blades coated with IVD Al compare closely with HCF results for IVD Al-coated Ti 8-1-1 test specimens.
3. Results of stresscoat and stress calibration analyses indicate no appreciable mode shape change in the first three modes of vibration due to airfoil coating.
4. Resonant frequencies of the first three modes of vibration for all coating configurations indicate that the Pt/Cu/Ni coating lowers the response frequencies slightly, possibly due to the mass effects of the coating. The IVD aluminum coating produces no appreciable effect on these frequencies.

CONCLUSIONS

Based on the results summarized previously, IVD Al and Pt/Cu/Ni coatings increase the resistance of titanium alloys to combustion without significantly affecting the substrate material. In addition, stress rupture life is enhanced by the Pt/Cu/Ni coating, IVD Al offers better adhesion and thermal shock resistance, and IVD Al is the better coating in reducing the severity of substrate combustion.

Because of this slight superiority exhibited by IVD Al, it was concluded that this was the best coating for the prevention of titanium combustion.

RECOMMENDATIONS

The following recommendations on continuing the study of the prevention of titanium combustion in advanced gas turbine engines are made:

1. Further work should be undertaken to evaluate the combustion suppression of additional duplex systems which would be designed to take advantage of results obtained during this program. Coating systems which may show promise include: copper plus aluminum, nickel plus aluminum, and aluminum-manganese over both copper and nickel.
2. A test program should be initiated to provide full-scale verification (via engine testing) of the capability of the IVD aluminum to perform as indicated during this program.

APPENDIX A

AFWAL/PL TITANIUM FIRE PROGRAM COMBUSTION TEST RESULTS

SUBSTRATE Ti 8Al-1Mo-1V

Specimen No.	Coating Type	Coating Thickness,		Chamber Pressure,		Chamber Temperature,		Air Velocity,		Burn Severity, %	Chordwise Burn Velocity,		Ignition Time, s
		mm	(in.)	Mpa	(psia)	°C	(°F)	m/s	(ft/s)		cm/s	(in./s)	
EB 23	Baseline	N/A		0.28	(40)	316	(600)	176	(578)	51	1.349	(0.531)	0.707
EC 2	Pt/Cu/Ni	0.05	(0.002)	0.28	(40)	316	(600)	175	(575)	2	N/A		N/A
EC 46	Pt/Cu/Ni	0.10	(0.004)	0.28	(40)	316	(600)	174	(572)	<1	N/A		N/A
EA 21	IVD Al	0.05	(0.002)	0.28	(40)	316	(600)	179	(587)	<1	N/A		N/A
EA 51	IVD Al	0.76	(0.003)	0.28	(40)	316	(600)	179	(587)	<1	N/A		N/A
EB 42	Baseline	N/A		0.55	(80)	441	(825)	203	(667)	80	3.884	(1.529)	0.629
EB 43	Baseline	N/A		0.55	(80)	441	(825)	202	(664)	78	3.879	(1.527)	1.064
EC 67	Pt/Cu/Ni	0.05	(0.002)	0.55	(80)	441	(825)	206	(675)	65	3.866	(1.522)	0.623
EC 80	Pt/Cu/Ni	0.05	(0.002)	0.55	(80)	441	(825)	205	(673)	78	3.487	(1.373)	0.828
EA 31	IVD Al	0.05	(0.002)	0.55	(80)	441	(825)	202	(662)	43	4.615	(1.817)	0.428
EA 32	IVD Al	0.05	(0.002)	0.55	(80)	441	(825)	204	(669)	75	3.266	(1.286)	0.624
EB 15	Baseline	N/A		0.28	(40)	316	(600)	226	(740)	95	2.060	(0.811)	1.297
EC 26	Pt/Cu/Ni	0.05	(0.002)	0.28	(40)	316	(600)	225	(737)	65	1.717	(0.676)	1.852
EC 55	Pt/Cu/Ni	0.10	(0.004)	0.28	(40)	316	(600)	222	(729)	9	0.998	(0.393)	2.589
EA 9	IVD Al	0.05	(0.002)	0.28	(40)	316	(600)	213	(700)	42	2.055	(0.809)	2.138
EA 45	IVD Al	0.76	(0.003)	0.28	(40)	316	(600)	213	(699)	41	1.544	(0.608)	1.558
EB 20	Baseline	N/A		0.41	(60)	385	(725)	238	(781)	100	3.266	(1.286)	0.945
EB 21	Baseline	N/A		0.41	(60)	385	(725)	234	(768)	99	3.264	(1.285)	0.588
EC 29	Pt/Cu/Ni	0.05	(0.002)	0.41	(60)	385	(725)	238	(781)	53	N/A		N/A
EC 30	Pt/Cu/Ni	0.05	(0.002)	0.41	(60)	385	(725)	238	(781)	49	3.145	(1.238)	1.192
EA 14	IVD Al	0.05	(0.002)	0.41	(60)	385	(725)	229	(752)	89	3.094	(1.218)	0.921
EA 15	IVD Al	0.05	(0.002)	0.41	(60)	385	(725)	234	(768)	49	3.048	(1.200)	0.827
EB 39	Baseline	N/A		0.55	(80)	441	(825)	241	(790)	77	4.729	(1.862)	0.841
EC 27	Pt/Cu/Ni	0.05	(0.002)	0.55	(80)	441	(825)	250	(819)	89	2.852	(2.123)	1.017
EC 66	Pt/Cu/Ni	0.10	(0.004)	0.55	(80)	441	(825)	249	(817)	56	4.321	(1.701)	0.964
EA 20	IVD Al	0.05	(0.002)	0.55	(80)	441	(825)	238	(780)	88	4.737	(1.865)	1.311
EA 50	IVD Al	0.76	(0.003)	0.55	(80)	441	(825)	239	(784)	90	4.470	(1.760)	0.735
EB 28	Baseline	N/A		0.28	(40)	316	(600)	272	(892)	95	2.357	(0.928)	1.039
EB 29	Baseline	N/A		0.28	(40)	316	(600)	238	(782)	36	2.045	(0.805)	1.497
EC 41	Pt/Cu/Ni	0.05	(0.002)	0.28	(40)	316	(600)	277	(908)	46	1.791	(0.705)	0.984
EC 61	Pt/Cu/Ni	0.05	(0.002)	0.28	(40)	302	(575)	240	(787)	20	1.651	(0.650)	1.882
EA 1	IVD Al	0.05	(0.002)	0.28	(40)	316	(600)	272	(891)	49	1.692	(0.666)	0.995
EA 4	IVD Al	0.05	(0.002)	0.28	(40)	316	(600)	245	(803)	51	1.715	(0.675)	0.736
EB 33	Baseline	N/A		0.41	(60)	385	(725)	245	(803)	95	3.302	(1.300)	0.629
EC 63	Pt/Cu/Ni	0.05	(0.002)	0.41	(60)	385	(725)	251	(824)	82	3.180	(1.252)	0.673
EC 58	Pt/Cu/Ni	0.10	(0.004)	0.41	(60)	385	(725)	251	(822)	54	3.190	(1.256)	1.334
EA 6	IVD Al	0.05	(0.002)	0.41	(60)	385	(725)	301	(989)	91	2.014	(0.793)	1.888
EA 44	IVD Al	0.76	(0.003)	0.41	(60)	385	(725)	296	(972)	71	3.299	(1.299)	0.591
EB 47	Baseline	N/A		0.55	(80)	441	(825)	303	(993)	89	5.834	(2.297)	0.620
EC 94	Pt/Cu/Ni	0.05	(0.002)	0.55	(80)	441	(825)	310	(1016)	82	5.657	(2.227)	2.695
EC 76	Pt/Cu/Ni	0.10	(0.004)	0.55	(80)	441	(825)	314	(1030)	68	4.978	(1.960)	3.177
EA 36	IVD Al	0.05	(0.002)	0.55	(80)	441	(825)	311	(1019)	74	5.872	(2.312)	1.066
EA 58	IVD Al	0.76	(0.003)	0.55	(80)	441	(825)	311	(1020)	74	4.509	(1.775)	0.728
EB 25	Baseline	N/A		0.28	(40)	385	(725)	186	(609)	98	1.849	(0.728)	1.726
EB 26	Baseline	N/A		0.28	(40)	385	(725)	190	(622)	98	1.638	(0.645)	1.481
EC 35	Pt/Cu/Ni	0.05	(0.002)	0.28	(40)	385	(725)	185	(608)	76	1.336	(0.526)	1.629
EC 39	Pt/Cu/Ni	0.05	(0.002)	0.28	(40)	385	(725)	186	(609)	50	1.110	(0.437)	2.048
EA 25	IVD Al	0.05	(0.002)	0.28	(40)	385	(725)	187	(615)	<1	N/A		N/A
EA 26	IVD Al	0.05	(0.002)	0.28	(40)	385	(725)	187	(614)	34	2.756	(1.085)	4.420
EB 11	Baseline	N/A		0.41	(60)	385	(725)	165	(541)	94	1.506	(0.593)	1.212
EC 37	Pt/Cu/Ni	0.05	(0.002)	0.41	(60)	385	(725)	215	(706)	64	2.484	(0.978)	1.339
EC 48	Pt/Cu/Ni	0.10	(0.004)	0.41	(60)	385	(725)	213	(700)	44	2.197	(0.865)	1.139
EA 27	IVD Al	0.05	(0.002)	0.41	(60)	385	(725)	188	(617)	37	3.007	(1.184)	3.091
EA 53	IVD Al	0.76	(0.003)	0.41	(60)	385	(725)	188	(617)	34	2.357	(1.928)	1.424

APPENDIX B ELECTRODEPOSITION PROCESSES

Chromium-Molybdenum Coating

Chromium-molybdenum coatings were applied using the electroplating procedure described below. After a light vapor blast of the surface and application of a thin chromium conversion coating, the parts are plated at 46.7 A/dm^2 (3.0 A/in.^2) with chromium-molybdenum from an electrolyte made up of a self-regulating chromium plating solution containing ammonium molybdate. The procedure is as follows:

Solution Makeup

Self-Regulating Plating Bath

Chromium acid⁽¹⁾ 300 g/l (40 oz/gal)
Ammonium molybdate $(\text{NH}_4)_6 \text{Mo}_7 \text{O}_{24} \times \text{H}_2\text{O}$ 75 g/l (10 oz/gal)

1. Dissolve the chromic acid in deionized water at room temperature.
2. Dissolve the ammonium molybdate in deionized water at $60^\circ\text{C} \pm 5^\circ\text{C}$ ($140^\circ\text{F} \pm 10^\circ\text{F}$).
3. Add the ammonium molybdate solution to the chromic acid and bring up to the operating level
4. Adjust temperature of plating solution to $38^\circ\text{C} \pm 2^\circ\text{C}$ ($100^\circ\text{F} \pm 5^\circ\text{F}$).

Vapor Blast

Novaculite 200⁽²⁾ 480-720 g/l (4 to 6 lb/gal)
Antisolidifying compound⁽³⁾ 113g/22.7 Kg (4 oz/50 lb) abrasive
Corrosion inhibitor⁽⁴⁾ 4 ml/l (15 ml/gal)

1. Fill tank to about $\frac{3}{4}$ of operating level with water.
2. Add abrasive slowly while circulating pump is on.
3. Add antisolidifying compound.
4. Add corrosion inhibitor.
5. Fill to operating level.

Etch Solution at 100°C

Hydrofluoric acid (48%) 48 ml/l
Sodium chromate 250 g/l

1. Dissolve the required amount of sodium chromate in deionized water.
2. Add required amount of hydrofluoric acid
3. Heat to 100°C (212°F).

Procedure

1. Mask area not to be plated with suitable stop-off lacquer.
2. Vapor blast surface to be plated with wet abrasive at 0.4 to 0.7 MPa (50 to 100 psi).
3. Rinse thoroughly in clean running water. Cleaned surface must not be allowed to dry prior to plating. Submerge part in deionized water.
4. Etch for 10 min to produce chrome conversion coating.
5. Using lead anodes, immerse part in plating solution with current off.
6. Raise current to 11.7 A/dm² (0.75 A/in.²) for 2.5 min.
7. Plate at 46.7 A/dm² (3.0 A/in.²) for 30 min.
8. Rinse thoroughly in deionized water. Discard first part used to dummy solution.
9. Heat-treat in vacuum as follows:

Ti 8Al-1Mo-1V:	954°C (1750°F) for 1 hr
followed by	593°C (1100°F) for 8 hr
Ti 6Al-4V:	760°C (1400°F) for 3 hr
followed by	538°C (1000°F) for 6 hr

For other titanium alloys, the diffusion heat-treat cycle should be compatible with previous heat-treat history and selected in accordance with MIL-H-81200.

10. Glass bead peen or vapor blast surfaces.

Chromium Cermet Coating

Chromium Cermet plating is applied to the test specimens using the procedure outlined below.

Solution Makeup

Chrome plating bath at room temperature (75-85°F) (24-29°C)
Chromic Acid (Unichrome) 247 g/l (33 oz/gal.)
Titanium Carbide (particle size <325 mesh)

Dissolve the chromic acid in room temperature distilled water. Add titanium carbide until solution appears saturated (approximately 60 g/l).

Surface Preparation

1. Lightly vapor blast parts — keep parts wet.
2. Cold water rinse.
3. Mild alkaline clean.
4. Cold water rinse.

Etch Solution

Hydrofluoric acid 1-3% + 20 g/l sodium chromate.

Procedure

1. Vapor blast specimen with a wet abrasive at 0.4 to 0.7 MPa (50-100 psi). Keep parts wet.
2. Wash specimen with alkaline cleaner, rinse.
3. Activate specimen for 10 sec in 1-3% HF + 20 g/l sodium chromate etch solution, rinse.
4. Using clean lead anodes, immerse parts in plating solution with current off.
5. Raise current to 15.5 A/dm² (1A/in.²) for 5 min.
6. Plate at 31.1 A/dm² (2A/in.²) for 10 min.
7. Complete plating at 46.7 A/dm² (3A/in.²).
8. Rinse and dry parts.
9. Heat treat in vacuum or inert atmosphere at 954°C (1750°F) for 1 hr followed by 8 hr at 593°C (1100°F).
10. Glass bead peen or vapor blast surfaces.

Aluminum-Manganese Coating

An aluminum-manganese electrodeposit was plated from a fused salt bath consisting of 79% AlCl₃, 10% NaCl, 10% KCl, and 1% MnCl. The coating produced had an approximate composition of 70-75% Al, 30-25% Mn. The plating bath was contained in a teflon beaker with a teflon cover to protect the hygroscopic electrolyte from moisture and minimized the amount of toxic vapor given off. Heat was supplied by a heating mantle. This process is very water sensitive and a small amount of water will contaminate the plating bath thereby preventing the desired electrodeposit from forming. The regulation of the bath composition was difficult due to the depletion of manganese during plating. Bath regulation could have been facilitated by employing anodes made of an aluminum-manganese composition instead of the high-grade aluminum that was used. The aluminum-manganese coating was applied using the following procedure.

Electrolyte Preparation

1. Mix constituents AlCl₃, NaCl, KCl. Chemicals must be anhydrous.
2. Heat until solution reaches desired temperature of 160 to 177°C (320 to 350°F) — electrolyte must be maintained at a temperature above 160°C for plating.
3. Insert dry dummy specimen.
4. Apply current with a current density of 3.2 to 5.4 A/dm² (30 to 50 A/ft²) for approximately 30 min.
5. Remove dummy specimen and discard.
6. Add MnCl₂. Allow sufficient time for MnCl₂ to diffuse if the bath is not agitated.

Specimen Preparation: Plating

1. Clean specimen with alkaline cleaner.
2. Cold water rinse.
3. Acetone rinse.
4. Allow specimen to dry.
5. Abrade surface with dry abrasive such as aluminum oxide particles entrained in a nitrogen or helium gas stream.
6. Insert specimen into electrolyte so that surfaces to be coated are aligned with anode.
7. Remove specimen when desired coating thickness is attained.
8. Wash with water.

Deposition by Ion Plating

Ion plating in the simplest form is a process whereby a coating material is evaporated in the positive glow region of a gas discharge. The evaporant is ionized and accelerated to the work piece under influence of electrical fields, and deposits are made on atomically clean surfaces with high energy. The deposits thus formed have very uniform thicknesses and exhibit excellent adhesion and density.

Gas Discharge Theory Relating to Ion Plating

A gas in its normal state is an insulator for electricity. However, when a small amount of gas is allowed to enter a previously evacuated chamber which has two properly spaced electrodes, and if sufficiently high voltage is applied, a gaseous discharge takes place and current can be carried between the electrodes. Electrons ejected from the negative cathode are accelerated toward the positive anode, gaining energy from the electrical field. As the electrons travel toward the anode, some collide with gas molecules, giving up part of their energy to

produce positive ions and extra free electrons as well as visible light. The heavy, slow moving positive ions remain in the space between electrodes longer than the lighter high-velocity electrons, giving a net positive space charge which, in turn, tends to further accelerate electrons from the cathode to produce a self-sustaining glow discharge.

Some of the positive ions are accelerated to the negative cathode, bombarding it sufficiently to knock off atoms of the cathode surface, disrupting the surface on an atomic scale and ejecting atoms of cathode material by momentum transfer. The positive ion bombardment of the cathode surface also releases electrons by secondary emission, which are attracted to the great density of positive ions congregated about the cathode. This cathode sheath of positive ions shields the cathode from the anode, causing the electric field lines to terminate on this sheath. Thus, an intense electrical field exists in a narrow region near the cathode with a high potential drop in this region. Only a small field intensity occurs over the remainder of the space between electrodes, and the potential drop is low, so that almost all the voltage drop between electrodes occurs near the cathode in the cathode sheath.

In the remaining space between the cathode sheath and the anode, electrons are accelerated only sufficiently to produce enough ions to neutralize the electron space charge. This region of the discharge emits visible light and is called the plasma glow region. The region closest to the cathode, where maximum voltage drop takes place, does not have the characteristic glow and is referred to as the cathode dark space.

If an ionizable material is evaporated in the plasma region of the discharge, while the above discharge is taking place, many of the evaporant atoms are struck by electrons and become ionized. They are then accelerated to the cathode. If the substrate to be coated is made the cathode, the positively charged evaporant ions follow electric field lines to impinge on the substrate surface with energy in electron volts very nearly equal to the full anode-to-cathode potential. The evaporant ions are deposited on the substrate surface and, at the same time, ionized gas atoms are removing material from the substrate surface by sputtering. Process parameters such as gas pressure, anode-to-cathode voltage, and evaporation rate must be adjusted such that more evaporant ions are deposited on the substrate surface than are sputtered off by action of the incident ions.

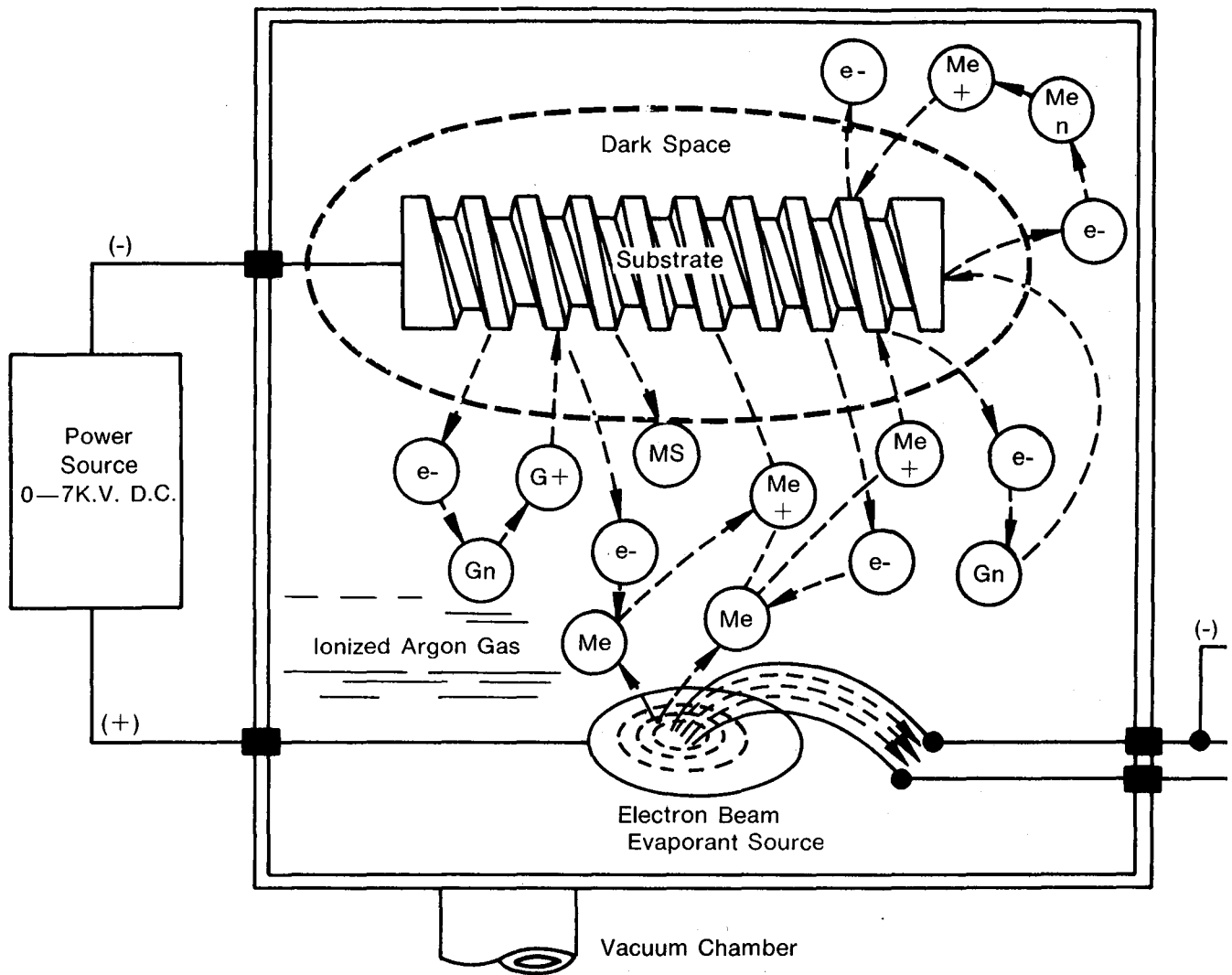
Because the evaporant ions follow electrical lines of force and the diffusion action of the gas, the plating action has the ability to reach all surfaces of the the substrate, not just those in a line of sight path from the evaporant. Figure 37 shows the ion plating process diagrammatically.

Process Procedure 20H

The process is carried out in a vacuum chamber equipped with a vacuum pumping system capable of a reduced pressure in the range of 5×10^{-7} mm of Hg.

The system pressure is reduced to 5×10^{-6} mm of Hg, thus eliminating most of the oxygen and other gases present. The vessel pressure is then brought to the proper level with argon, which is inert. For obtaining different properties, other gases or gas mixtures may be used. By proper throttling and gas metering, the pressure is maintained in a range between 0.005 and 0.04 mm of Hg during the coating cycle.

The part or parts to be coated are made the cathode and are given a negative bias of several thousand volts with respect to the plasma. The surface is thus cleaned by bombardment with ionized gas, freeing it of surface oxides and, to some extent, disrupting the surface on an atomic scale and creating nucleating sites.









-  Indicates Negatively Charged Electrons
-  Indicates Neutral Gas Atoms
-  Indicates Positively Charged Gas Ions
-  Indicates Substrate Atoms
-  Indicates Evaporant Atoms
-  Indicates Positively Charged Evaporant Ions

Figure 37. Schematic Diagram of the Ion Plating Process

After the surface is cleaned (usually 10 to 30 min), evaporation of the coating material is begun and continued until the proper coating thickness is reached. Evaporation and the gas discharge are then terminated and the substrate allowed to cool in the vacuum or inert gas atmosphere.

Obviously, the evaporant and gas ions arriving at the cathode give up their energy in the form of heat, necessitating that the fixturing and process parameters must be adjusted to prevent overheating of the selected substrate.

Nonconductive surfaces can be coated by proper fixturing in a mesh enclosure called a Faraday cage.

Merits of the Process

1. The surface to be coated is cleaned on an atomic scale and remains clean during the entire coating process.
2. Due to the surface heat, clean surfaces, and high energy of the arriving coating material, some diffusion occurs at the interface so that coatings of superior adhesion are obtained. Under certain conditions, some ion implantation occurs. It is not unusual to observe stronger bonds than the parent metal.
3. Since deposition takes place on an atomic scale using high energy, pore-free coatings are obtainable. Pore-free coatings offer superior corrosion protection, and in many cases where the coating material has absolute resistance to its environment, extremely thin coatings provide excellent corrosion resistance.
4. Coating combinations not obtainable by other methods can be achieved. Metals such as aluminum, beryllium, cadmium, chromium, cobalt, copper, gallium, gold, hafnium, indium, iron, lanthanum, lead, manganese, molybdenum, neodymium, nickel, niobium, palladium, platinum, rhodium, ruthenium, silicone, silver, tungsten, tin, titanium, vanadium, and zirconium may be put on selected substrates.
5. Many hard-to-coat materials such as aluminum, magnesium, titanium, beryllium, molybdenum, tungsten, borides, nitrides, carbides, etc., can be satisfactorily coated with the ion plating process.
6. Gas mixtures using reactive gases may be used to form tightly adherent coatings of carbides, nitrides, borides, etc.
7. Many ion-plated thin films on hard-to-coat substrates may be subsequently electroplated for heavy buildups or other properties.
8. Graded coatings using different material combinations for special properties can be achieved.

Sputtering as a Deposition Process

In the broadest sense, sputtering is a process wherein the material from a source (target) is transported in a vapor phase through a plasma (ionized gas) to the part to be coated (substrate) where it is deposited as a coating having essentially the same chemical characteristics as the original target material.

Under ideal conditions, excellent adhesion will occur if the substrate is clean and the arriving material carries sufficient energy to cause nucleation. The sputtering process offers these potentials.

The basic sputtering configuration (called diode sputtering) consists of placing a desired target material and substrate to be coated in a vacuum chamber. The chamber is then evacuated and subsequently back-filled to a low pressure with an inert gas, usually argon. By valving the gas input and throttling the vacuum pumps, proper gas pressure and throughput can be accurately controlled during the process cycle in the working range of 2×10^{-5} to 0.05 mm of Hg.

A suitable power supply (DC or RF) is arranged to provide a negative voltage on the target, and under this influence it becomes a cold cathode electron emitter. The electrons emitted from the target ionize part of the gas, creating positive ions. Because of the negative bias on the target, the positive gas ions are accelerated toward it and strike the surface with sufficient energy to dislodge atoms of the target material. The dislodged atomic particles move through the plasma in all directions, striking the surface to be coated with sufficient energy to create an atomic bond between the substrate and coating material. The energy of the coating material is derived by a momentum transfer from the bombarding gas ions upon the target surface. Under most sputtering conditions, the coating particles will arrive at the substrate surface with energies ranging between ten and several hundred electron volts. By comparison, electroplating usually devops only a few tenths of an electron volt.

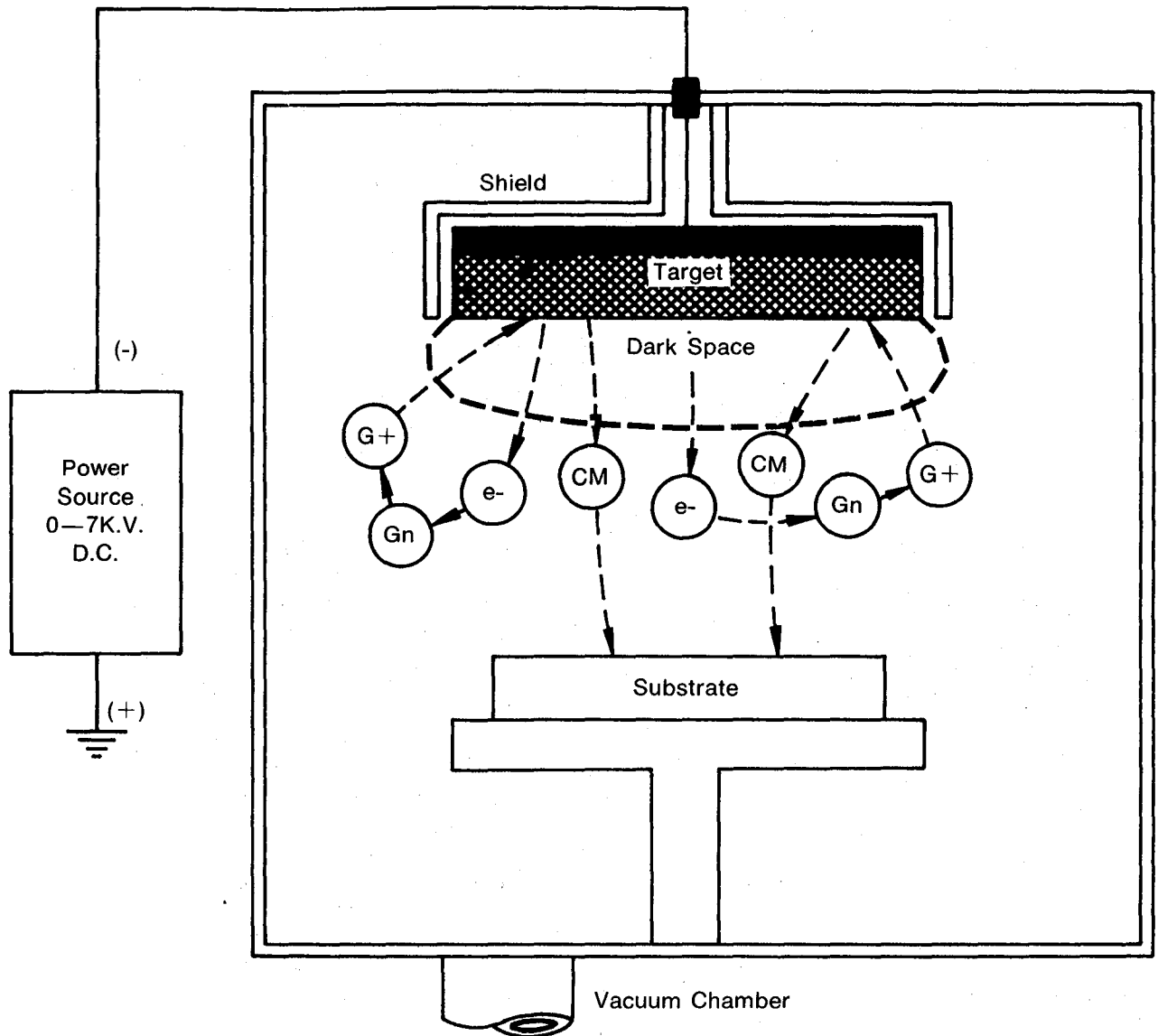
Most sputtering systems will have the electrical power supplies connected so that the part to be coated can be made the cathode, thus sputter cleaning the surface by ion bombardment prior to coating. During sputter cleaning, contaminants are removed and atomically clean surfaces are obtained. This surface conditioning disrupts the surface on an atomic scale, creating nucleating sites which promote excellent adhesion of the coating material to the substrate surface.

Figure 38 is a schematic representation of the basic sputtering process.

Activation of a Platinum Surface for Subsequent Electroplating

The following process is used to activate a platinum surface for subsequent electroplating.

1. Wash surface with detergent.
2. Rinse with deionized water.
3. Immerse surface in 10% HCl solution with an alternating current applied (current density = 62 A/dm^2) for 1 min.
4. Rinse with deionized water.







-  Indicates Negatively Charged Electrons
-  Indicates Neutral Gas Atoms
-  Indicates Positively Charged Gas Ions
-  Indicates Coating Material

Figure 38. Schematic Diagram of the Sputtering Process

APPENDIX C TEST SPECIMEN CONFIGURATIONS

Combustion Tests

Laser Ignition Specimen

Test specimens were prepared for Tasks I and II combustion tests in the configuration shown in figure 39. The dimensions of each machined specimen were measured and recorded; specimens which did not meet the specifications noted in figure 39 were rejected. An average of micrometer readings taken at the seven points shown in figure 40 determined specimen thickness.

Prior to testing, the coated and uncoated specimens received a coating of electroplated black nickel or black chromium in the shaded triangular area shown in figure 40. The nonreflective black coating served to maximize the coupling of laser energy to the specimen by eliminating variations caused by reflectivity differences among the various coatings.

Cascade Ignition Specimen

Test specimens were prepared for cascade combustion tests in the configuration shown in figure 41. The dimensions of each sheared specimen were measured and recorded; specimens which did not meet the specifications noted in figure 41 were rejected. Specimen thickness was recorded as the average of micrometer measurements taken at the seven points shown in figure 40.

Cascade Ignitor Specimen

The upstream specimen for cascade combustion tests were sheared in accordance with the configuration shown in figure 42 from AMS 4916 (Ti 8Al-1Mo-1V) sheet stock. Prior to testing, the ignitor sample was anodized to a blue or violet color to maximize the coupling of laser energy to the specimen.

High-Cycle Fatigue Tests

Utilizing a constant-stress fatigue specimen for high-cycle fatigue testing allowed the testing of relatively large, coated areas. Figure 43 shows the configuration used in screening tests, and figures 44 and 45 detail the configurations used in the secondary phase of testing. The high-cycle fatigue testing of Ti 3Al-8V-6Cr-0.4Mo-4Zr utilized the configuration shown in figure 46. Material availability dictated these specimen configuration changes.

Tensile Tests

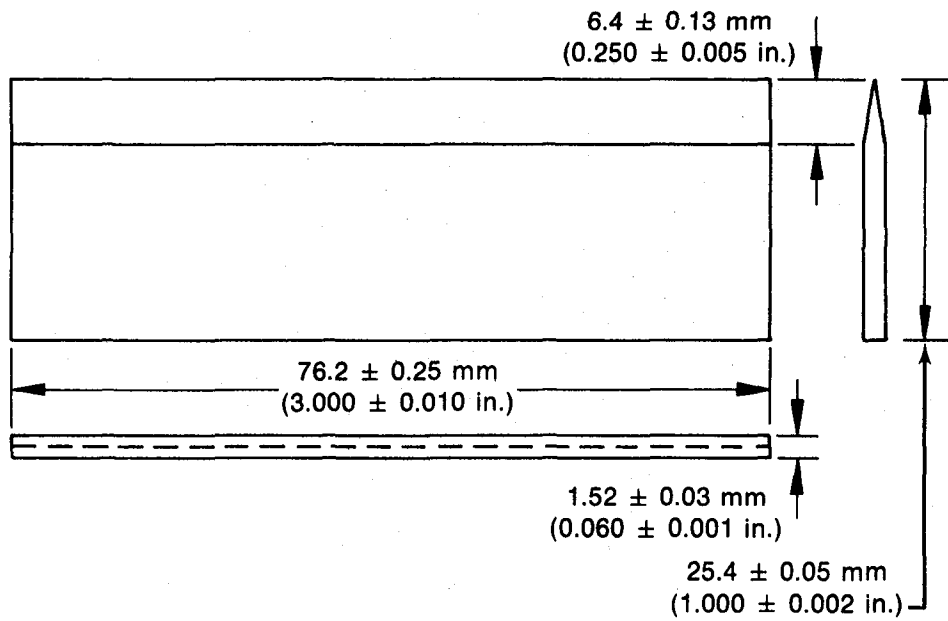
The specimen design is shown in figure 47. Specimens were machined from 0.15 cm (0.060 in.) sheet stock.

Creep and Stress-Rupture Tests

Test specimens, both creep and stress rupture, were machined from 0.15 cm (0.060 in.) material to the configuration shown in figure 47.

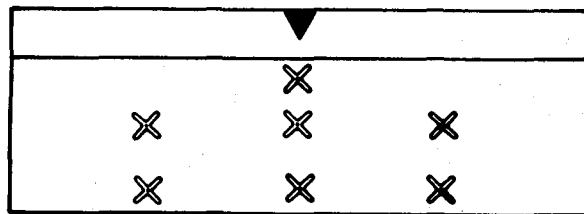
Hot Salt Stress Corrosion Tests

Test specimens were machined from 0.10 cm (0.040 in.) AMS 4916 (Ti 8-1-1) sheet stock in accordance with the specifications listed in table 15. The specimens were machined such that the long axis of the specimen was perpendicular to the direction of rolling.



FD 139562

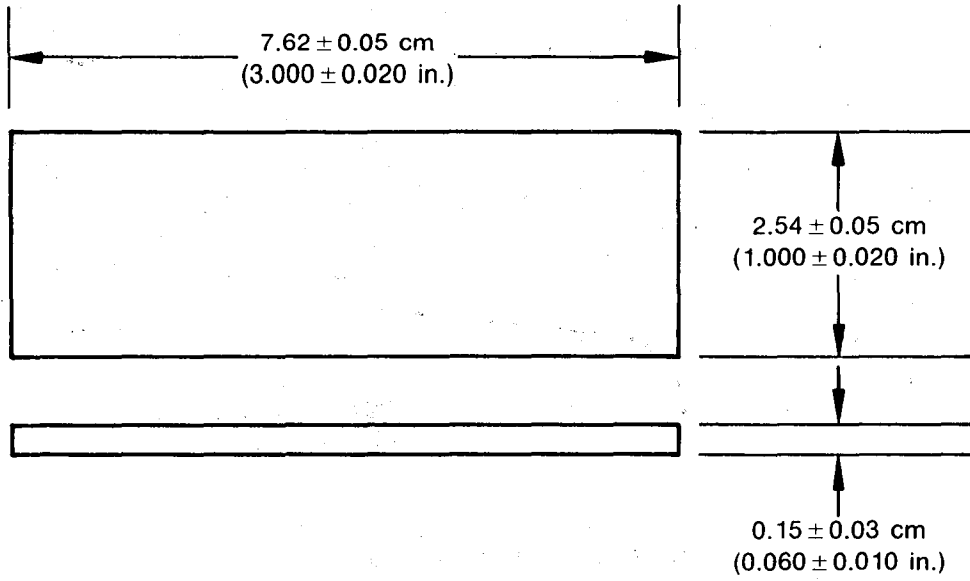
Figure 39. Specimen Configuration



X = Thickness Measurement Point

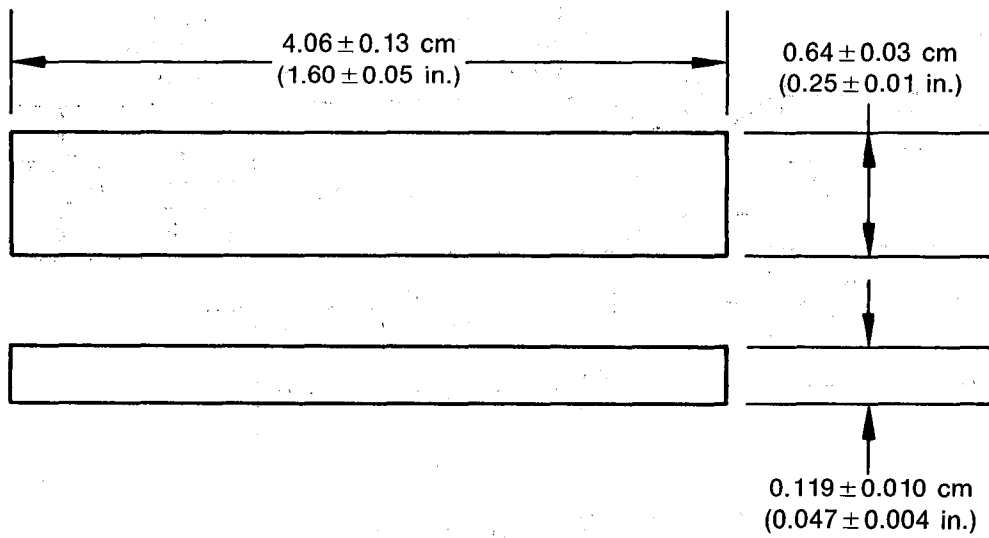
FD 139563

Figure 40. Specimen Thickness Measurement Points



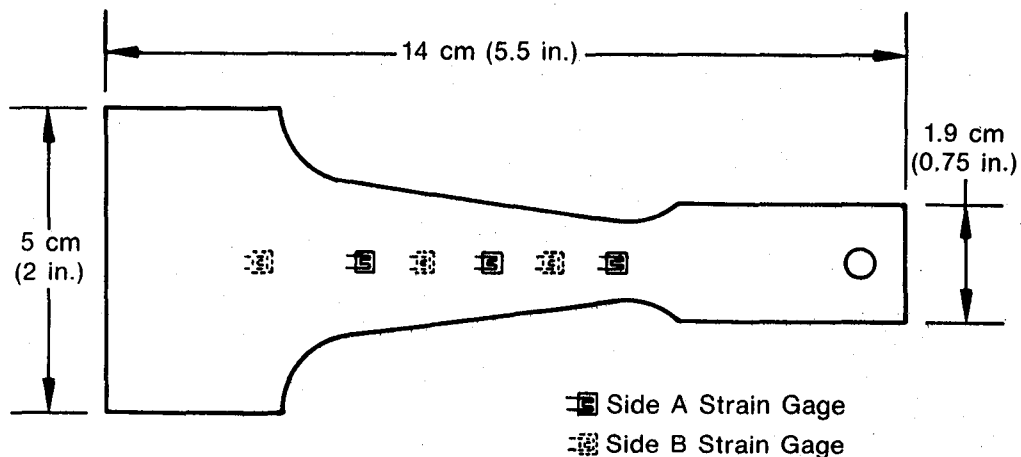
FD 201848

Figure 41. Cascade Combustion Specimen



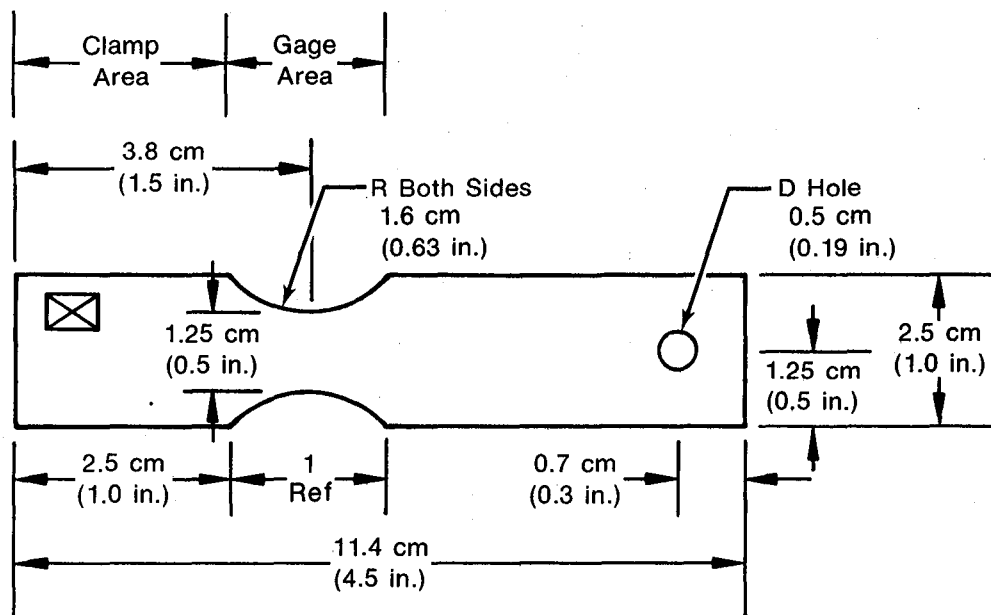
FD 201849

Figure 42. Ignitor Combustion Specimen



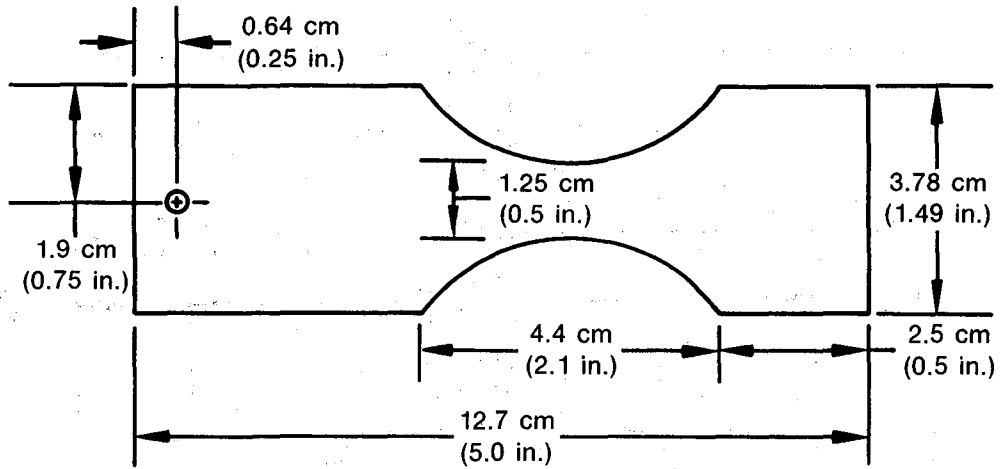
FD 201850

Figure 43. High-Cycle Fatigue Specimen



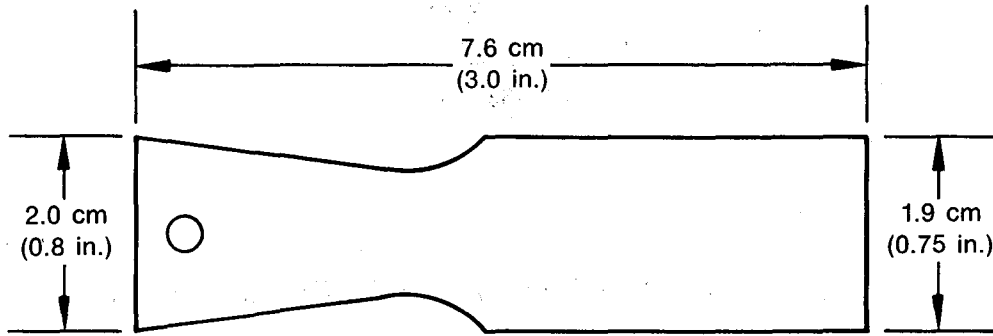
FD 201851

Figure 44. High-Cycle Fatigue Specimen



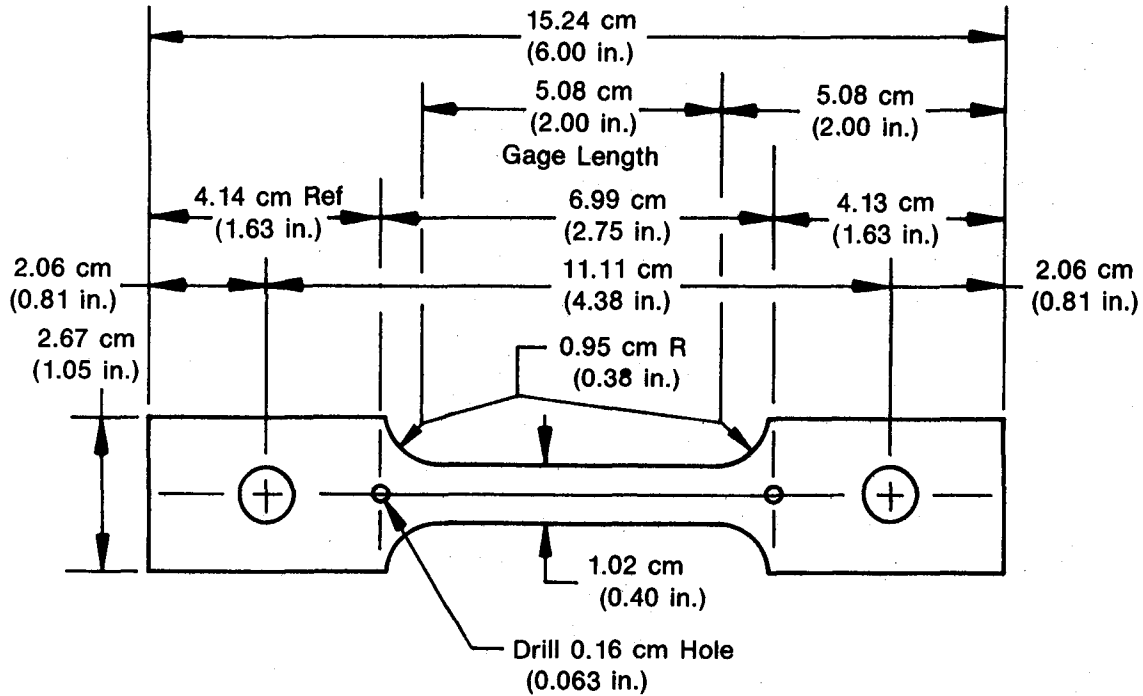
FD 201852

Figure 45. High-Cycle Fatigue Specimen



FD 201853

Figure 46. High-Cycle Fatigue Specimen



FD 139569A

Figure 47. Stress Rupture/Creep/Tensile Test Specimen

TABLE 15. SPECIMEN DIMENSIONS

Thickness		Width		Length Type I		Length Type II	
± 0.0254 mm (± 0.001 in.)	0.030	± 2.54 mm (± 0.1 in.)	0.5	± 0.127 mm (± 0.005 in.)	5.780	± 0.127 mm (± 0.005 in.)	5.930
0.762	0.030	12.7	0.5	146.812	5.780	150.622	5.930
0.787	0.031	12.7	0.5	146.305	5.760	149.809	5.898
0.813	0.032	12.7	0.5	145.847	5.742	149.047	5.868
0.838	0.033	12.7	0.5	145.440	5.726	148.412	5.843
0.864	0.034	12.7	0.5	145.085	5.712	147.828	5.820
0.890	0.035	12.7	0.5	144.780	5.700	147.320	5.800
0.914	0.036	12.7	0.5	144.475	5.688	146.812	5.780
0.940	0.037	12.7	0.5	144.221	5.678	146.431	5.765
0.965	0.038	12.7	0.5	143.967	5.668	145.999	5.748
0.991	0.039	12.7	0.5	143.713	5.658	145.669	5.735
1.016	0.040	12.7	0.5	143.510	5.650	145.288	5.720

Specimens machined to the dimensions shown will receive a stress of approximately 345 MPa (50 ksi) (Type I) or 415 MPa (60 ksi) (Type II) when inserted in the fixture shown in figure 10.

Specimens For Other Tests

Erosion Tests

The erosion test specimen was a rectangular configuration with dimensions of $2.5 \times 5.1 \times 0.15$ cm ($1.0 \times 2.0 \times 0.06$ in.).

Adhesion Tests

The dimensions of the rectangular adhesion test specimen were $12.7 \times 2.5 \times 0.10$ cm ($5.0 \times 1.0 \times 0.04$ in.).

Static Oxidation Tests

The dimensions of the rectangular static oxidation test specimen were $2.5 \times 0.5 \times 0.05$ cm ($1.0 \times 0.2 \times 0.02$ in.).

Diffusion Tests

The dimensions of the rectangular diffusion test specimen were $2.5 \times 2.5 \times 0.15$ cm ($1.0 \times 1.0 \times 0.06$ in.).

Thermal Shock Tests

The dimensions of the thermal shock specimen were $2.5 \times 2.5 \times 0.15$ cm ($1.0 \times 1.0 \times 0.06$ in.).

Stress Analysis

F100 6th-stage compressor blades (P/N 4034806/PWA 1202) were utilized as stress analysis specimens.

DISTRIBUTION LIST

Mr. G. C. Deutsch/RW
NASA Headquarters
600 Independence Ave
Washington, DC 20546

Library (2)
MS 60-3
NASA Lewis Research Ctr
21000 Brookpark Road
Cleveland, OH 44135

Mr. J. P. Merutka (Bal)
MS 49-1
NASA Lewis Research Ctr
21000 Brookpark Road
Cleveland, OH 44135

Mr. R. Rudey
MS 60-4
NASA Lewis Research Ctr
21000 Brookpark Road
Cleveland, OH 44135

Mr. B. Stein MS 188-B
NASA
Langley Research Ctr
Langley Field, VA 23665

Technical Library, Code JM6
NASA
Manned Space Craft Ctr
Houston, TX 77058

Dr. R. I. Jaffee
E.P.R.I.
3412 03 Hillview Ave.
Palo Alto, CA 94304

Dr. M. Greenfield/RWM
NASA Headquarters
600 Independence Avenue
Washington, DC 20546

Report Control Office
MS 5-5
NASA Lewis Research Ctr
21000 Brookpark Road
Cleveland, OH 44135

Dr. L. Harris/RW
NASA Headquarters
600 Independence Avenue
Washington, DC 20540

Technology Utilization
MS 3-19
NASA Lewis Research Ctr
21000 Brookpark Road
Cleveland, OH 44135

Mr. N. T. Saunders
MS 49-1
NASA Lewis Research Ctr
21000 Brookpark Road
Cleveland, OH 44135

Mr. Mike Bauccio DRDAV-DS
Army Av. Res. & Dev. Com.
4300 Goodfellow
St. Louis, MO 63120

Library/Acquisitions
Jet Propulsion Lab.
4800 Oak Grove Drive
Pasadena, CA 91103

Library
NASA
Marshall Space Flight
Center
Huntsville, AL 35812

Applied Technology Lab
DAVDL-ATP-ATP
Attn: J. Lane
Ft. Eustis, VA 23604

Matls. & Struct. Section
MS 501-11
NASA Lewis Research Ctr
21000 Brookpark Road
Cleveland, OH 44135

Acquisition Dept. (25)
NASA S&T Info. Facility
P. O. Box 8757
Balt-Wash Int Airport
MD 21240

DISTRIBUTION LIST (Continued)

Mr. S. J. Grisaffe
MS 105-1
NASA Lewis Research Ctr
21000 Brookpark Road
Cleveland, OH 44135

Mr. Al Powers
MS 500-127
NASA Lewis Research Ctr
21000 Brookpark Road
Cleveland, OH 44135

Library
NASA
Goddard Space Flight Ct
Greenbelt, MD 20771

Mr. Randy C. John
Shell Development Corp.
P. O. Box 1380
Houston, TX 77001

Mr. G. A. Wacker
Head, Metals Division
Naval Ship R&D Ctr.
Annapolis, MA 21402

Mr. A. L. Baldi V.P. R&D
Alloy Surfaces Co. Inc.
100 S. Justison St.
Wilmington, DE 19899

Mr. George A. Graves
University of Dayton
Research Center R 162 KL
300 College Park Ave.
Dayton, OH 45409

Dr. Donald Wood Build, ID4
General Electric Co.
R&D Center
P. O. Box 8
Schenectady, NY 12341

Mr. A. R. Stetson
Solar Turbines Int'l
2200 Pacific Hwy.
P. O. Box 80966
San Diego, CA 92138

Materials Division File
MS 49-1
NASA Lewis Research Ctr
21000 Brookpark Road
Cleveland, OH 44135

Dr. S. R. Levine
MS 49-1
NASA Lewis Research Ctr
21000 Brookpark Road
Cleveland, OH 44135

Library M.S. 185
NASA
Langley Research Ctr
Langley Field, VA 23365

Mr. J. Fairbanks
DOE
Division of FFU
MSE 178
Washington, DC 20545

Reports Acquisition
Aerospace Corporation
P. O. Box 92957
Los Angeles, CA 90009

Mr. S. Shannkar
Howmet Corporation
Technical Center
555 Benston Road
Whithall, MI 49461

Dr. Paul Siemers K1, 4A21
General Electric Co.
R&D Center
P. O. Box 8
Schenectady, NY 12341

Mr. D. Hanink
Engineering Operations
Detroit Diesel Allison
General Motors Corp.
Indianapolis, IN 46206

Mr. J. W. Vogan
Solar Turbines Int'l
2200 Pacific Hwy
P. O. Box 80966
San Diego, CA 92138

DISTRIBUTION LIST (Continued)

Mr. John Kocis
TRW Inc-AECR
1400 N. Cameron St.
Harrisburg, PA 17105

Library
AVCO Systems Division
201 Lowell Stret
Lowell, MA 01851

UTC Library, M. Donnelly
United Tech. Corp.
400 Main Street
East Hartford, CT 06108

Mr. W. R. Freeman, Jr.
Howmet Turbine Comp. Corp.
475 Steamboat Road
Greenwich, CT 06830

Dr. W. B. Hillig K1, 4A21
General Electric Co.
R&D Center
P. O. Box 8
Schenectady, NY 12341

Mr. S. Rangaswamy
METCO, Inc.
11 01 Prospect Avenue
Westbury, LI, NY 11590

Ms. Lulu Hsu
Solar Turbines Int'l.
2200 Pacific Hwy
P. O. Box 80966
San Diego, CA 92138

Dr. D. K. Gupta
J Build. (MERL)
Pratt & Whitney Aircraft
400 Main Street
East Hartford, CT 06108

MCIC
Battelle Memorial Inst.
505 King Avenue
Columbus, OH 43201

Library
Pratt & Whitney Aircraft
United Tech. Corp.
West Palm Beach, FL 33402

Dr. T. E. Strangman
AiResearch Mfg. Co.
111 S. 34th St.
Phoenix, AZ 85034

Library
Cabot Corporation
Stellite Division
P. O. Box 746
Kokomo, IN 46901

Mr. Vern Anderson
P&WA Group
Government Prod. Div.
P. O. Box 2691
West Palm Beach, FL 33402

Mr. Charles Ammann
Tech. Dir., Coated Products
Chromalloy R&D Div.
Blaisdell Rd
Orangeburg, NJ 10962

Mr. J. R. Rairden K1
General Electric Co.
R&D Center
P. O. Box 8
Schenectady, NY 12341

Mr. H. Herman W8
Detroit Diesel Allison
General Motors Company
P. O. Box 894
Indianapolis, IN 46206

Dr. Owen
TRW Inc-AECR
1400 N. Cameron St.
Harrisburg, PA 17105

Technical Reports Library
Oak Ridge National Lab.
Oak Ridge, TN 37830

Library
Research & Delv. Center
General Electric Company
P. O. Box 8
Schenectady, NY 12301

DISTRIBUTION LIST (Continued)

Mr. N. Geyer
AFWAL/MLLM
Wright Patterson AFB, Ohio 45433

Dr. N. Linblad MPTL
Mail Drop M-85
General Electric Co.
Cincinnati, OH 45215

Mr. Joseph J. Falco
Army Mat. & Mech. Res. Ctr.
Arsonel Street
Watertown, MA 02192

Dr. David M. Thompson
Corning-Zircoa
31501 Solon Road
Solon, OH 44139

Mr. P. C. Johnson
Mgr., Engineering Services
American Airlines
Main. and Engr. Center
Tulsa, OK 74151

Mr. Russel Beahm
Power Plant Engineering
United Airlines
International Airport
San Francisco, CA 94128

Mr. L. Hjelm
AFWAL-MLL
Wright-Patterson AFB, OH 45433

Mr. E. E. Bailey
AFWAL-NASA
Wright-Patterson AFB, OH 45433

Mr. H. Heckler
Mail Drop D-83
General Electric Co.
Cincinnati, OH 45215

Mr. D. K. Ratcliffe
Corning-Zircoa
31501 Solon Road
Solon, OH 44139

Mr. R. Hecht
Pratt & Whitney Aircraft
United Tech. Corp.
Florida R&D Center
West Palm Beach, FL 33402

Mr. I. Machlin
Code AIR-5163C1
Department of the Navy
Naval Air Sys. Command
Washington, DC 20361

Mr. David Rigney
Mail Drop D-83
General Electric Co.
Cincinnati, OH 45215

Mr. John M. Richardson III
Alloy Surface Co.
100 S. Justison Street
Wilmington, DE 19899

Mr. Duane Ruckle
Pratt & Whitney Aircraft
United Tech. Corp.
400 Main Street
East Hartford, CT 06108

Mr. Donald Cardinal
3M Co. 3M Center
Building 219-1
St. Paul, MN 55144

Dr. R. C. Tucker, Jr.
Linde Div.
Union Carbide Corp.
1500 Polco Street
Indianapolis, IN 46224

Dr. Jerry L. Arnold
Senior Staff Metallurgist
Matls. Sci., R&T
ARMCO Inc.
Middletown, OH 45043

Mr. R. Mahorter
Code 60631
Department of the Navy
Naval Air Devl. Center
Warminster, PA 18974

DISTRIBUTION LIST (Continued)

Dr. William P. Minnear
Build. K-1, Room 4A45
General Electric Co.
Corp. R&D Ctr.
Schenectady, NY 12301

Mr. Harry A. Hokanson
Dir., Power Plant Engr.
Eastern Airlines, Inc.
International Airport
Miami, FL 33148

Prof. R. A. Rapp
116 West 19th Ave.
Ohio State University
Columbus, OH 43220

Prof. L. Seigle
Dept. of Mat'ls Science
State Univ. of New York
Stonybrook, LI NY 11794

Dr. R. Bratton, Mgr.
Ceramic Science
Westinghouse Res. Labs.
Beulah Road
Pittsburgh, PA 15235

Mr. Fred Mahler
Teledyne CAE
1330 Laskey Road
Toledo, OH 43612

Mr. D. E. Schwab
Materials Engineer
AiResearch Mfg. Co.
2525 W. 190th Street
Torrance, CA 90509

Dr. Donald H. Boone
Lawrence Berkeley Lab.
Bldg. 62 RM. 351, U of CA
Berkeley, CA 94720

Mr. Frank Hermanek
Mgr., Technical Services
Alloy Metals Inc.
501 Executive Drive
Troy, MI 48084

Mr. C. Levy Build. 312
Army Mat. & Mech. Res. Ctr.
Arsonel Street
Watertown, MA 02192

Mr. Donald E. Snedecker
Corning-Zircoa
31501 Solon Road
Solon, OH 44139

Dr. E. R. Thompson
Mgr., Matls. Science
UTC Research Ctr.
Silver Lane
East Hartford, CT 06108

Mr. C. A. Fisher
Dir., Power Plant Engr.
Trans World Airlines
P. O. Box 20126-R2-452 MCI
Kansas City, MO 64195

D. T. A. Taylor
Linde Div.
Union Carbide Corp.
1500 Polco Street
Indianapolis, IN 46224

Prof H. Herman
Dept. of Mat'ls Science
State Univ. of New York
Stonybrook, LI NY 11794

Dr. R. F. Bunshah
Matls. Dept.
6532 Boelter Hall
U. of California
Los Angeles, CA 90024

Dr. M. A. H. Howes
Metals Division
ITT Research Inst.
10 W. 35th Street
Chicago, IL 60616

Mr. William G. Barker
Naval Air Propulsion Ctr.
P. O. Box 7176
Trenton, NJ 08628

DISTRIBUTION LIST (Continued)

Curtiss-Wright Corp.
Attn: Dr. Sam Wolosin
Matls. Engr. Dept.
One Passaic Street
Woodridge, NJ 07075

Dr. T. S. Piwonka TM-2966
TRW Equipment
23355 Euclid Avenue
Cleveland, OH 44117

Dr. S. C. Singhal
Ceramic Science
Westinghouse Res. Labs.
Beulah Road
Pittsburgh, PA 15235

Mr. H. Doering Bld 53-316
Gas Turbine Prod. Div.
General Electric Co.
1 River Road
Schenectady, NY 12345

Propulsion Engineering
The Boeing Co.
P. O. Box 3707
Seattle, WA 98124

Dr. David P. Whittle
Lawrence Berkeley Lab.
Bldg. 62 RM. 141, U of CA
Berkeley, CA 94720

Argonne National Lab
Attn: Harold Herman
9700 South Cass Avenue
Argonne, IL 60439

Mr. Manohar Asnani
TRW, Inc.
1455 E. 185th Street
Cleveland, OH 44110

Mr. Daniel D. Profant
AVCO-Lycoming
550 S. Main Street
Stratford, CT 06497

Mr. L. M. Bianchi VP & GM
Turbine Coat. Facility
AIRCO TEMESCAL
2850 Seventh Street
Berkeley, CA 94720

AVCO Corporation
Lycoming Division
Attn: A. F. Deferrari
550 S. Main St.
Stratford, CT 06497

METCO Inc.
Mr. M. Ortner
Dir. U. S. Marketing
1101 Prospect Ave.
Westbury, LI NY 11590

Dr. S. Raghuramantm-2966
TRW Equipment
23355 Euclid Avenue
Cleveland, OH 44117

Mr. Robert Beck
Mgr. Mat'ls Engr.
Teledyne CAE
1330 Laskey Road
Toledo, OH 43612

Dr. H. Beale
Battelle Labs.
505 King Ave.
Columbus, OH 43201

Mr. Sylvester Lee
AFWAL-MLTM
Wright-Patterson AFB, OH 45433

Mr. S. Mutialic
Turbine Coat. Facility
AIRCO TEMESCAL
2850 Seventh Street
Berkeley, CA 94720

Mr. Lyle B. Speigel
AVCO-Eve. Labs
550 S. Main Street
Stratford, CT 06497

DISTRIBUTION LIST (Continued)

NASA
Attn: Curt Liebert
Lewis Research Center
21000 Brookpark Road
Cleveland, OH 44135

Naval Sea Systems Command
Attn: S. B. Shepard
Code 5231
Washington, DC 20362

TRW Equipment TM-2110
Attn: J. N. McCarthy
23355 Euclid Avenue
Cleveland, OH 44117

Dr. Istvan J. Toth TM-2966
TRW Equipment
23355 Euclid Avenue
Cleveland, OH 44117

Mr. Ram Darolia MPTL
Mail Drop M-85
General Electric Co.
Cincinnati, OH 45215

Mr. Shiro-Fujishiro
AFWAL/
Wright-Patterson AFB, Ohio 45433

Mr. R. Jackson K1
General Electric Co.
R&D Center
P. O. Box 8
Schenectady, NY 46206

NASA
Attn: Dr. S. Stecura
Lewis Research Center
21000 Brookpark Road
Cleveland, OH 44135

Pratt & Whitney Aircraft
Attn: D. Scott Duvall
400 Main Street
E. Hartford, CT 06108

Mr. Tom Sherlock-Lab 101
Westinghouse Electric
P. O. Box 251
Concordville, PA 19331

Mr. Kenneth Ryan
GMC-DDA
P. O. Box 894
Indianapolis, IN 46806

NASA
Attn: Library
AMES Research Center
Moffett Field, CA 94035

NASA
Attn: Frank Stepka
Lewis Research Center
21000 Brookpark Road
Cleveland, OH 44135

Rockwell International
Attn: G. E. William
Rocketdyne Division
6633 Canoga Avenue
Canoga Park, CA 91304

Mr. S. T. Scheirer
Westinghouse Electric
Combustion Turbines Sys.
P. O. Box 251 (M-Code 210)
Concordville, PA 19331

Dr. R. G. Carlson MPTL
Mail Drop M-85
General Electric Co.
Cincinnati, OH 45215

Mr. Charles E. Fetheroff
TRW Equipment TM-2966
23355 Euclid Avenue
Cleveland, OH 44117

Mr. R. L. Shamakian
P&WA Group
Government Prod. Div.
P. O. Box 2691
West Palm Beach, FL 33402

Mr. E. Kerzicnik MPTL
Mail Dro M-85
General Electric Co.
Cincinnati, OH 45215

DISTRIBUTION LIST (Continued)

Westinghouse Electric
Attn: C. A. Anderson
Research Laboratory
1310 Beulah Road
Pittsburgh, PA 15668

Mr. Tom Derkacs
TRW Inc.
23555 Euclid Avenue
Cleveland, OH 44117

Mr. Merle Funkhouser
P&WA Group
Government Prod. Div.
P. O. Box 2691
West Palm Beach, FL 33402

Mr. Don Kearns Suite 422
Solar Turbine Inter.
499 South Capital St. SW
Washington, DC 20003

Mr. Frank N. Longo
METCO Inc.
1101 Prospect Avenue
Westbury, LI NY 11590

Mr. Sherman D. Brown
Ceramic Eng. Dept.
U of Illinois
Urbana, IL 61801

Mr. Robert Benden
TRW Inc.
23355 Euclid Ave.
Cleveland, OH 44117

Mr. Stanley L. Bost
Corning-Zircoa
31501 Solon Road
Solon, OH 44139

Mr. R. J. Bratton
R&D Center
Westinghouse Electric
1310 Beulah Road
Pittsburgh, PA 15235

NASA
Attn: Mr. Gene Cataldo
Geo. C. Marshall SPC Ct
Marshal SFC, AL 358121

Dr. William Lee
Rockwell International
Energy Systems Group
8900 Desoto Ave.
Canogo Park, CA 91304

TRW Equipment TM-2966
Attn: I. M. Matay
23355 Euclid Avenue
Cleveland, OH 44117

Mr. James Clare
METCO Inc.
1101 Prospect Ave.
Westbury, LI NY 11590

Mr. Y. Horada
IIT Res. Inst.
10 West 35th Street
Chicago, IL 60616

Mr. George A. Grave, Jr.
U of Dayton
Dayton, OH 45409

Mr. John Klein
METCO Inc.
1101 Prospect Ave.
Westbury, LI NY 11590

